Wideband reconfigurable antenna designs

BY

OMID MANOOCHEHRI
B.S., Shiraz University of Technology, Shiraz, Iran, 2008
M.S., Tarbiat Modares University, Tehran, Iran, 2011

THESIS

Submitted as partial fulfillment of the requirements
for the degree of Doctor of Philosophy in Electrical and Computer Engineering
in the Graduate College of the
University of Illinois at Chicago, 2019

Chicago, Illinois

Defense Committee:

Danilo Erricolo, Chair and Advisor
Besma Smida
Amit Trivedi
Piergiorgio L.E. Uslenghi
Jing Liang, Google Inc.
Francesco Monticone, Cornell University
Nicolaos G. Alexopoulos, University of California Irvine.

ACKNOWLEDGMENTS

I am indebted to many people for their continuing support leading to this dissertation. First, I would like to thank my advisor, Prof. Danilo Erricolo, for his support and trust. His supportive guidance helped me navigate through the problems and his trust gave me enough freedom to enjoy exploring the field. I would also like to thank my collaborators namely, Dr. Farhad Farzami, Mr. Amin Darvazehban and Mr. Mohammadali Salari and Ms. Seiran Khaledian from their advice and guidance through the fabrication processes and test. I am also thankful to Prof. Francesco Monticone and Dr. Jing Liang for providing valuable insights and suggestions in specific portions of my dissertation.

Being a member of Andrew Laboratory at the University of Illinois at Chicago (UIC) was an excellent experience for me. The collaborations and discussions over the years helped me grow, personally and intellectually. Many of the ideas in our work emerged from our discussions and teamwork.

OM

PREFACE

This dissertation is an original intellectual product of the author, O. Manoochehri. All of the work presented here for RF, antenna and microwave circuits was conducted in the Andrew Laboratory at the University of Illinois at Chicago.

Reconfigurable antennas are important for many applications such as satellite communication systems (1; 2; 3), cell phone communications (4; 5) and direction finding systems (6; 7; 8). I have focused on direction finding system antennas and worked primarily on designing the antennas to be used in direction finding systems. Then, I also provided some contributions to design and fabricate RF components needed by the antennas. Therefore, the main focus of this project is to introduce some novel ultra-wide band reconfigurable antennas (9) with dual band ultra-wide-band omnidirectional antenna (10) used in direction finding systems. Optimization of the fabrication process and experimentation with different methods are the contribution of these projects.

Moreover, a wideband and high efficient multi feed multi beam reflector to be used in direction finding and satellite communication systems fed by double ridge horn and Vivaldi antenna are designed.

We also designed and fabricated two reconfigurable microstrip antennas by using reflective surfaces and PIN diodes to be used in wireless and medical purposes to detect tissue tumors.

The results have previously appeared (or is appearing) as an article in Journal of IEEE Antennas (11), and Wireless Propagation Letters (12), Microwave and Optical Technology Letters (13) an article in IEEE Transactions on Microwave Theory and Techniques (14), and several workshops and conference publications: (15), (16), USNC-URSI'16 (17; 18; 19; 20), USNC-URSI'17 (21; 22) and USNC-

PREFACE (Continued)

URSI'18 (23; 24). The copyright permissions for reusing the published materials have been presented in Appendix B.

Omid Manoochehri
March 21, 2019

CONTRIBUTION OF AUTHORS

The content of chapter 2 is based upon the design and fabrication of a novel reconfigurable parallel plate lens antenna. The lens antenna measurement and simulation manuscript results have been published in IEEE Transactions on Antennas and Propagation (9). I was responsible for designing, modeling and finally, composing the manuscript with the help of my advisor, Prof. Danilo Erricolo. Mr. Amin Darvazehban and Mr. Mohammad Ali Salari helped me with part of the experimental data.

The content of Chapter 3 is based upon the design and fabrication of a wideband Rotman lens antenna. A portion of the content of this Chapter has been published in IEEE Transactions on Microwave Theory and Techniques (14). I was responsible for the fabrication and testing of the Rotman lens antenna. Amin Darvazehban, Mohammad Ali Salari, Professor Tavakoli and Dehkhoda, our collaborators from Amirkabir University helped during the simulation and fabrication of substrate and they also edited the manuscript.

The content of Chapter 4 is based upon the design and fabrication of a wide band reconfigurable reflector antenna fed by double ridged horns. A portion of the content of this Chapter has been published in IEEE Antennas and Propagation Society (15). I was responsible for the design, fabrication and testing of the reflector antenna. Mr. Amin Darvazehban, Mr. Ahmad Emadeddin and Prof. Erricolo helped me to improve the proposed formulas used in the paper and also edited the manuscript.

The content of Chapter 5 is based upon the design and fabrication of a wideband reconfigurable reflector antenna fed by double ridged horns. A portion of the content of this Chapter has been published in IEEE Antennas and Propagation Society (25). I was responsible for the design of the SIW antenna

CONTRIBUTION OF AUTHORS (Continued)

array. Mr. Amin Darvazehban, Mr. Mohammad Ali Salari helped me to optimize the antenna and Prof. Erricolo helped me to improve the manuscript.

The content of Chapter 6 is based upon the design and fabrication of a novel TEM horn antenna with an active matching circuit. A portion of the content of this Chapter has been published in IEEE Antennas and Wireless Propagation Letters (12). I was responsible for design, fabrication and testing of microdevices along with guidance from my advisor, Prof. Danilo Erricolo and contribution of Mr. Amin Darvazehban and Mr. Mohammad Ali Salari to edit the manuscript.

The content of Chapter 7 is based upon the design and fabrication of a novel Biconical antenna with 5 layer polarizers. A version of this Chapter has been published in Microwave and Optical Technology Letters (10). I was responsible for design, fabrication and testing of microdevices along with guidance from my advisor, Professor Danilo Erricolo and contribution of Amin Darvazehban and Mohammad Ali Salari and Seiran Khaledian to test and edit the manuscript.

The content of Appendix 8 is based upon design and fabrication of an ultra-wide band waveguide coupler. A portion of the content of this Appendix has been published in Microwave and Optical Technology Letters (26). I was responsible for analysis, simulation and fabrication of the coupler. Mr. Amin Darvazehban is responsible for developing the theory for tapered double ridge coupler. Prof. Danilo Erricolo was in charge of this project and help us to edit the paper and improve the theory behind the proposed waveguide coupler.

TABLE OF CONTENTS

TABLE OF CONTENTS (Continued)

CHAPTER **PAGE**

LIST OF TABLES

LIST OF FIGURES

LIST OF FIGURES (Continued)

FIGURE **PAGE**

LIST OF FIGURES (Continued)

FIGURE **PAGE**

LIST OF FIGURES (Continued)

LIST OF FIGURES (Continued)

FIGURE **PAGE**

LIST OF ABBREVIATIONS

DGS	Defected Ground Structure
EMC	Electromagnetic Compatibility
CSRR	Complementary Split-Ring Resonator
UIC	The University of Illinois at Chicago
GPR	Ground Penetrating Radar
GRIN	Gradient Refractive Index Material
LC	Liquid Crystal
NIC	Negative Impedance Converter
PPW	Parallel Plate Waveguide
PTFE	Polytetrafluoroethylene
PSO	Particle Swarm Optimization
VSWR	Voltage Standing Wave Ratio
UWB	Ultra Wide Band

SUMMARY

Modern wireless communications systems require the integration of multiple radios into a single reconfigurable platform to maximize connectivity. In order to have a reconfigurable platform, each component should be designed to be compatible and agile to meet the system demands. The UIC Andrew Electromagnetics Lab has contributed to several solutions for antennas that are reconfigurable in frequency and pattern and I studied wideband reconfigurable lens antennas because these antennas are used in two main types of applications: (i) automotive radar systems (27) and (ii) direction finding radar systems (28).

Today, designing small automotive radar systems is a big challenge in automobile industry navigation systems. These systems can be used to help drivers to increase safety. Moreover, direction finding radar systems can be used for military, rescue and cellular operator applications to find unknown targets. All of these systems need special antennas and the antennas should have low profile, wideband and the capability to handle high RF power. Most radar systems do not have enough space for their antennas; therefore the primary challenge for antenna designers is proposing small antenna. These antennas can also be used for satellite communications where all the above requirements are not easily achieved. Automotive radar systems typically operate in the microwave region or mm-wave region where lens structures are good candidates to be used for reconfigurable antennas(14). A good example is the Luneburg lens antenna. A Luneburg lens is fed by microstrip or horn antennas. The primary challenge of Luneburg antennas is their size and fabrication process. Some authors proposed a semi-spherical dielectric lens fed by microstrip antennas to reduce the size, but microstrip antenna could not handle high power. Others

used one-layer dielectric instead of multi dielectric layers to have more natural fabrication process, but the total efficiency is not sufficient. We have addressed some of these challenges in our preliminary results: low profile, wideband, the capability to handle high RF power and minimum difficulty to fabricate (9). We designed and fabricated an ultra-wideband multibeam microwave lens antenna operating from 8 GHz to 18 GHz to cover X and Ku band for radar systems. The antenna consists of four excitation ports connected to a parallel plate waveguide filled with a cylindrical dielectric slab. We simplified the fabrication process by proposing a material with a uniform dielectric constant whose value is optimized to maximize gain performance while simplifying the manufacturing process, instead of having an index of refraction that varies with the radial distance from the axis of the cylindrical lens. We addressed the capability to handle high RF power and reducing the size by replacing the antenna feed with coaxial connector pins to reduce the overall size and increase the bandwidth compared to prior designs. Many direction finding systems typically have 8 to 10 antennas placed along a circle and another one, the reference antenna, placed at its center (6; 7; 8). When a wave from an unknown direction is incident on the system, its phase and amplitude are measured by all antennas along the circle and compared with the reference antenna to estimate the direction of arrival of the signal. The reference antenna is omnidirectional and should have low ripple pattern in all directions to minimize the estimation error. Biconical antennas are good candidates as reference antennas, but the primary challenge is designing a wideband biconical antenna to receive both vertical and horizontal polarizations, since the polarization of the incident signal is unknown. To address the lack of knowledge about the polarization of the incident signal, some authors proposed the use of polarizers to rotate the polarization of the incident wave. However, the biconical antenna pattern has ripples in the azimuth plane at a higher frequency, and the

main antenna beam drifts away from the horizontal plane, and this could create amplitude estimation errors. We designed and fabricated a reference antenna consisting of an ultrawideband biconical antenna operating from 2 GHz to 18 GHz surrounded with strip polarizers to have the capability to receive both horizontal and vertical polarization and cover the S,C,X, Ku bands (10). This antenna uses 5 layers of strips and un-balanced cones with two different cone angles to create stable patterns. Several layers of polarizers are used to rotate the plane of polarization of the incident signals so that it becomes polarized at a slant angle of 45°. A direction finding system should be able to detect signals in the VHF and UHF bands, and the primary challenge is designing a physically small antenna. TEM horn antennas are good candidates, and some solutions include using metamaterials and lumped loading elements to decrease the frequency operation. However, these (passive) methods are not sufficient to decrease the frequency operation to the VHF band. We also designed and fabricated TEM horn antennas operating from 20 MHz to 2.5 GHz (12). 8 TEM horn antennas can be placed on a circle with 1 m radius with 45° of angular separation. We proposed an active circuit instead of a passive matching circuit to compensate for the capacitive behavior of the antenna at low frequencies. A negative impedance capacitor circuit decreases the lowest frequency from 200 MHz to 20 MHz. We also proposed an ultra-wideband 6 GHz to 18 GHz phased array antenna with a beam scanning angle of 52° is proposed. Microstrip Rotman lens has been designed to act as the beamforming network, and optimized to achieve minimum phase-error over the whole frequency range. In order to satisfy the condition needed for avoiding grating lobes, as well as achieving a wide radiation bandwidth and a high power handling capability, an E-plane double-ridged horn antenna is used as the radiating element. A novel wide-band end-launcher coaxial to double-ridged waveguide transition has also been developed for connecting the beamforming network to the antenna

array. An excellent agreement between the measurements of the fabricated system and the simulated results are observed. This antenna cab be used in directional finding systems.

We also proposed a novel design technique to design a highly efficient multi-feed reflector antenna. This method controls the arrangement of feed positions in order to increase the efficiency and gain of the whole structure. A broadband multiband antenna based on offset parabolic reflector in order to use in broadband multiband applications is presented. The structure has been designed, simulated and measured based on the proposed method at the frequency range of 6 GHz to 18 GHz, and takes the advantages of low profile, high efficiency, and high gain. The proposed antenna system is a good candidate for broadband access where wide coverage and high gain are simultaneously required. The maximum gain is 27 dB at 18 GHz and the overall coverage is 30° in the elevation plane and 7° in the azimuth plane by producing 4 distinct beams and aperture efficiency of more than 51%.

We also proposed a substrate integrated waveguide (SIW) slot array antenna with a reconfigurable liquid crystal (LC) phase shifter for operation at X-band and Ku-band is proposed. The frequency range of operation for a VSWR of better than 2 is from 11.85 GHz to 12.25 GHz with a realized gain of around 18 dB. Using LC phase shifter makes it possible to carry signals with higher power than conventional phase shifters. Moreover, continuous phase shifting, as well as wideband operation, are among the advantages of using a LC phase shifter. The proposed antenna can be used in satellite communication systems.

CHAPTER 1

INTRODUCTION

1.1 Thesis Organization

Today, fast-growing demand for wideband and miniaturized communication systems will drastically need more strong strategies to use multipurpose antennas with different frequency and pattern bandwidths. Reconfigurable antennas are the best candidates to be used in portable and small systems, because they are cheap and occupies less space compared with conventional antennas. Pattern reconfigurable antenna are one of the most promising candidates for the new-generations of communication systems. The main challenges of designing reconfigurable antennas are cost and frequency bandwidth. Fabrication complexity increases the cost and size dramatically. Antenna frequency bandwidth is directly related to the antenna size and making small antennas limits their frequency bandwidth. In this thesis, I present some techniques to decrease the proposed reconfigurable antenna size and fabrication cost such as using active matching circuits, dielectric and liquid crystals.

Reconfigurable antennas can be controlled by digitally control systems and if we make active antennas, we can simplify digitally control systems greatly. Digitally control systems use switches and active diodes to control the antenna frequency bandwidth and each active element can limit whole frequency bandwidth. Therefore, by using active reconfigurable antennas we can decrease the number of used switches and diodes in the control systems. Reconfigurable antennas can also allow frequency hopping and be used as filters. direction finding systems have different type of antennas. These antennas cover

required frequency bandwidths such as VHF, UHF, C, S, X and Ku band. In each Chapter one of these antennas is described. It is interesting to say that each antenna can be used in other applications such as radar, satellite communication systems. This thesis is organized into nine chapters. Descriptions of each chapter of the dissertation are as follows:

Chapter 1: This chapter provides the reader with the motivations for this work and identifies the research questions that the work is focused on. Our approach to these problems is explained and a list of related contributions is included in this chapter, as well.

> In this Chapter, I have designed and fabricated a novel parallel waveguide lens antenna from 8 GHz to 18 GHz to be used in direction finding systems. I was the main responsible for the work, and the coauthors helped me to edit the paper manuscript and test the antenna.

Chapter 2: This chapter presents the concepts of the lenses and focuses on the Luneburg and parallel waveguide lens antenna used in direction finding systems (DF). We proposed an UWB parallel waveguide lens that works from 8 GHz to 18 GHz. Design procedure with advantages and disadvantages are mentioned. The proposed antenna fabricated and the measured and simulation results are in a good agreement. This antenna can be used in satellite communication systems because it has a high gain and miniaturized dimension, the antenna has low loss and can handle high RF powers.

Chapter 3: This chapter presents the concepts of Rotman lens antenna and proposed an UWB Rotman lens antenna used in directional finding systems with the simulation and measurement results and indicates the advantage and disadvantage of Rotman Lens. This antenna can also be used in satellite communication systems and scan 60° space angle by using horn antennas. Moreover, this antenna can handle high RF power so it can be used in satellite transponders.

In this Chapter, I have designed a multibeam reflector antenna fed by double ridged antennas to be used in a direction finding system from 6 GHz to 18 GHz. The antenna can be used in satellite communication systems too and the proposed formula has been approved by using genetic algorithm optimization. I was the main responsible for the work, and the coauthors helped me to edit the paper manuscript and test the antenna in the anechoic chamber.

Chapter 4: This chapter presents a novel design technique to design a highly efficient multi feed reflector antenna. This method controls the arrangement of feed positions in order to increase the efficiency and gain of the whole structure. The proposed antenna system is a good candidate for broadband access where wide coverage and high gain are simultaneously required. This antenna can be used in satellite communication and direction finding systems. Two types of the antennas are proposed to feed the reflector. 1) Double ridge horn antenna, 2) antipodal corrugated Vivaldi antenna. These antennas are wideband and have a stable gain in the whole frequency bandwidth

from 6 GHz to 18 GHz. We use some methods such as using corrugated edges and tapered matching line to create stable patterns for the antennas.

In this Chapter, I have designed and simulated an SIW slot array antenna using liquid crystal at Ku band and also designed a reconfigurable cross-slot microstrip antenna at C band. The antennas can be used in electromagnetic imaging systems too. The SIW antenna can scan the space by changing the DC bias applied on the liquid crystal and the cross-slot antenna used PIN diodes to rotate the pattern in the two perpendicular planes. I was the main responsible for the work, and the coauthors helped me to edit the paper manuscript.

Chapter 5: In this chapter, a substrate integrated waveguide slot array antenna with a reconfigurable liquid crystal phase shifter for operation at X-band and Ku band is proposed. Liquid crystals (LCs) are used in microwave circuits recently because of their characteristics. LCs permittivity can be changed when the E field bias changes. They can be good candidates for solid-state phase shifters. We also proposed cross-slot antennas with parasitic slots and PIN diodes to rotate the main pattern. A reflective surface is used to suppress the back lobes. This antenna can be used in wireless communications and medical purposes to detect tissue tumors. Lung and chest tumors can be detected using electromagnetic monitoring systems since there is a significant dielectric contrast between the lung tissues and accumulated fluids. So, by analyzing the scattered wave, tumor volumes and locations can be detected easily.

In this Chapter, I have designed a novel wideband TEM horn antenna to be used in direction finding systems as a reference receiver antenna. The antenna has an active RF matching circuit to receive low frequencies from 20 MHz to 200 MHz. I was the main responsible for the work, and the coauthors helped me to edit the paper manuscript and test the antenna.

Chapter 6: In this chapter, we review the concept of TEM horn antennas then proposed ultra-wideband antenna works from 20 MHz to 2.5 GHz using active negative impedance capacitor (NIC) to match the antenna at low frequencies. Eight numbers of this antenna can be used as receiving antennas in Direction finding systems. These antennas should be wideband and small to cover wider frequency bandwidth, especially at low frequencies. The main reason for using small antennas is minimizing detection error at higher frequencies. The antennas should have a stable gain at whole frequency bandwidth to minimize target range errors. TEM horn is an excellent candidate to be used in DF systems.

In this Chapter, I have designed and a wideband dual polarized biconical antenna to be used in direction finding systems as a reference receiver antenna. The antenna can receive horizontal and vertical polarization simultaneously. I was the main responsible for the work, and the coauthors helped me to edit the paper manuscript and test the antenna in the anechoic chamber.

Chapter 7: In this chapter the concept of the biconical antenna described then we proposed an Ultra-wide band dual polarized asymmetric biconical antenna using polarizers to rotate the waves. This antenna can be used as a reference antenna in the direction finding systems. The antenna should have stable pattern in the azimuth plane because the other antenna received powers used in DF systems are compared with this antenna received power. Therefore, the antenna gain should be stable to minimize the target range error. Some techniques are used to stabilize the antenna gain and pattern from 6 GHz to 18 GHz frequency band. The antenna gain variation is less than 2 dB in the whole frequency band.

In this Chapter, I have designed a wideband Rotman lens antenna to be used in a direction finding system from 6 GHz to 18 GHz. The antenna can scan the space from -30° to $+30^{\circ}$. I tested the antenna and helped Mr. Amin Darvazehban to simulate the antenna. I also helped the coauthors to edit the paper manuscript.

Chapter 8: This part concludes the dissertation with highlights and achievements of the project with emphasis on bandwidth, RF power handling, and their applications.

1.2 Reconfigurable antenna

A reconfigurable antenna is an antenna capable of modifying its frequency and radiation properties dynamically in a controlled and reversible manner. In order to provide a dynamical response, reconfigurable antennas integrate an inner mechanism (such as RF switches, varactors, mechanical actuators or tunable materials) that enable the intentional redistribution of the RF currents over

the antenna surface and produce reversible modifications over its properties. Reconfigurable antennas differ from smart antennas because the reconfiguration mechanism lies inside the antenna rather than in an external beamforming network. The reconfiguration capability of reconfigurable antennas is used to maximize the antenna performance in a changing scenario or to satisfy changing operating requirements.

1.3 Types of antenna reconfiguration

Reconfigurable antennas can be classified according to the antenna parameter that is dynamically adjusted, typically the frequency of operation, radiation pattern or polarization(29).

1.3.1 Frequency reconfiguration

Frequency reconfigurable antennas can adjust their frequency of operation dynamically. They are particularly useful in situations where several communications systems are used because the required antennas with different frequency bandwidths can be replaced by a single reconfigurable antenna. Frequency reconfiguration is generally achieved by modifying physically or electrically the antenna dimensions using RF-switches, impedance loading or tunable materials (30).

1.3.2 Radiation pattern reconfiguration

Radiation pattern reconfigurability is based on the intentional modification of the spherical distribution of radiation pattern. Beam steering has a diverse applications and consists of steering the direction of maximum radiation to maximize the antenna gain in a link with mobile devices. Pattern reconfigurable antennas are usually designed using movable/rotatable structures (31) or including switchable and reactively-loaded parasitic elements (32). In the last 10 years,

metamaterial-based reconfigurable antennas have gained attention due to their small form factor, wide beam steering range and wireless applications (33).

1.3.3 Polarization reconfiguration

Polarization reconfigurable antennas are capable of switching between different polarization modes. The capability of switching between horizontal, vertical and circular polarization can be used to reduce polarization mismatch losses in portable devices. Polarization reconfigurability can be provided by changing the balance between the different modes of a multimode structure (34).

1.3.4 Compound reconfiguration

Compound reconfiguration is the capability of simultaneously tuning several antenna parameters, for instance, frequency and radiation pattern. The most common application of compound reconfiguration is the combination of frequency agility and beam-scanning to provide improved spectral efficiencies. Compound reconfigurability is achieved by combining in the same structure different single-parameter reconfiguration techniques or by reshaping a pixel surface (35) dynamically.

In this thesis, we design different radiation reconfigurable antennas to be used in direction finding and satellite communication systems (14; 9; 15; 25; 36).

Part I

Reconfigurable Antennas

CHAPTER 2

PARALLEL PLATE WAVEGUIDE ANTENNA LENS

2.1 Literature review of the lens antenna

Lenses are well-known structures used for modifying the shape of a wavefront by introducing an engineered delay in the path of the wave. For dielectric lenses, the lens' shape, as well as its dielectric constant, can be controlled to provide the desired wavefront. In most microwave applications, the primary purpose of using a lens structure is to increase the gain of the antenna by transforming a spherical wavefront to a plane wavefront (38).

Making a multibeam antenna system is another application, where a lens structure can become very useful. Multibeam ultra-wideband antennas, with selective directional beams, high gain and low grating lobes, are useful to many communication and radar systems including automotive radars (5). Pencil beams as well as fan beams can be created using lens structures, where fan beams are more suitable for some Doppler radars as well as direction finding systems (39). The Luneburg lens is one of the most well-known dielectric lenses used in microwave lens antennas to create multibeam patterns. This lens has a spherical shape with a gradual variation of its relative permittivity from 2 at its core to 1 on its surface. By placing several feeds around the lens, a high-gain multibeam antenna with independent beams is created (see Fig .2). High costs, bulkiness, and manufacturing problems are the

main drawbacks of the Luneburg lens (40; 41). In contrast, the Rotman lens has low cost and it can be made ultra-wideband (14); however, it gets very lossy due to the sidewall reflections (42)(see Fig. 14).

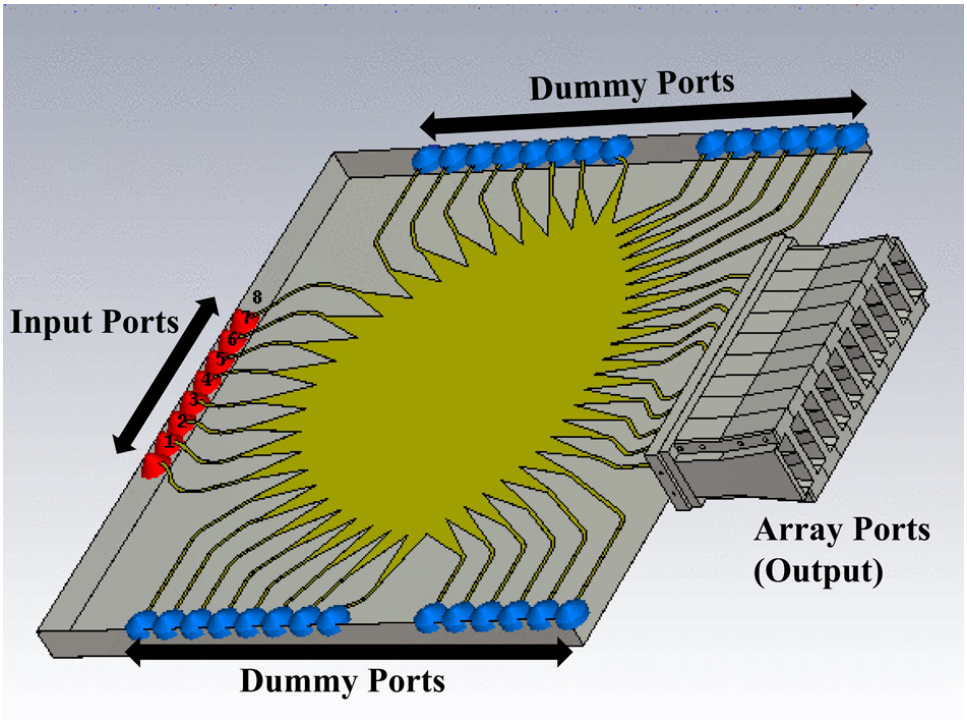

Figure 1: Top view of the microstrip Rotman lens.

Several variations of Luneburg lenses with fan-beam scanning capability have been designed by using parallel plate techniques (43). In these techniques, one is interested in the propagation of the TE_{10} mode of a parallel plate waveguide parallel plate waveguide therefore a cylindrical Luneburg lens is designed by varying the plate spacing so that the resulting index of refraction mimics the Luneburg lens

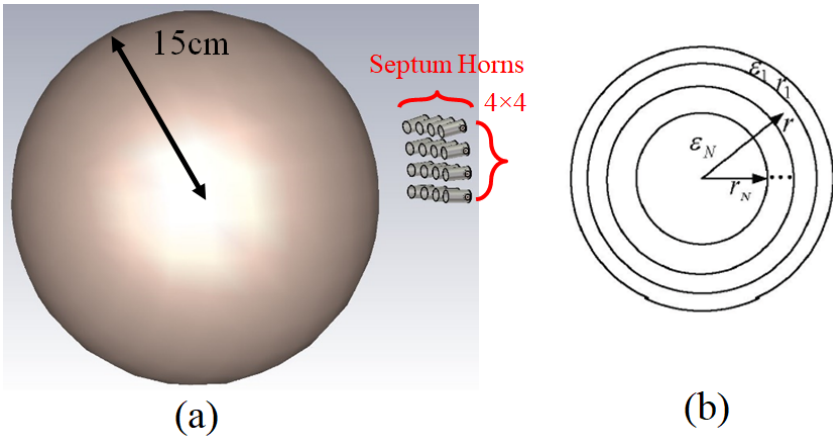

Figure 2: (a) 40 GHz multilayer 15 cm Luneburg lens antenna excited by 16 septum horn antennas, (b) inside view of the multilayer spherical luneburg lens with different dielectric relative permittivities.

law (44). Typically, a planar linear tapered slot antenna requires an antenna feed at the focal point of the lens.

2.2 Lens system design

2.2.1 Proposed parallel waveguide lens antenna

We are also going to adopt a parallel plate structure with a ”Luneburg inspired” cylindrical lens, but with two main differences: (1) instead of having an index of refraction that varies with the radial distance from the axis of the cylindrical lens, we consider a material with a uniform dielectric constant whose value is optimized to maximize gain performance while simplifying manufacturing process; (2) the replacement of the antenna feed with a coaxial connector pin to reduce the overall size and increase the bandwidth compared to (44).

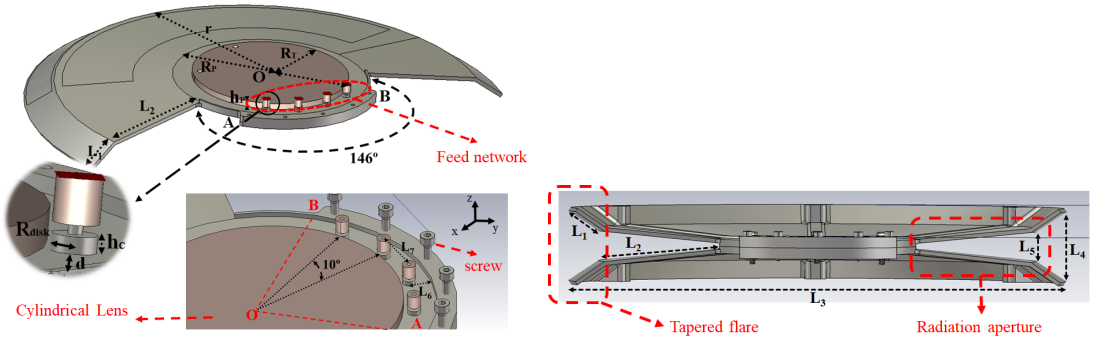

(a) (b)

Figure 3: The multibeam ultra-wideband antenna made of three main parts: (a) the feed structure consisting of 4 coaxial cable connectors, and the ”Luneburg inspired” cylindrical lens. (b) A view of the inside parts of the proposed antenna (radiation aperture). The dimensions are given in Table I.

As it is shown in Fig. 3, the structure is fed by a simple coaxial cable, which creates a cylindrical wavefront, that passes through a parallel plate waveguide filled with a single slab of dielectric with a permittivity of 2.1 (Teflon). The dielectric plays the role of a lens and modifies the cylindrical wavefront to create a planar wavefront at its output, which is shown in Fig. 4. This planar wavefront is then guided towards the aperture of the antenna, and due to the uniform phase distribution on the planar wavefront, a directive fan beam is created. The beam steering is simply done by exciting the corresponding input. The main advantage of the proposed structure is its simplicity, where a single slab dielectric is used as the lens structure with no need to use a layered dielectric structure and no geometrical modifications or are necessary to be applied to the parallel plate waveguide. Moreover, no sophisticated design for the feed antenna is necessary, since a simple coaxial feed is used. Most importantly, the proposed structure

TABLE I: Dimensions of the lens antenna (mm)

Parameter	L_1	L_2	L_3	L_4	L_5	L_6	L_7	
Dimension	17.5	60	248	35	15	5.15	16.7	
Parameter	d	h_p	h_c	h_L	R_p	R_T	R_{Post}	r
Dimension	1	3	1.5	2.5	50	40	1	122

is capable of handling high power, since no microstrip antenna is used as the feed and it is only limited by the breakdown voltage of the dielectric and the power handling capability of the connectors. The designed antenna system scans 40° in the azimuth plane using 4 distinct beams which overlap by 3 dB with adjacent beams at 18 GHz and 1.5 dB at 8 GHz. The 3 dB radiation pattern beamwidth in the azimuth plane is 9.1° at 18 GHz and 19.7° at 6 GHz. The structure has a fan beam radiation pattern where the 3 dB beamwidth radiation pattern in the elevation plane varies from 30° at 18 GHz to 60° at 8 GHz. Such an antenna with steering capability can be widely used in radars, direction finding systems (45; 46; 16; 47; 48). Preliminary results were provided in (16), and they have been expanded by providing more explanations and including additional simulations and measurement results. All parts of the system are simulated with CST Microwave Studio software (49). As can be seen in Fig. 3, the proposed system consists of three main parts: the feed, the cylindrical lens, and the radiation aperture. The excited cylindrical wavefront, created by coaxial feeds, is guided towards the lens and modified to generate a plane wavefront at its output, where this plane wavefront is guided towards the radiation aperture. We are going to give a step by step discussion of each part.

2.2.1.1 Lens design

The proposed cylindrical lens sandwiched between two parallel conducting plates is illustrated in Fig. 3. The lens, which is made out of a low-cost Polytetrafluoroethylene (PTFE) Teflon material ($\varepsilon_r = 2.1$ and $\tan\delta = 0.0002$), has a cylindrical cross-section to give the desired step-variation of the index of refraction. The cylindrical cross-section is easy to fabricate and flexible enough to obtain the desired performance. The lens is fed by four SMA connectors placed at an appropriate distance away from the edge of the cylindrical lens to obtain better matching with the lens. This distance increases the degrees of freedom to optimize the lens' return loss value.

The mode of propagation in the proposed parallel plate waveguide is determined by the direction of the electric field due to the connector pin. Referring to Fig. 3, there is a sectional parallel plate waveguide defined by the 4 feed pins and the center of the cylindrical lens (see the region limited by OAB). Within this region, waves travel along the radial direction with the equiphase surfaces represented by curved surfaces of constant radius. In the previous work (44), the TE_{10} mode is the dominant mode because the excitation ports are miniaturized microstrip antennas and microstrip antennas excite TE_{10} modes inside a waveguide. However, in this paper, connector pins excite the E_z field component in the waveguide. Therefore, the radial variations of this field are represented by Hankel functions, and in the sectional-plate geometry the propagation mode is TEM^{ρ} with E_z and H_ϕ components (50).

In Fig. 4, the transformations of a cylindrical wavefront to a planar one for different permittivity values are compared. One can observe that when the permittivity is lower (for $\varepsilon_r = 1.5$) the shape of the wavefront is convex. Then, by increasing the permittivity one obtains a sufficiently flat wavefront (for $\varepsilon_r = 2.1$). Further increases of the permittivity cause the wavefront to become concave (for $\varepsilon_r = 4$) and,

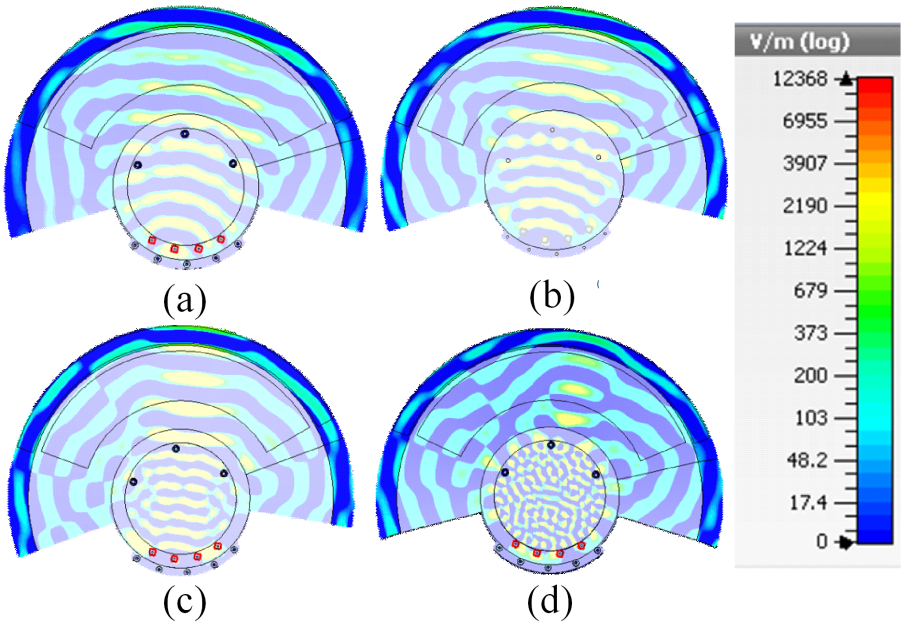

Figure 4: Simulation results are showing the magnitude of the electric field of the propagating wave for lenses with different permittivities at 13 GHz. (a) $\varepsilon_r = 1.5$; (b) $\varepsilon_r = 2.1$; (c) $\varepsilon_r = 4$; and, (d) $\varepsilon_r = 10$.

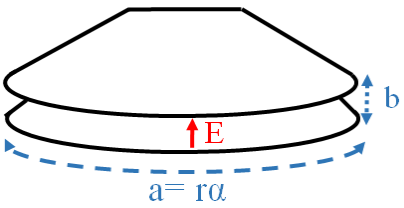

Figure 5: Parameter definitions for a narrow horn antenna to determine the radiation beamwidths.

finally, even larger values of the permittivity cause the wavefront to differ significantly from the desired planar wavefront.

As the permittivity increases a smaller disk is needed to create a planar wavefront. However, when the wave is launched from the excitation ports, a portion of the wave leaks from the sides of the lens (assuming all the other dimensions are kept fixed), hence the sidelobe level (SLL) will increase. Therefore, there should be a compromise between the size of the system, the SLL, and the gain. As it turns out, the relative permittivity of 2.1 is the optimal value that results in dimensions compatible with our design requirements. The planar wavefront is essential for generating a focused beam, which, in turn, depends on the location of the feed. In order to achieve the best illumination, the phase center of the SMA feed connectors must be located at the focal point of the lens and the radius of the lens should be more than $\lambda_g/4$ where λ_g is the wavelength inside the lens at the lower frequency of the design bandwidth (44).

It is interesting to note that in a Luneburg lens antenna designers use a dielectric profile where ε_r varies from the center of the lens to the lens surface. The variation of ε_r is related to the radius of the lens. However, the lens fabrication process is complicated. In this paper we succeeded to obtain excellent result only by using single material (PTFE) with a uniform value of the dielectric permittivity $\varepsilon_r = 2.1$, which makes the fabrication easier compared to other designs based on the use of the Luneburg lens.

2.2.1.2 Aperture design

.

The radiation aperture of the lens is the final step in the antenna system design. A radiation aperture is chosen among different types of the antennas because: (1) it has a wide-bandwidth behavior; (2) it

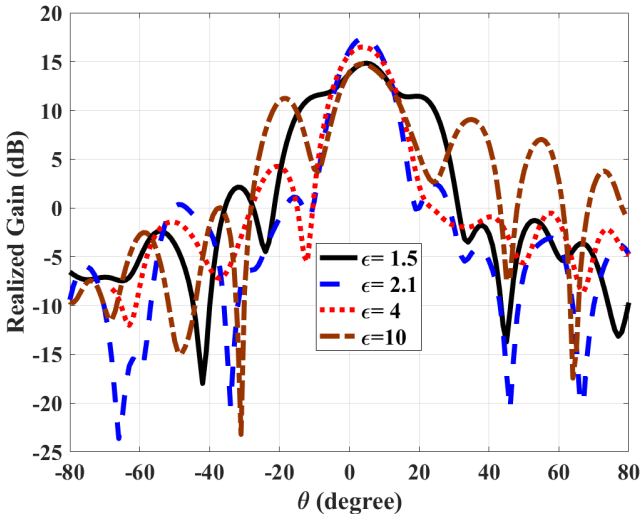

Figure 6: Simulation results of the realized gain at f = 13 GHz for lenses with different permittivities. (a) $\varepsilon = 1.5$; (b) $\varepsilon = 2.1$; (c)$\varepsilon = 4$; and, (d) $\varepsilon = 10$.

.

does not require a matching circuit, such as in the case of microstrip antennas; (3) it can handle higher levels of RF power compared to microstrip antennas because microstrip slot or Vivaldi antenna often are used to feed the cylindrical lens and microstrip antennas due to substrate power handling limitation. In addition, the lens should have a wide fan beam for each excitation port so that a narrow aperture can be used for this structure. Accordingly, we can approximate the radiation aperture as a narrow horn antenna and calculate the initial dimensions of the aperture using the approximate formulas for the azimuth and

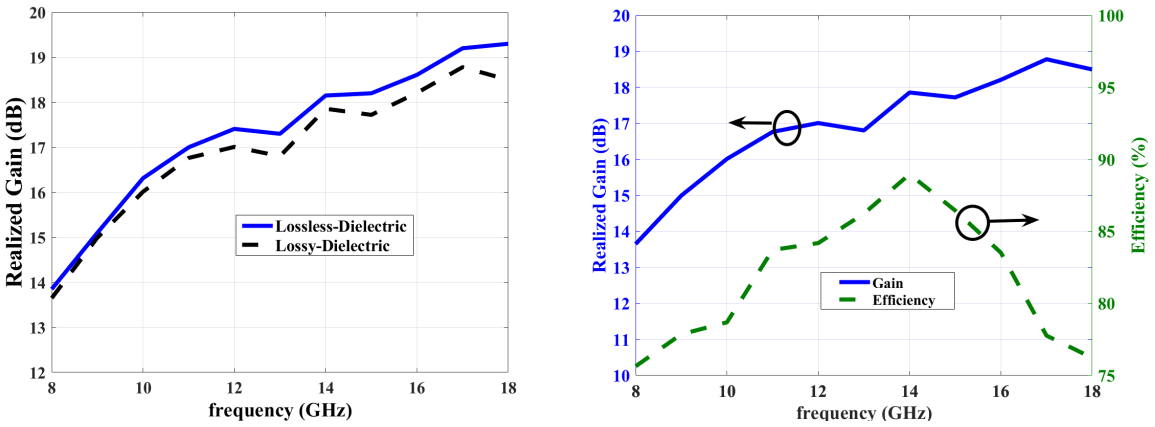

(a) (b)

Figure 7: Simulation results for (a) realized gain for a lossless and lossy dielectric lens. (b) frequency response of the realized gain and radiation efficiency.

elevation plane radiation beamwidth for a narrow horn antenna (51). Referring to Fig. 5, the azimuth and elevation plane radiation beamwidth are

$$\Psi_{3dB}^{El} = \frac{53\lambda}{b}, \Psi_{3dB}^{Az} = \frac{68\lambda}{a} \tag{2.1}$$

where b corresponds to the distance L_5 in Fig. 37b, $a = r\alpha$ is the effective horizontal width for the lens aperture, where $\alpha = 60\pi/180$ and $r = \lambda_g/4$ is the radius of the lens. These expressions provide the initial values for the design parameters in Fig. 3. Then, the final dimensions are obtained using the Particle Swarm Optimization feature of the CST software. Table II reports the optimized values and

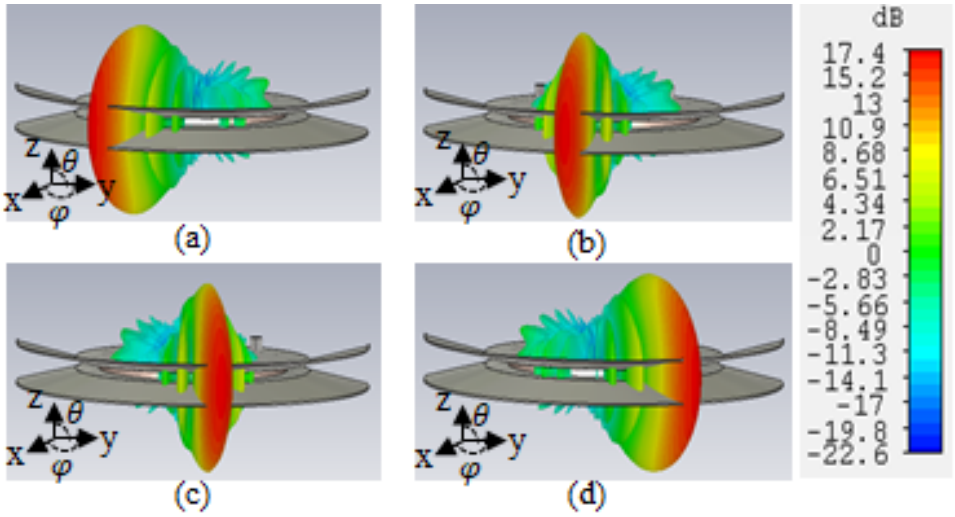

Figure 8: Simulated radiation patterns for excitation of (a) port 1; (b) port 2; (c) port 3; and, (d) port 4.

shows that there is good agreement between the initial approximations obtained with formulas (2.1), and the simulation results for port 1.

Fig. 6 compares the radiation patterns of lenses with different relative permittivities at 13 GHz, because this is the center frequency of operation. Similar to the results shown in Fig. 4, the gain improves going from $\varepsilon_r = 1.5$ to $\varepsilon_r = 2.1$, then it becomes worse for larger values of the relative dielectric permittivity. We also note that $\varepsilon_r = 2.1$ is achieved with Teflon that has low values of $\tan\delta$ at high frequencies (more than 10 GHz). To better understand the effect of dielectric losses, the realized gain of the antenna is simulated versus the frequency in Fig. 7a. While it is clear that there is an advantage at having a dielectric with low $\tan\delta$, the effect of $\tan\delta$ in the realized gain is more significant at higher frequencies by about 1 dB. Fig. 7b shows the realized gain of the antenna and its efficiency. One can observe that

TABLE II: Comparison of the simulation and calculated radiation beamwidth for port 1

Plane	8 GHz	10 GHz	13 GHz	18 GHz
$\phi^{Az}(simulation)$	19.7°	16.6°	15.1°	9.1°
$\phi^{Az}(calculation)$	19.95°	16°	12.3°	8.9°
$\theta^{El}(simulation)$	61°	46.5°	37.1°	31.1°
$\theta^{El}(calculation)$	56.7°	45°	35°	25.3°

there is a variation of about 5 dB within the operation bandwidth and that the efficiency is maximum around 14 GHz. Since the behavior of both the gain and the efficiency are not linear with the frequency, this explains the reason for designing the antenna and its feed at the center frequency.

It should also be mentioned that the dispersion, i.e., frequency dependent permittivity, also affects the shape of the wavefront at different frequencies. Therefore, low dispersion and low loss materials are more suitable for lens applications. Since the input ports are placed next to each other, the coupling between them is inevitable. As can be seen in Fig. 8, by exciting each input port, a distinct beam is created in the desired direction.

2.2.1.3 Feed SMA design

Four coaxial connector pins are used to excite the lens because connector pins have the advantage of having small size compared to the use of microstrip antennas and the transition from the coaxial pin to the waveguide has wider bandwidth than a microstrip antenna. Referring to Fig. 3, the four pins are

placed in the air between the dielectric lens and the reflector wall AB. The connector pin and the coaxial probe have an inductive behavior, which limits the whole frequency bandwidth. Hence, this inductive behavior can be compensated by using a capacitive loading. Referring to Fig. 3, the capacitive loading is introduced by adding a disk to the end of the pin, so as to create a capacitance between the floor of the waveguide and the disk itself. The disk acts as an impedance matching section, where the design parameters R_{disk} and h_c can be tuned to achieve the desired matching. The distance L_6 of the connector pin from the cavity wall is initially set to be a quarter wavelength at the central frequency (13 GHz) so that this results in an open circuit seen by the coaxial probe. Moreover, The approximate value of the capacitance introduced by the disk is

$$C = \varepsilon_0 \frac{\pi R_{disk}^2}{d} \tag{2.2}$$

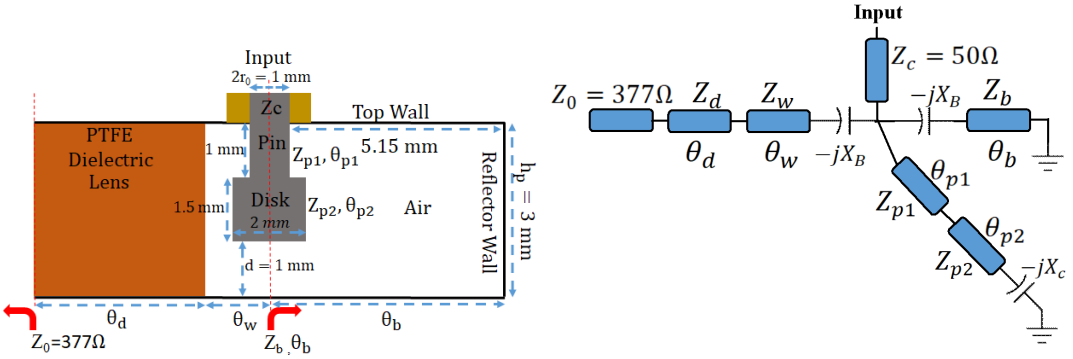

(a) (b)

Figure 9: (a) Schematic of the cross-section of the single probe to waveguide transition ; (b) Approximate transmission line equivalent circuit of the cross-section shown in Fig. 9a

where R_{disk} is defined in Fig. 9a and d is the distance between the disk and the floor of the waveguide (52). The location of the feed and the geometrical parameters that define them were then fine-tuned using CST Microwave Studio software with the goal to maximize the bandwidth and minimize the reflections.

Impedance matching is sensitive to the fabrication especially at a higher frequency (more than 15 GHz), and some dimensions are so important to get desirable results. For instance, the disks attached to the pin, the gap distance between the pins and the reflector, top and wall (see Fig 9a). The reason is that capacitor values to compensate inductive behavior of the pins are directly related to these distances. In order to create a strong coupling between the coaxial probe and the cavity, the distance d is chosen to be very small. To further justify this design, we present in Fig. 9b the cross-section of the overall antenna system and its equivalent transmission line model as it is seen from the feeding port. The elements that appear in Fig. 7b are: Z_d is the characteristic impedance of the transmission

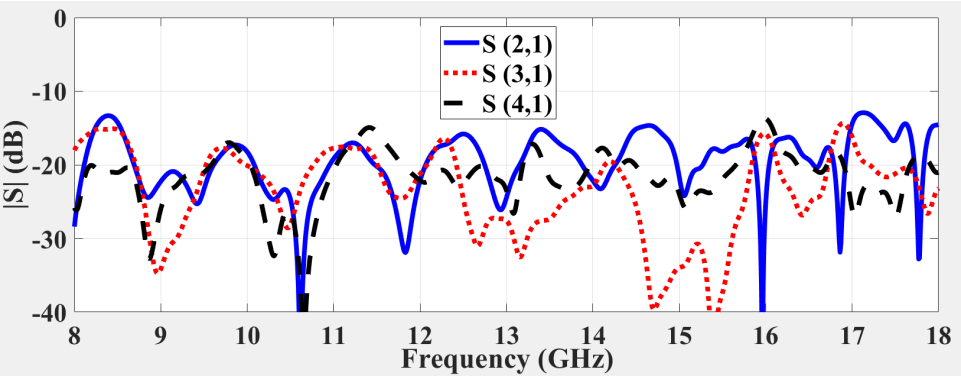

Figure 10: Measurement results showing coupling between the ports.

line representing the dielectric lens (θ_d is its electrical length); Z_w is the characteristic impedance of transmission line representing the free space between the dielectric lens and the disk (θ_w is its electrical length); Z_{p1} is the characteristic impedance of the transmission line representing the connector pin (θ_{p1} is its electrical length); Z_{p2} is the characteristic impedance of the transmission line representing the disk (θ_{p2} is its electrical length); Z_b is the characteristic impedance of the transmission line representing the free space between the pin plus the disk and the reflector wall AB (θ_b is its electrical length).

The stored reactive energy in the proximity of the coaxial pin and the top wall causes a reactive impedance $-jX_B$, with (52)

$$X_B = \frac{f_0 \pi^2 r_0^2}{cL} \tag{2.3}$$

where r_0 is the radius of the coaxial feed and $L = L_7$ is the distance between the coaxial feed connectors, shown in Fig. 9a.

The connector pin impedance Z_p is given by the expression for an unbalanced cylindrical stripline (53; 54)

$$Z_p = \frac{60}{\sqrt{\varepsilon_{\text{eff}}}} \ln \frac{2h}{a} \tag{2.4}$$

where ε_{eff} is the effective dielectric for the coaxial transmission line when the left region (PTFE) is filled with dielectric and the right region (from the connector pin to the reflector wall) is air . The distance between the transmission line and ground is $h = d$ and for Z_{p1}, $a = r_0$ and for Z_{p2}, $a = R_{disk}$ is the radius of the disk. The radial parallel plate waveguide impedance can be easily given by (50)

TABLE III: Measured and simulated gain and beamwidth of port 1 at 4 frequencies

Port 1	**Simulated**			**Measured**		
f	ϕ	θ	Gain (dB)	ϕ	θ	Gain (dB)
8 GHz	19.7°	61°	13.6	20°	61.4°	13.1
10 GHz	16.6°	46.5°	15.9	17°	45.9°	15
13 GHz	15.1°	37.1°	16.8	15.5°	38°	16
18 GHz	9.1°	31.1°	18.5	9.3°	32°	17.5

$$Z_w^{\rho}(TEM^{\rho}) = \frac{E_z}{-H_{\phi}} = \frac{j\beta_{\rho}}{\omega\varepsilon}\frac{H_0^{(2)}(\beta_{\rho}\rho)}{H_1^{(2)}(\beta_{\rho}\rho)} \tag{2.5}$$

here $H_0^{(2)}(\beta_{\rho}\rho)$ and $H_1^{(2)}(\beta_{\rho}\rho)$ are the second kinds Hankel functions , ρ is the radius in the cylindrical coordinate system and β_{ρ} is the propagation constant in the $\hat{\rho}$ direction given by

$$\beta_{\rho} = \sqrt{\beta^2 - \beta_z^2} = \sqrt{\omega^2\varepsilon_r\varepsilon_0\mu_0 - 0} = \omega\sqrt{\varepsilon_r\varepsilon_0\mu_0} \tag{2.6}$$

The above formulas provide a good initial approximation for the design. Then full wave CST Microwave Studio software and particle swarm optimization, determine the dimensions given in Table I.

2.3 Parallel lens fabrication and measurement

In this section, radiation pattern measurements, as well as S-parameter measurements are discussed for the fabricated antenna. The measured mutual couplings between the ports are shown in Fig. 10. The measured VSWR of all ports are shown in Fig. 11. As can be seen the bandwidth for VSWR$<$3 is 10 GHz. At each measurement step, one of the input ports is excited, and all the other ports are terminated to a matched load. The coupling between ports is less than 12 dB throughout the frequency band of operation. Due to the structure symmetry, other ports have the same coupling. Table III compares the results of the simulations and measurements for beamwidth and gain at different frequencies, which show a good agreement between simulations and measurements. The overlap between neighboring radiation patterns is also shown in Fig. 12.

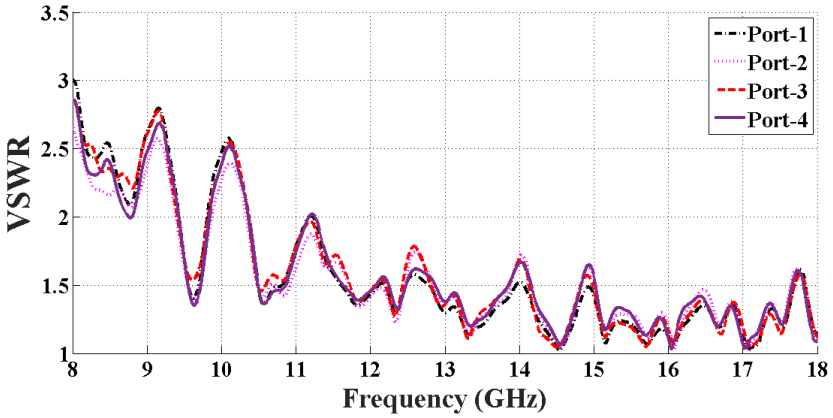

Figure 11: Measured VSWR of the antenna.

2.4 Conclusion

A compact ultra-wideband multibeam microwave lens antenna for operation in the frequency range from 8 GHz to 18 GHz has been proposed. A parallel plate waveguide structure with 4 input ports with a dielectric lens to manipulate the wavefront and a linearly tapered radiation aperture has been designed an optimized using particle swarm optimization to achieve minimum return loss and desired radiation pattern over the frequency band of operation. Four distinct radiation beams can be generated by the proposed structure, which covers a scan angle of 40° in the azimuth plane. The beamwidth in the elevation plane is about 30°. The main advantage of the proposed structure lies in its simple design and high power handling capability. This design can be easily modified by, for example, increasing the number of connectors to obtain more beams with an overall higher gain value. For the excitation, a simple coax input is used without any need for complicated antennas such as linear tapered slot line. A single dielectric slab is used to manipulate the curvature of the wavefront and obtain a planar wavefront, without any need for multilayer dielectric structures such as Luneburg lens. The manipulated wavefront is then guided towards a radiation aperture resembling a parallel plate horn antenna. This antenna has been comprehensively simulated and optimized and the final design has been fabricated and measured. A good agreement between measurements and simulations has been achieved.

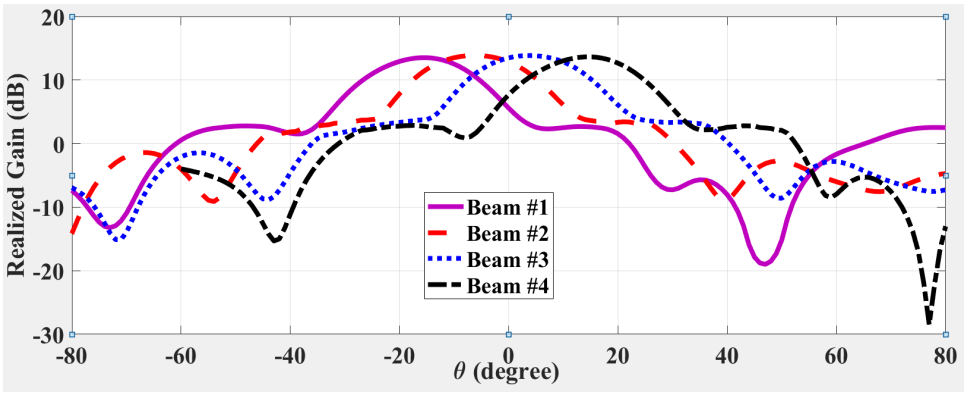

(a)

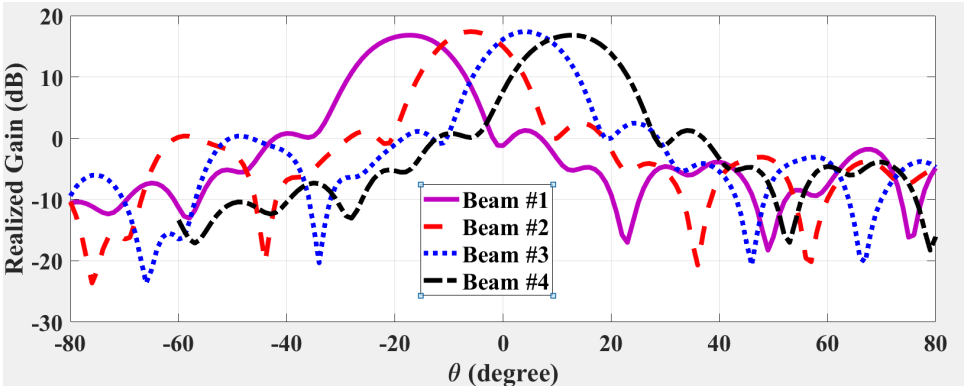

(b)

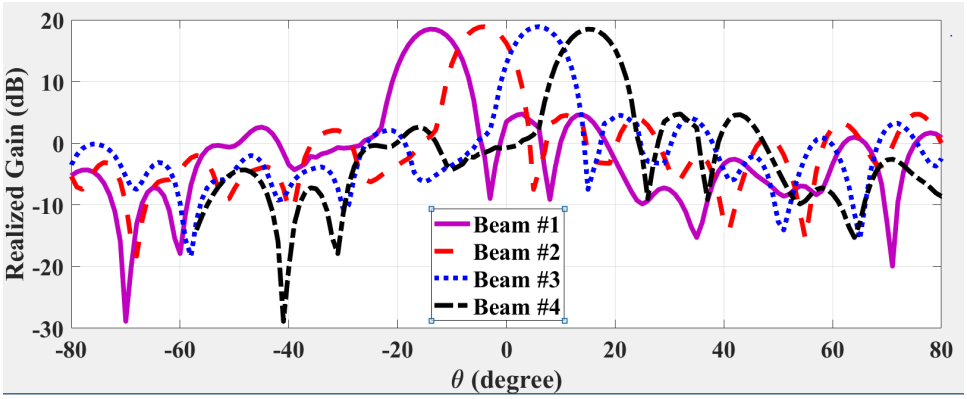

(c)

Figure 12: Measured radiation gains of the antenna at (a) 8 GHz; (b); 13 GHz (c) and 18 GHz.

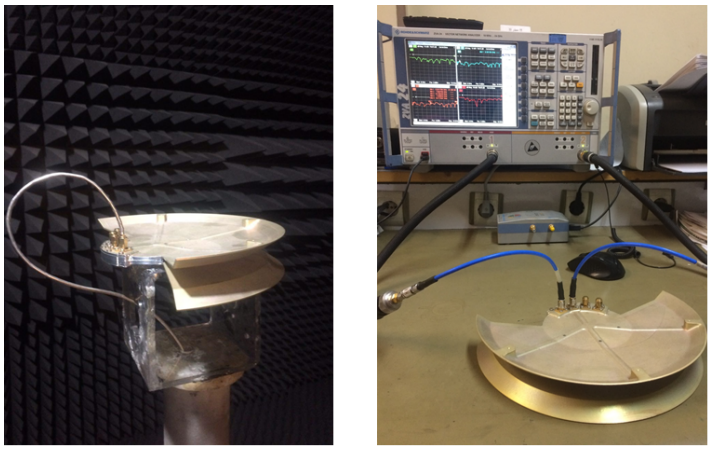

(a) (b)

Figure 13: Measurement setup in Amirkabir University of Technology (a) antenna in anechoic chamber (b) S-parameter measurements by a network analyzer ZNB40.

CHAPTER 3

MICROSTRIP ROTMAN LENS ANTENNA DESIGN

3.1 Ultra-wideband scanning antenna literature review

An increased interest in low profile ultra-wideband (UWB) scanning antenna array with high gain, low grating lobe and large scan area for applications such as ground-based and airborne communication, bio-medical imagining, automotive anti-collision radars and electronic warfare, has been recently observed. For most of these applications, beam steering is highly desired. Various methods have already been developed to increase the coverage of broadband multibeam systems. The most popular beam-steering methods are phased array antenna based on phase shifters, Butler matrix, Luneburg lens and Rotman lens. The effectiveness of phase shifters at high frequencies may be limited due to excessive front-end loss and added system complexity. The advantages of a Butler matrix are the simplicity of construction and implementation, however; it requires crossovers on the lines. The Rotman lens has the advantages of lightweight, wideband, PCB fabrication, wide scanning array and true-time-delay (TTD) meaning that it contains a constant time delay over a broadband frequency range. The Rotman lens acts as a beam forming network (BFN) for phased array antenna in which by exciting each of the input ports, an appropriate wavefront travels to create the needed time delay across the array antenna and consequently the desired phase distribution over the antenna will be created. The question is that why have we chosen a Rotman lens antenna instead of a Luneburg lens? The Luneburg lens is a spherical lens

designed to have a gradual variation of permittivity from 2 at the core of the lens, to 1 on its surface. By placing several feeds around the lens, it is possible to create a high-gain multibeam antenna with several beams working independently of each other. The main drawbacks of the Luneburg lens are high costs, construction problems, and bulk. In contrast, the Rotman lens has the advantages of being low cost and wideband; however, it shows significant losses due to the sidewalls reflections.

The schematic of the proposed phased array antenna system, consisting of a Rotman Lens as Beam Forming Network (BFN) and 10 double-ridged horn antenna as a radiating element is indicated in Fig. 14. We could increase number of the horn antennas, but based on the antenna array theorem, 10 double-ridged horn antennas are enough to obtain more than 14 dBi antenna gain (55). As indicated in the Figure, the Rotman lens consists of three main parts, the input ports, the output ports connected to the phased array radiating elements and dummy-ports, which are designed to reduce the reflection from the sidewalls of the Rotman lens. The number of input ports determines the number of beams produced with the lens (scanning steps) and the number of output ports is determined by the desired gain and half-power beamwidth (HPBW) of the array. Since the antenna may be used for high power applications, the double-ridged horn antenna is used as a radiating element because has better power handling in comparison to a microstrip antenna. Moreover, using ridges in horn antenna causes the impedance of the antenna to be matched gradually to the impedance of the free space, which makes the antenna more wideband compared to conventional horn antennas. An end-launched coaxial to double ridged waveguide transition is designed in order to connect the output ports of the microstrip lens to double-ridged E-plane horn radiating element.

The designed antenna system scans 56° of space by 8 distinct beams which have 1 dB overlapping level of adjacent beams at 6 GHz and 3 dB overlapping level of adjacent beams at 18 GHz. Its 3 dB beamwidth radiation pattern is 20° at 6 GHz and 7° at 18 GHz. The return loss of the structure consisting of the Rotman lens BFN, end launched coaxial to double ridged waveguide transition and the antenna is below -10 dB in the whole frequency band from 6 GHz to 18 GHz.

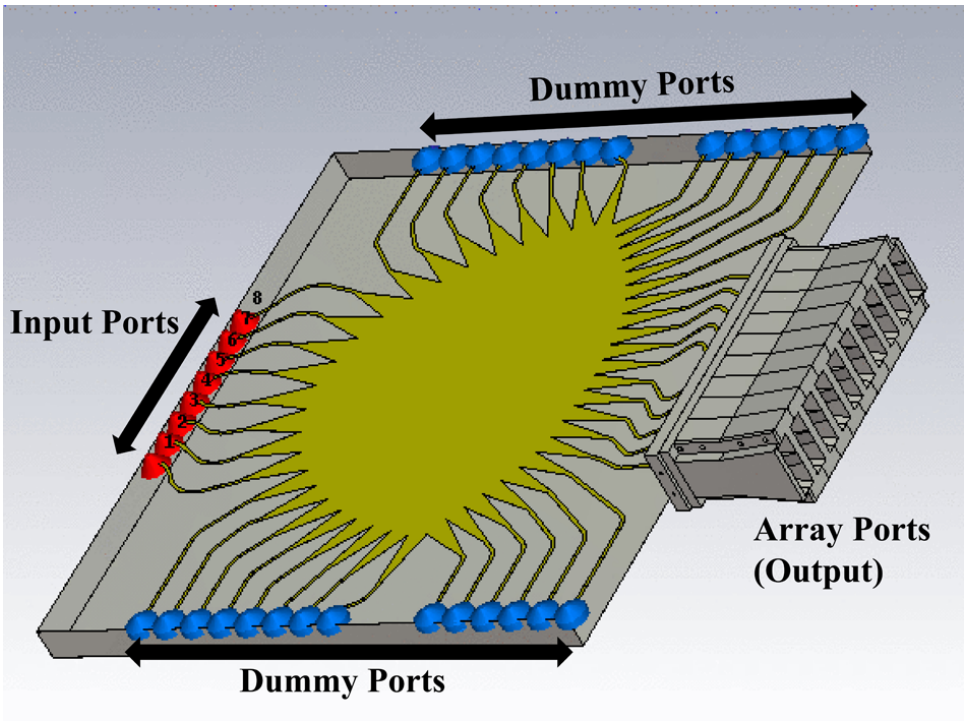

Figure 14: Top view of the microstrip Rotman lens with a ten-element array of E-plane double-ridged horn antenna.

In order to minimize the radiation lobe in the grating lobe in scanning antenna the distance between adjacent radiating elements should meet the following condition (56)

$$d < \frac{\lambda_{min}}{1 + |sin\theta_{max}|} \tag{3.1}$$

where λ_{min} is the minimum wavelength and θ_{max} is the maximum scanning angle. It should be noticed that decreasing the distance between adjacent elements will decrease the directivity of the proposed array as well, so there is a trade off between the directivity and grating lobe appearance. The proposed antenna array consists of three parts; i) the Rotman lens as a beam forming network, ii) the double ridged horn antennas as radiating elements and iii) the end launched coaxial to double ridged antenna transition in order to connect the lens to the array.

3.2 Rotman lens

Fig. 15 shows the configuration and design parameter of the Rotman lens. The input ports are located on geometrical beam contours, and the output ports are located on the receiver contour. These ports are connected to the lens structure by the microstrip trace lines that are tapered in order to minimize the reflection coefficient. The conventional Rotman lens consists of three focal points for which the phase-error is theoretically zero. However, in practical applications, more than three ports are needed. Please note that, the number of input ports (called beam ports) determines the steps of scanning, and the number of output ports is determined by the desired gain (57). In the conventional Rotman lens the receiver and beam contours are supposed to be circular. In this project, however, we do not limit our design to a selected number of focal points (beam ports), where they generate no phase error. Instead, the lens is designed to achieve a minimum average phase-error for all the ports rather than achieving no errors for

a limited number of beam ports. To overcome the problem of generated phase error, we propose a lens structure in which the locations of both beam ports on the beam contour and the array ports on the inner receiver contour are optimized.

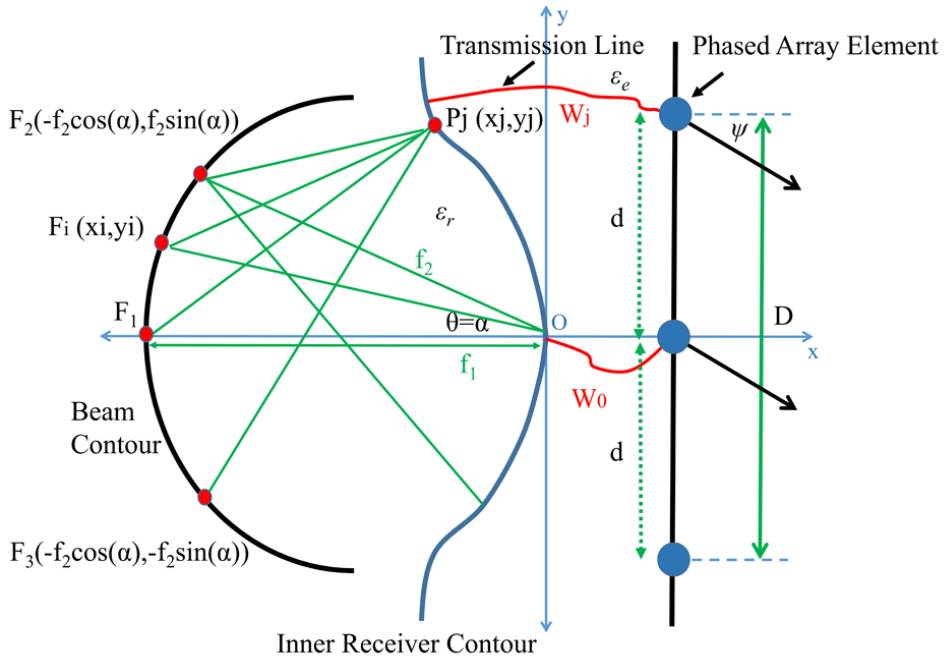

Figure 15: Configuration of the Rotman lens and design parameters.

According to the phase error relation reported in (58), the cost function can be defined as:

$$o = \sum_{i=1}^{N} \sum_{j=1}^{M} |L_2 - L_1| \tag{3.2}$$

where N and M are the number of beam and array ports on the respective contours. L_1 and L_2 are electrical path length from the i-th beam port to the central phase array element on the x-axis; (see Fig. 15) and from i-th beam port to j-th phase array element.

$$L_1 = F_i O\sqrt{\varepsilon_r} + W_0\sqrt{\varepsilon_e} \tag{3.3}$$

$$L_2 = F_i P_j\sqrt{\varepsilon_r} + W_j\sqrt{\varepsilon_e} + d\sin\psi_a \tag{3.4}$$

where F_i and P_j are the position of i-th beam port on the beam contour and the position of j-th array port on the inner receiver contour, respectively. O is the center coordination of the inner receiver contour that is the reference point of the lens topology in Fig. 15. W_0 is the electrical length of the transmission line that connects O to the central phased array element, and W_j is the electrical length of the transmission line that connects j-th array port on the inner receiver contour to the corresponding radiating element ε_r and ε_e are the permittivity constants of the Rotman lens and the transmission lines,respectively. In addition, d is the distance between the phase array radiating elements, and ψ_a is the maximum scanning angle. We utilize the GA toolbox in MATLAB software to optimize F_i, for i = 1,2,3, . . . ,8 and P_j, for j = 1,2, . . . ,10.

3.3 Radiating element with transition

The configuration of the double ridged antenna can be seen in Fig. 16. A horn antenna is typically fed by an SMA connector attached to its side wall, however in this project in order to satisfy the required spacing between adjacent radiating elements we have devised a way for feeding antennas from the

waveguide cross section, which enables a direct connection between the output of the Rotman lens and the E-plane double-ridged horn antenna. For this purpose, a novel end-launched coaxial to double-ridged transition has been developed. As indicated in Fig. 17, the transition consists of a mode converter in order to convert the coaxial TEM-mode to TE-mode of the horn antenna. The rest of the adaptor provides the impedance matching.

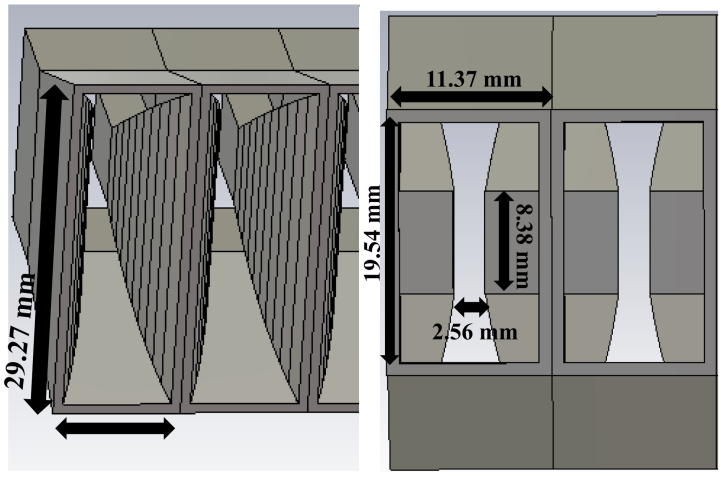

(a) (b)

Figure 16: (a) Front view of the E-plane double-ridged horn antenna. (b) Back view of the E-plane double-ridged horn antenna.

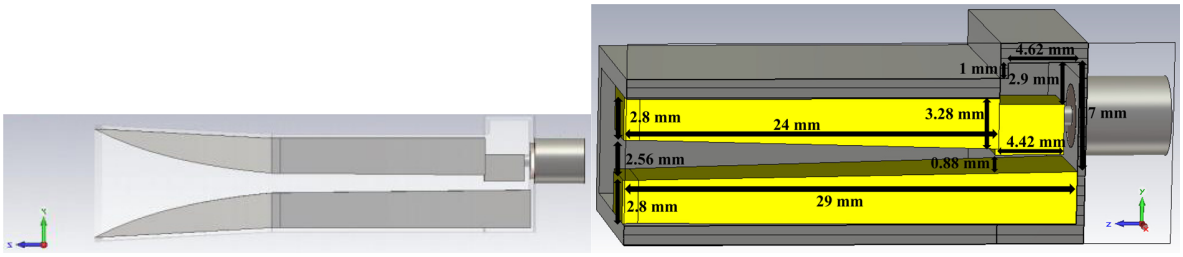

(a) (b)

Figure 17: (a) Side View of the horn antenna with the end-launched coaxial to double-ridged waveguide transition. (b) Dimensions of the end-launched transition.

3.4 Fabrication and measurement

The designed antenna array element together with the Rotman lens beam forming network is fabricated and tested. Fig. 18 shows the fabricated phased array system.

At each measurement, one of the input ports is excited, and all other ports terminated to a matched load. Since the system is symmetric, only four of the input ports are tested. The return loss of the whole system is depicted in Fig. 19. As it can be seen, the return loss of the whole structure is below -10 dB in the whole frequency range from 6 GHz to 18 GHz.

The measured array pattern of the antenna array system at a different frequency bands is depicted in Fig. 20 By exciting each of the input ports, a distinct beam is created in the desired direction. Due to the design spacing between the elements, there are no grating lobes at all, when the first port is excited. Grating lobes just occur at the frequency of 18 GHz for patterns with a scanning angle of 20° and larger, and these grating lobes are out of the field of the view of the array.

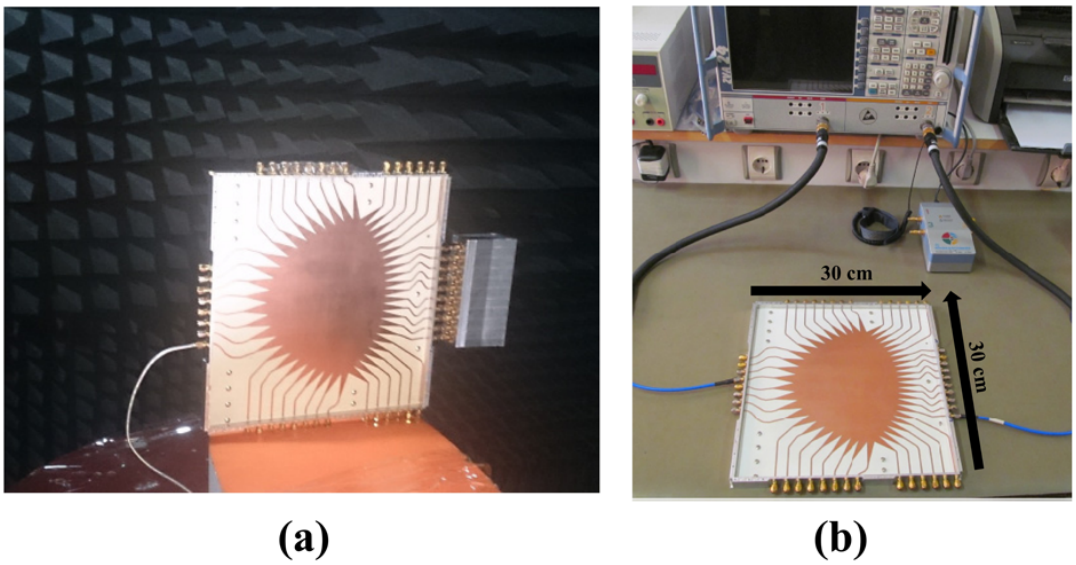

Figure 18: Measurement setup. (a) Lens and array in anechoic chamber. (b) Return loss measurement by the network analyzer.

A Rotman lens is called a true-time-delay (TTD) device meaning that it maintains a constant time delay over a broadband frequency range of operation. In order to verify the true time-delay behavior of the Rotman lens, Fig 21, shows the radiation pattern for different frequencies versus the angle. As it can be seen, the location of the power peak remains almost unchanged as we scan the frequency, which shows that the proposed lens is true time-delay and has a very small phase-error.

3.5 Conclusion

In this work an ultra-wideband phased array system with a total scanning angle of 56° in the frequency range from 6 GHz to 18 GHz has been proposed. A microstrip Rotman lens with 8 input ports and 10 output ports has been designed, optimized and fabricated to achieve a minimum phase-error.

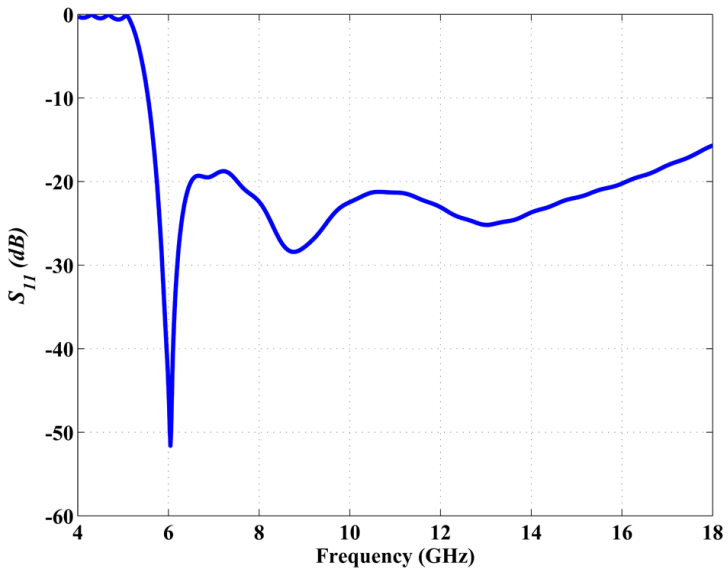

Figure 19: Return loss of the antenna with the end-launcher coaxial to waveguide transition.

Considering properties such as power handling capability, high bandwidth and small inter-element spacing, an E-plane double-ridged horn antenna is designed as the radiating element. Due to the small inter-element spacing it is required to feed the horn antenna from the waveguide cross section. Therefore, an optimized wide-band end-launcher coaxial to waveguide adapter has also been designed. This phased array system has been comprehensively simulated, optimized, fabricated and measured. A very good agreement between the measured and simulated results has been achieved.

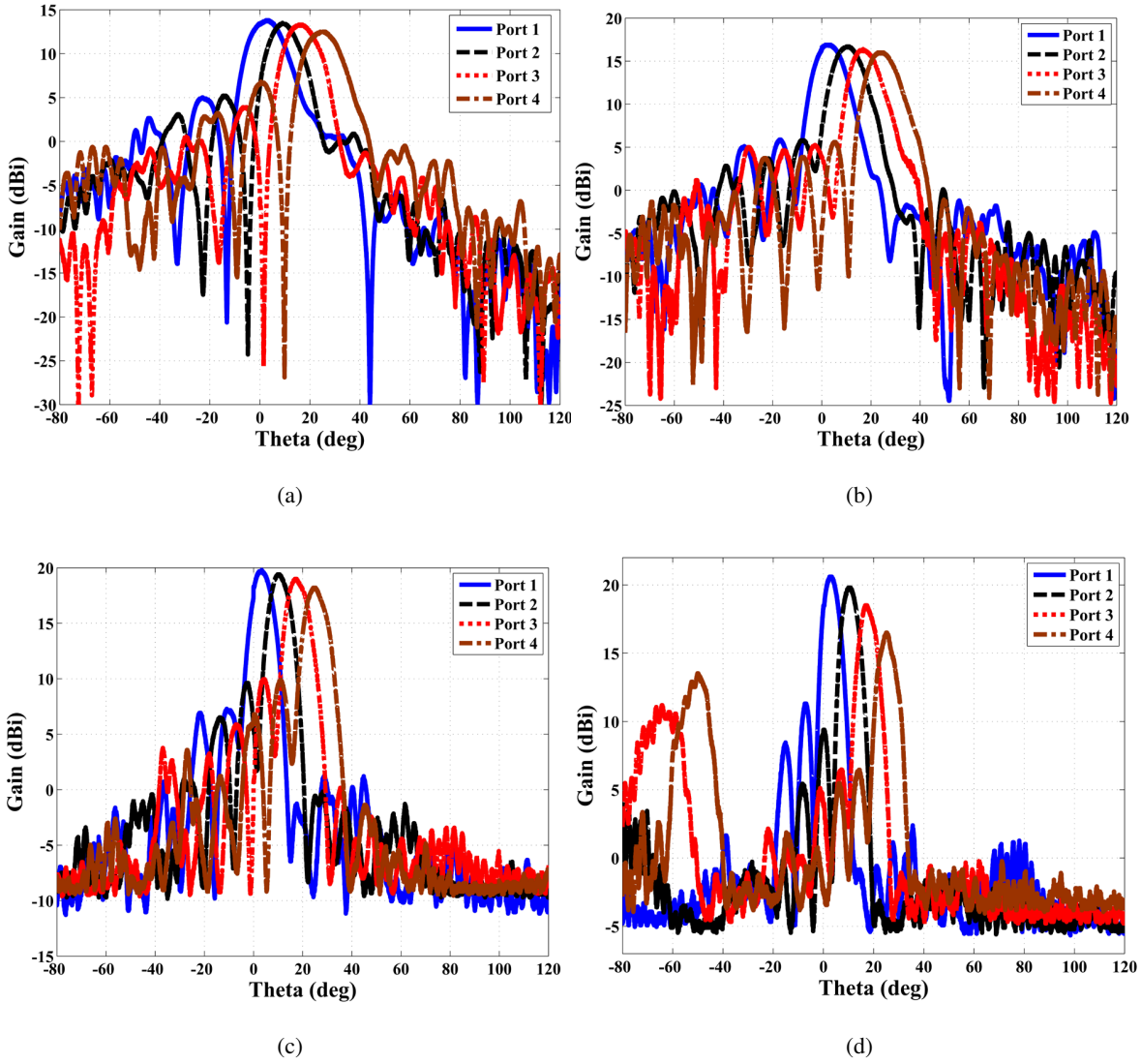

Figure 20: Measured patterns generated by exciting all four ports at (a) 6 GHz, (b) 10 GHz, (c) 14 GHz. and (d) 18 GHz.

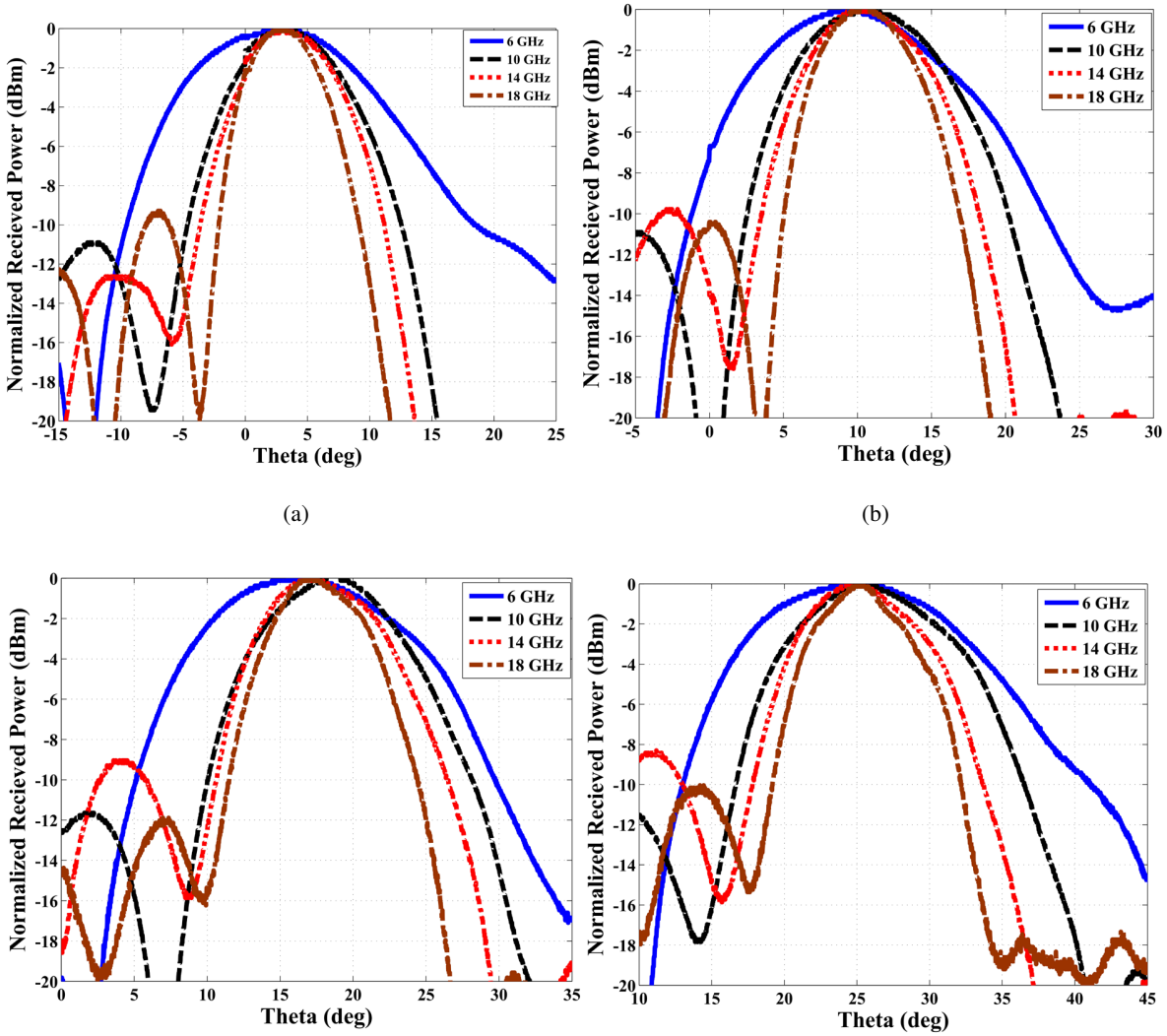

Figure 21: Verification of the true time-delay property of the designed lens. The location of the peaks remains almost unchanged by exciting the (a) first port, (b) second port, (c) third port, and (d) fourth port.

CHAPTER 4

RECONFIGURABLE REFLECTOR ANTENNA DESIGN

4.1 Literature review of multi-beam antennas

Phased array fed single reflector is another candidate for high gain multiband satellite antennas and direction finding systems (2).

In this method, the feed array has a uniform or tapered amplitude distribution and a slowly varying phase distribution, and a reflector (or a sub-reflector in a dual reflector antenna) is partially illuminated by the array. Each antenna beam is formed by appropriate phase distribution over the whole feed array. These beams cannot excite the whole reflector surface. Therefore, the aperture efficiency of the reflector will be reduced (60). They also suffer from the disadvantages of increased mass compared to singly fed shaped reflector, and the BFN also gives rise to loss (3). A multifocal antenna is an extended concept of a bi-focal antenna (61). This is achieved by placing several primary sources in the focal plane and then by switching them alternatively. However, this leads to the fact that the sources are no longer at the reflector focus, and consequently, the efficiency of reflector would decrease, and the side lobe level would increase (62). A multifocal paraboloidal reflector provides a homogeneous pattern in different beam directions, but its aperture efficiency is poor. The efficiency drastically drops when the number of foci increases, because the design flexibility of the foci arrangement is inadequate (63). In this chapter,

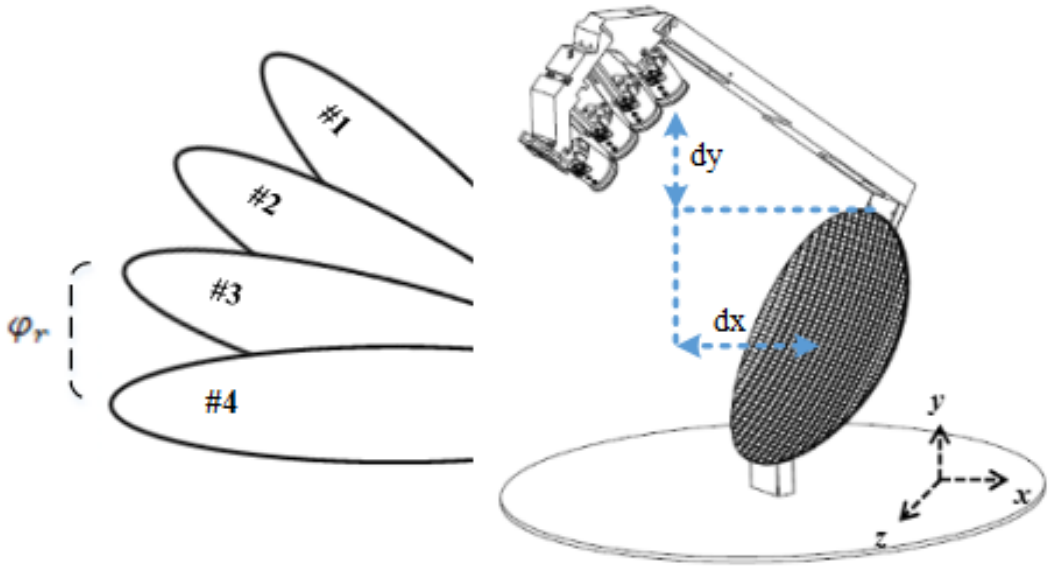

Figure 22: Paraboloidal offset reflector, feeds and desired beams

a new method for designing a multi-feed multi-beam parabolic reflector is presented. The new design method controls the arrangement of the feed positions in order to increase the efficiency and gain of the whole structure. The advantage of this method from other ones is that this is much simpler and has more efficiency than previous solving and optimization methods such as genetic optimization or invasive weed optimization (64)-(65). Moreover, in previous methods, only the maximum efficiency has been defined for one feed, and other feeds have not been optimized to achieve maximum efficiency. But in this method, all feeds have been optimized for achieving maximum efficiency simultaneously. To validate the proposed method, a reflector with four feeds is considered. The positions of offset feeds are optimized by means of genetic algorithm optimization method with HFSS software to obtain high

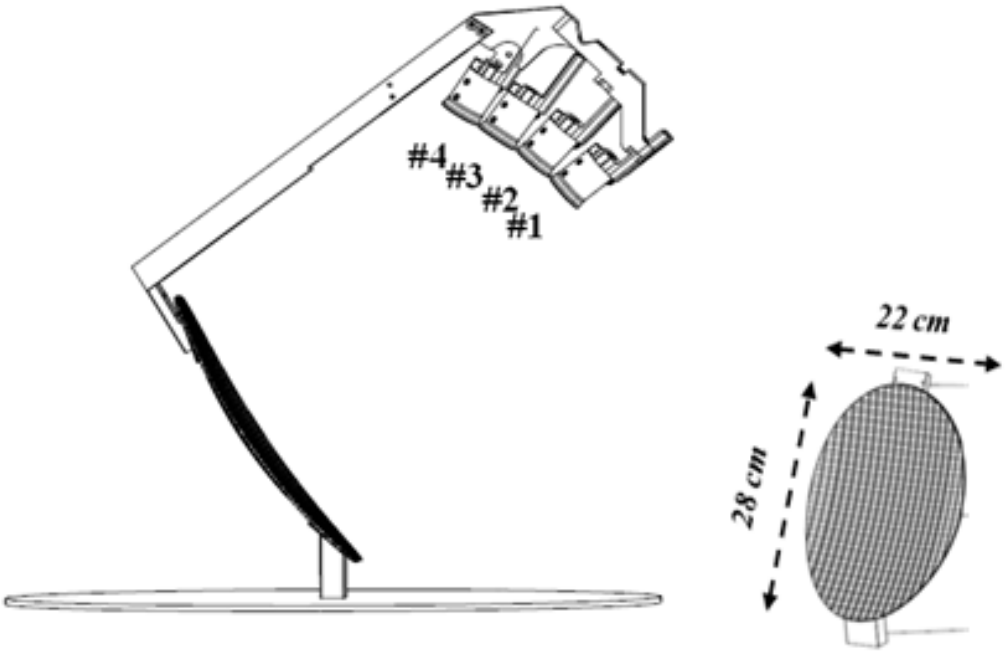

Figure 23: The basic configuration of the reflector antenna with its feeds

gain and efficiency simultaneously. The results have a good comparison with the genetic algorithm optimization method. This structure is consisting of four distinct beams in order to coverage 6 degree of the azimuth plane and 30 degree of the elevation one with a nominal gain of more than 27 dBi. The maximum gain of the antenna is 29.6 dB at 18 GHz, and the minimum efficiency of the antenna is more than 51%.

4.2 Design Principle

The design of a multiple-beam antenna depends on the beam size related to the minimum-coverage-area requirement. A multi-beam reflector system is composed of a paraboloidal main reflector and

multiple feeds as indicated in Fig22. In this chapter,a three step procedure for designing high performance multiband offset reflector is presented. In the first step, according to the coverage area and the 3 dB beam width of each beam, positions of feeds are obtained. Then, according to the beam positions , the angle of rotation for different beams in elevation plane φ_r are then obtained as indicated in Fig22. In the next step, according to the desired gain and 3 dB beam width for each beam, we can design an offset reflector, with an appropriate diameter D, focal length F, offset height H and angle subtended in the bisection direction Ψ_{B2}. The procedure for designing one feed offset reflector is mentioned in (66). After designing the appropriate one feed offset reflector and according to angular rotation obtained in the first step can be calculated as below:

$$\Psi_{B2} = \Psi_{B1} + \varphi_r \tag{4.1}$$

According to Ψ_{B2} and equations for designing offset reflector a new reflector with the same D but different focal length and offset height can be designed. The same procedure can be applied for the other beams. First, find F_3 and H_3. Second, repeat that for the next n beams. According to (F_1,H_1), ($F_{\frac{n}{2}+1}$,$H_{\frac{n}{2}+1}$) and (F_n , H_n) we can find the locus of feed x-position as:

$$F_n < x < F_1 \tag{4.2}$$

and the optimum feed y-position can be obtained as:

$$y = ax^2 + bx + c \tag{4.3}$$

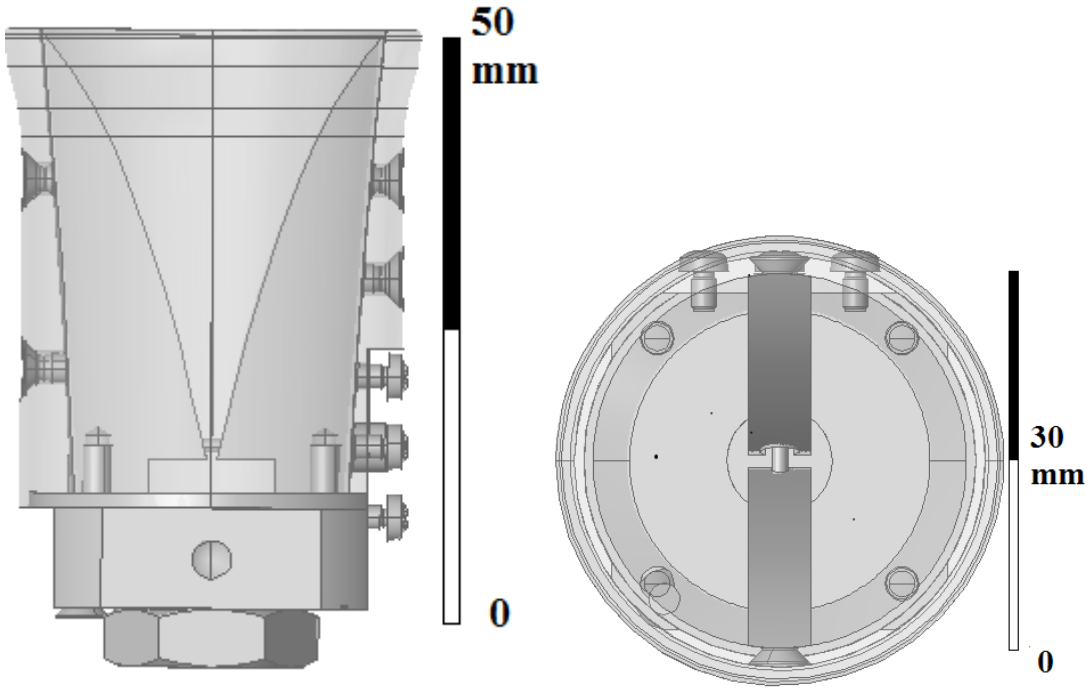

(a) (b)

Figure 24: Double ridged aperture-matched horn antenna(a)side view, (b) top view

where a, b and c are defined as,

$$a = \frac{(H_n - H_m)(F_m - F_1) - (H_m - H_1)(F_n - F_m)}{(F_n^2 - F_m^2)(F_m - F_1) - (F_m^2 - F_1^2)(F_n - F_m)} \tag{4.4}$$

$$m = \frac{n}{2} + 1 \tag{4.5}$$

$$b = \frac{(H_m - H) - a(F_m^2 - F_1^2)}{F_m - F_1} \tag{4.6}$$

$$c = H_1 - aF_1^2 - bF_1 \tag{4.7}$$

From the above equations, the optimum locus for feeds can be obtained. The advantage of this method is using the whole surface of the reflector for all of the beams and increasing the reflector efficiency. In addition, the structure is compact due to the efficient placement of feed.

TABLE IV: Comparison between the positions of feeds obtained by the proposed method and the positions optimized with Genetic Algorithm in HFSS software (the units are cm and dx and dy are defined in Fig. 1).

Method	**beam1 (d_x,d_y)**	**beam2 (d_x,d_y)**	**beam3 (d_x,d_y)**	**beam4 (d_x,d_y)**
GA	**(15.15,-1.77)**	**(13.08,1.40)**	**(9.92,4.33)**	**(7.8,5.82)**
Equation	**(14.84,-1.24)**	**(13.95, 1.98)**	**(11.24,4.67)**	**(8.94,5.91)**

4.3 Simulated and experimental results

In this work, an offset reflector with four distinct double ridged aperture-matched horn antenna has been designed. The location of the feeds has been obtained by the method in previous section. Half power beamwidth of each beam is 6 degrees in the azimuth plane and 6 degrees in the elevation plane. The basic configuration is illustrated in Fig.23. Double ridge aperture-matched horn is used for reflector feeding in order to obtain a good impedance matching in the whole frequency bandwidth from 6 GHz

TABLE V: Aperture efficiencies of optimized offset reflector obtained by Genetic Algorithm with HFSS

Freq. (GHz)	**Feed #1 eff.**	**Feed #2 eff.**	**Feed #3 eff.**	**Feed #4 eff.**
8	**60.38 %**	**58.61 %**	**56.20 %**	**52.47 %**
12	**69.56 %**	**65.47 %**	**62.32 %**	**59.84 %**
15	**67.19 %**	**63.58 %**	**60.07 %**	**56.39 %**
18	**64.66 %**	**61.24 %**	**58.12 %**	**53.78 %**

TABLE VI: Aperture efficiencies of offset reflector obtained by the proposed method

Freq. (GHz)	**Feed #1 eff.**	**Feed #2 eff.**	**Feed #3 eff.**	**Feed #4 eff.**
8	58.86 %	57.14 %	53.67 %	50.01 %
12	66.83 %	63.46 %	60.03 %	56.91 %
15	63.19 %	61.08 %	57.65 %	53.32 %
18	61.86 %	60.26 %	56.04 %	51.97 %

TABLE VII: Single feed efficiency

Freq. (GHz)	**8**	**12**	**15**	**18**
Aperture efficiency	**67**	**72**	**70**	**69**

to 18 GHz (VSWR$<$2) and slant polarization bandwidth. The performance of double ridge aperture-matched horn is optimized to have a constant 3 dB beamwidth in the whole frequency bandwidth. The variation of 3 dB beamwidth over whole frequency bandwidth is less than 30°.

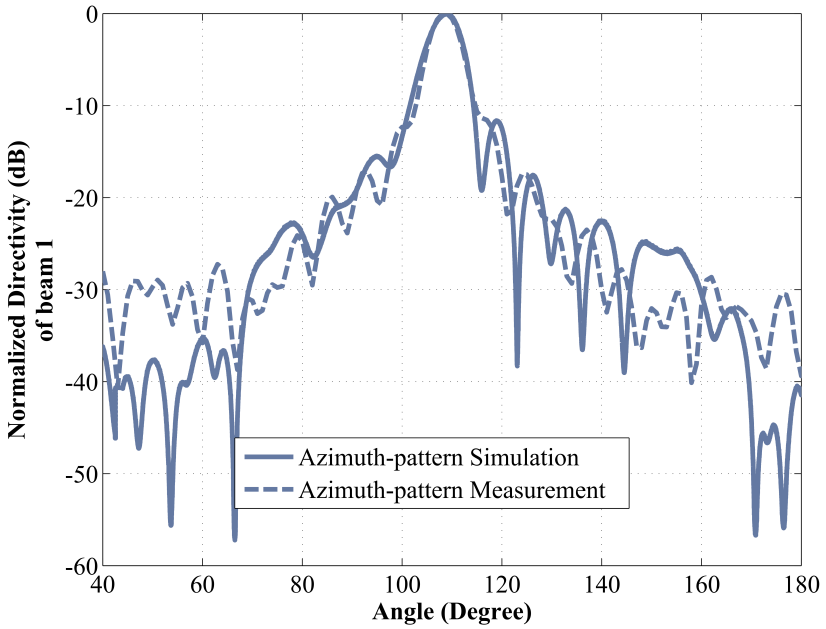

Figure 25: Simulated and measured radiation pattern in the azimuth plane for peak beam 1.

The configuration of the double ridged match horn antenna is illustrated in Fig. 24a. The whole structure is simulated with HFSS Software. In order to verify the validity of the design procedure, the same offset reflector and double ridged aperture-matched horn antenna are considered. The positions of feeds are obtained from optimization in HFSS software using a genetic algorithm (GA). The goal of this optimization is achieving the appropriate location for feeds to obtain the maximum gain and efficiency of whole structure. In Table IV, positions of the feeds obtained from the proposed method and the positions optimized with Genetic algorithm in HFSS are compared. The results show a good compromise between the two methods. The aperture efficiency of the reflector is calculated based on the feed horn pattern with respect to the $\frac{F}{D}$ ratio (67). The calculated aperture efficiency in different

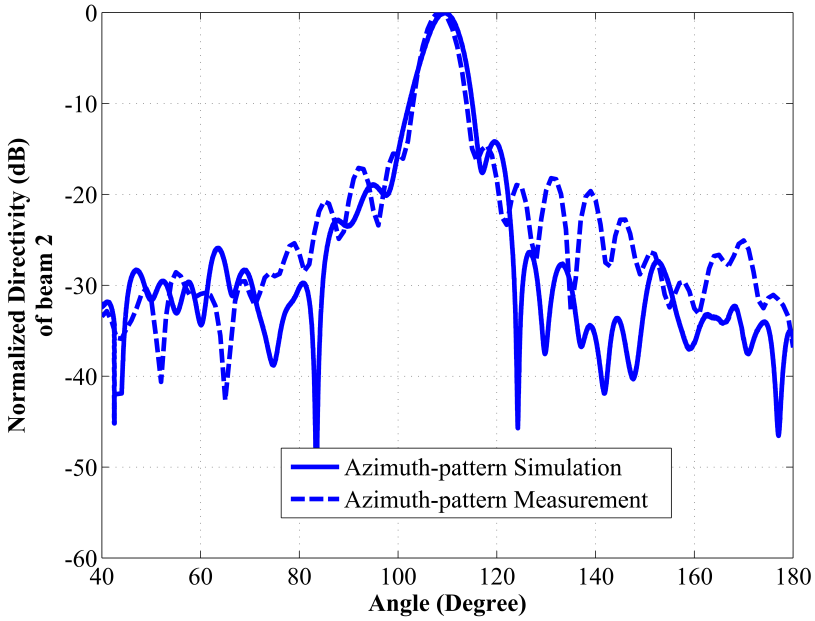

Figure 26: Simulated and measured radiation pattern in the azimuth plane for peak beam 2.

frequencies for the case in which the feed positions are optimized with the HFSS genetic algorithm are listed in Table V. In Table VI measured aperture efficiencies at different frequencies for all feeds are mentioned. The single feed efficiency in different frequencies is mentioned in Table VII. In this case, the power radiating patterns of feeds based on the measured patterns of double ridged aperture-matched horn antenna are calculated. The simulated and measured radiation patterns in the azimuth plane for four distinct beams at the center frequency have been illustrated in Fig. 25. to Fig. 28. The elevation radiation patterns for four distinct beams have also depicted in Fig. 29.

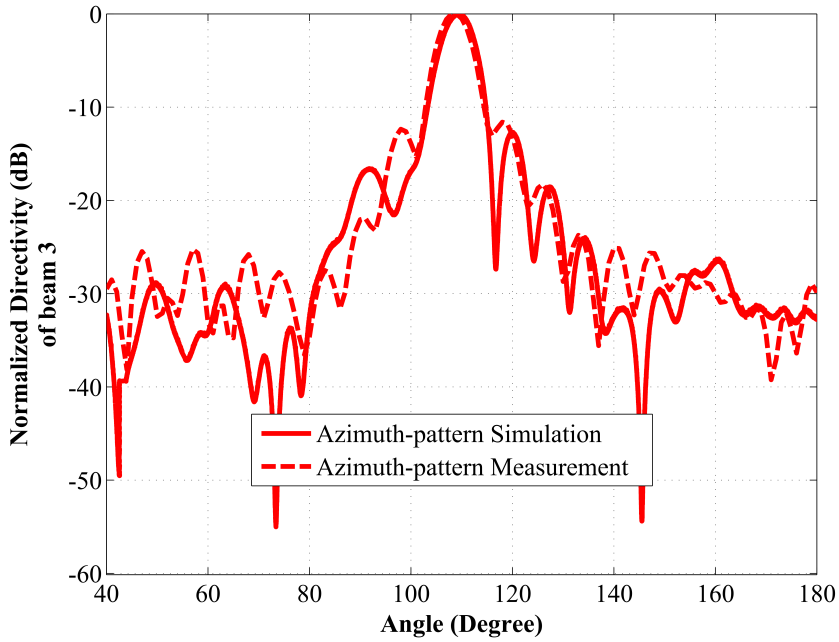

Figure 27: Simulated and measured radiation pattern in the azimuth plane for peak beam 3

We also design an antipodal Vivaldi antenna instead of the double ridged horn antenna. The Vivaldi antenna can be used in DF applications without using reflector too because they have smaller dimensions and are low cost.

4.4 Introduction to Vivaldi antennas

Today, high-speed communications, direction finding, wireless and radar systems are widely developed. Many of these applications require UWB and compact antennas (14; 12). Several types of UWB antennas are discussed in the literature such as helical, bicone, bowtie, horn and Vivaldi (10). Each antenna type has its disadvantages and advantages. For short pulse wireless and high RF power with linear polarization, horn antennas are good candidates but they cannot be used near the ground, and they

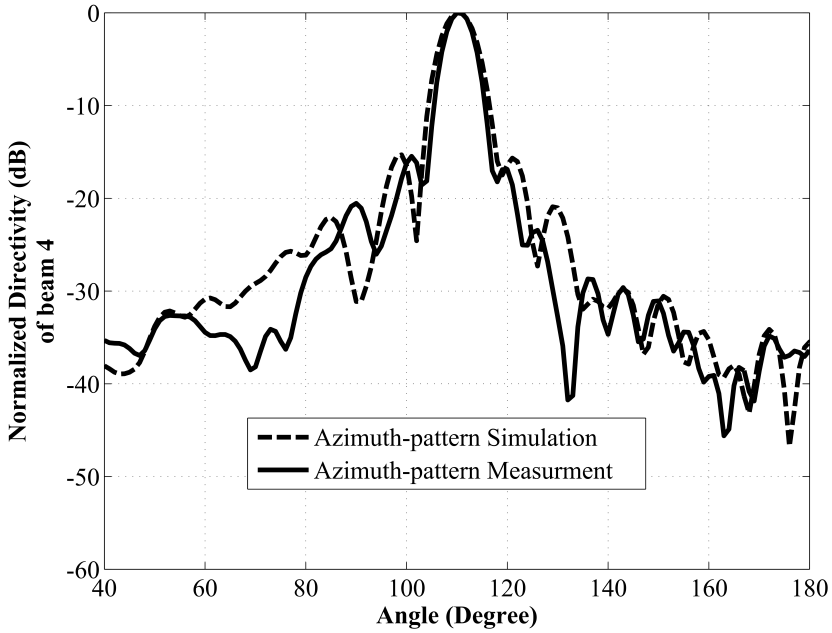

Figure 28: Simulated and measured radiation pattern in the azimuth plane for peak beam 4

are costly to fabricate. Bowtie antennas have higher gain than dipole antennas however for high gain applications they are not suitable. Bicone and helical antennas are not compact and cannot be used in miniaturized systems. Therefore, one of the best UWB and compact candidate is the Vivaldi antenna with a lot of advantages such as planar and small structure, low cost, ease of fabrication, high gain and low side lobe level. Two types of Vivaldi antennas were introduced: the coplanar Vivaldi antenna (68) and the antipodal Vivaldi antenna (69; 70). Coplanar Vivaldi antennas have exponentially tapered radiation parts printed on the same side of the substrate.

We can use an antipodal Vivaldi antenna to feed the reflector instead of the double-ridge horn antenna because it does not need any balun and can be fed by coaxial cable easily. An antipodal Vivaldi

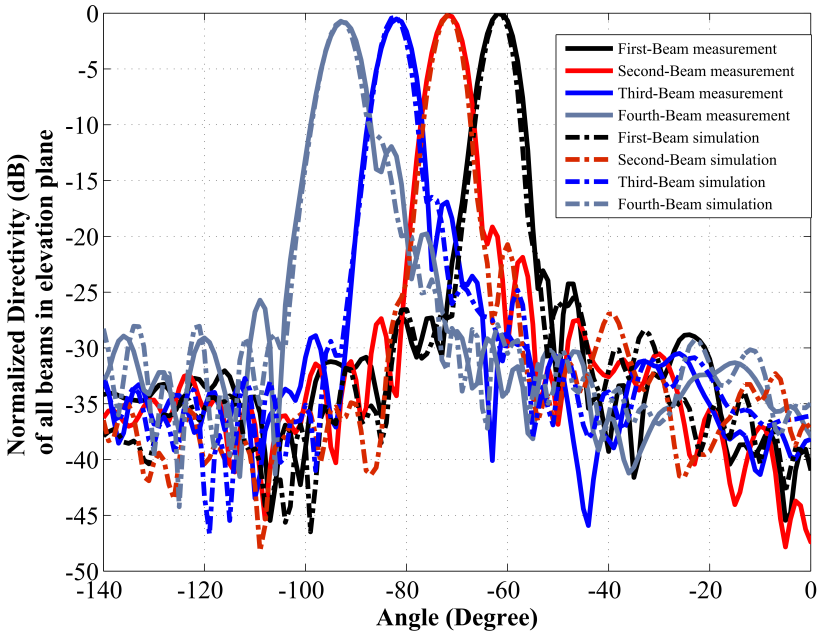

Figure 29: Simulated and measured radiation pattern in the elevation plane

antenna a with tapered corrugated edge from 6 GHz to 18 GHz is designed and fabricated. This antenna can be used in ultra-wide band applications that need stable patterns such as in direction finding systems. The two tapered microstrip antennas are printed on the top and bottom sides of a substrate. The microstrip ground plane is eliminated since one of the tapered microstrips is used as a ground plane. In this technique, an unbalanced to balanced balun is not required. The measured antenna gain is 8 dBi while maintaining VSWR less than 2. There is a good agreement between the simulated and measured results.

Different types of feeding networks were introduced such as using vias or coupled lines. The main problems of coplanar Vivaldi antennas are having cross-polarized radiations and using an unbalanced to balanced balun to feed the antenna, so they cannot be suitable for radar systems.

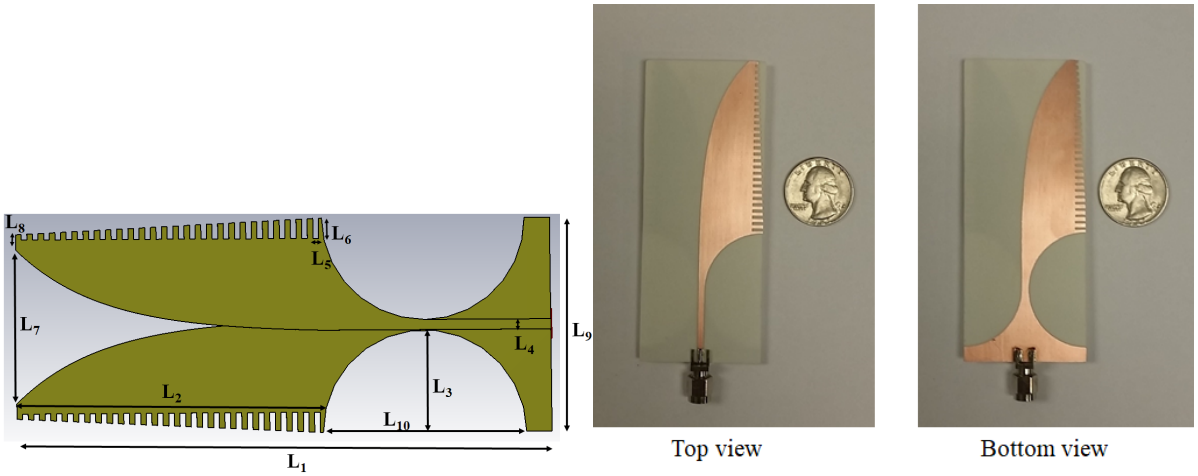

Figure 30: The geometry of the proposed antenna. (a) dimension parameters in Table VIII (b) fabrication photo.

In antipodal Vivaldi antennas, one of the radiation parts is printed on the top, and another one is printed on the bottom of the substrate. In antipodal Vivaldi antennas, cross-polarization is removed so that they can be used in polarization sensitive systems. Different corrugated types have been proposed such as rectangular, circular and triangular to improve the antenna gain and VSWR.

In this design, an antipodal Vivaldi antenna with linear tapered corrugated rectangular shape is proposed to improve the antenna gain. The antenna is fabricated on a 813 mm Rogers RO 4003 with $\varepsilon_r = 3.55$. The frequency of operation is from 8 GHz to 18 GHz. By removing two semicircles from the ground plane, the return loss is improved, and the antenna gain also is stable in the whole frequency bandwidth.

4.5 Antipodal Vivaldi antenna design

The antenna structure including its dimensions is shown in Fig. 30. In this design, the connector and the radiator are carefully considered to obtain a good matching condition because an unbalanced to balanced balun is not used. Therefore, a circular taper is used to match the connector to the antenna. The antenna input impedance is 50 Ω and should be constant. This explains why the taper rate is opposite on both antenna sides. Moreover, the antenna symmetry must be kept to minimize cross-polarization. The tapered slots have an exponential profile. Several parameters were optimized to achieve minimum return loss and stable patterns such as L_1, L_2, and L_9. We also added corrugated edges on the tapered slots to improve S_{11} and the antenna gain. In previous designs, Vivaldi antennas were designed using constant height rectangular or triangular corrugated edges that resulted in a gain that was frequency dependent. To reduce the frequency dependence of the gain, we introduced a taper in the height of the rectangular corrugation, which results in a gain curve that is flatter across the whole operation frequency. We compared the gain, return loss and SLL of several types of corrugations such as rectangular, circular

TABLE VIII: Dimensions of the antenna (mm)

Parameter	L_1	L_2	L_3	L_4	L_5
Dimension	105	60	20	2	1.1
Parameter	L_6	L_7	L_8	L_9	L_{10}
Dimension	4	30	1	42	45

and triangular. The best results were obtained with a linearly tapered rectangular shape. The tapered corrugation also improved the SLL compared to the constant corrugated edge by about 3 dB.

4.6 Simulation and measurement results

The final dimensions are obtained using particle swarm algorithm with CST. The simulated and measured S_{11} are shown in Fig. 31d. As shown in Fig. 31, there is a good agreement between the simulated and measured results.

4.7 Conclusion

A novel method has been proposed for designing highly efficient multi-feed multi-beam offset reflector. A three step procedure for designing multi feed offset reflector has been proposed. In order to validate the proposed method an offset reflector with four distinct feeds has been designed using the proposed method and has been compared with an optimized method using genetic algorithm. The results show a good agreement between the two methods. A broadband multi beam antenna based on offset reflector is designed, simulated and fabricated. The maximum gain is 29.6 dB at 18 GHz and the overall coverage is 30° in elevation plane and 6 degrees in the azimuth plane by producing 4 distinct beams and the minimum efficiency of the antenna is more than 51%.

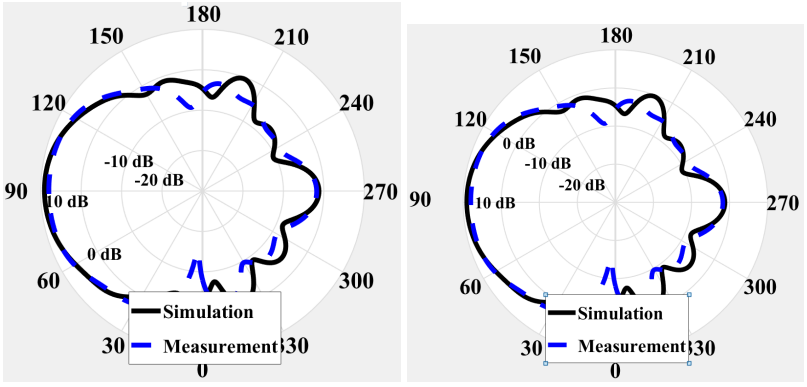

(a) (b)

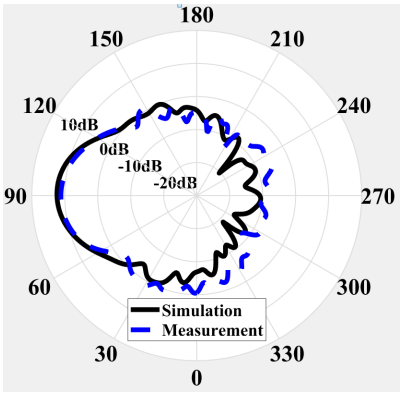

(c)

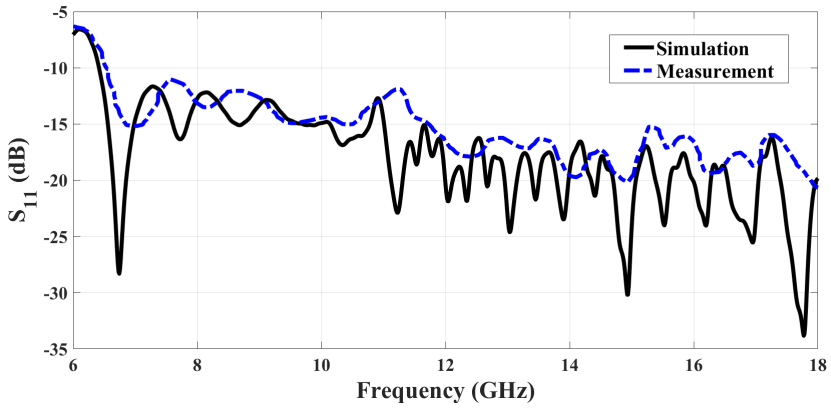

(d)

Figure 31: (a) Simulated and Measured radiation patterns in the yz plane at (a) 8 GHz, (b) 12 GHz, (c) 18 GHz, and (d) simulated and measured S_{11}.

CHAPTER 5

RECONFIGURABLE ANTENNA USING METASURFACE AND LIQUID CRYSTAL

5.1 Introduction to Liquid Crystal antennas

Multibeam compact antennas, with selective directional beams, high gain and low grating lobes, are useful to many communication systems such as DVB-T and radar systems including automotive radars (14). The idea of making a rectangular waveguide inside a dielectric substrate by using a dense array of via-holes to mimic the side walls of the waveguide led to the substrate integrated waveguide (SIW) structures (71; 72; 73). These structures combine the advantages of planar microwave technology and metallic waveguides. Making tunable structures such as reconfigurable antennas has become increasingly popular in recent years, since it reduces the cost of implementation and improves the flexibility of operation. In this Chapter, we are going to use liquid crystal (LC) material to make a tunable phase shifter, which is used in the feed network of an SIW slot array antenna. Using LC crystal has several advantages over conventional phase shifters such as wideband continuous phase shifting and higher power handling capability. Liquid crystal molecules are in a state; in which they can flow even though they have orientational order with a rod-like shape (74; 75). It means that the LC crystal permittivities can be changed by applying external DC E-field. Therefore, the wave speed and phase can be adjustable. The anisotropy in the shape results in anisotropies in its physical parameters such as dielectric

properties. LC materials are especially useful for planar microwave structures with tunable properties such as tunable phase shifters. For microwave applications LC materials with positive anisotropy are used, i.e., $\varepsilon_{r||} - \varepsilon_{r\perp} > 0$ (where the E-field senses $\varepsilon_{r||}$ for its parallel components and $\varepsilon_{r\perp}$ for its prependicular components versus to the wave propagation direction). In our design, the tunable parameter is the permittivity, which can be adjusted by a bias voltage. For zero bias voltage the molecules are aligned parallel to the SIW transmission line (LC phase shifter)with the minimum permittivity of $\varepsilon_{r\perp}$. By increasing the voltage ($V_{bias} > V_{threshold}$), molecules are aligned with the electric field created by the voltage and the ε_{eff} increases as long as the molecules are aligned perpendicular to the transmission line ($V_{bias} > V_{threshold}$) and the maximum permittivity $\varepsilon_{r||}$ is reached. $V_{threshold}$ is the minimum voltage that all of the molecules are aligned parallel to the DC bias E-field.

5.2 Antenna design

The antenna consists of three main parts (Fig. 45), 1) SIW slot array as radiating elements 2) LC phase shifters together with a network of bias voltages to control the phase of each LC phase shifter and 3) a 1-to-8 Wilkinson power divider as the feed line. The dimension of the antenna is 140 mm $\times$ 205 mm and is fabricated on GML 1000 substrate with $\varepsilon_r = 2.2$, $h =$ 1.52 mm and $\tan\delta = 0.005$. The slot array consists of eight SIW linear arrays with eight slots. Each slot length is about ($\lambda_g/2$). The maximum possible value for the substrate thickness for the array is chosen to increase the liquid crystal permittivity change and the slot radiation efficiency. On the other hand, to reduce the radiation loss from feed lines, the thickness of the substrate (Rogers RO4003C with $\varepsilon_r = 3.38$, $h =$ 0.2 mm and $\tan\delta = 0.0027$) underneath the feed line was made smaller as it can be seen in Fig. 54c. To prevent distorting radiation

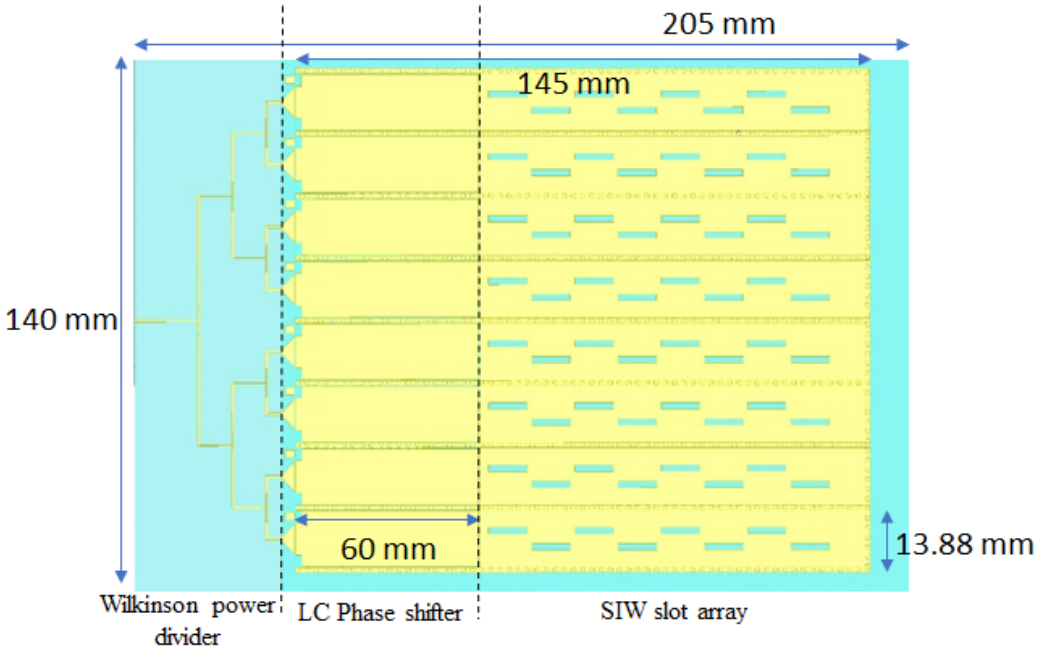

Figure 32: Top view of the SIW slot array with 1-to-8 Wilkinson power dividers and the LC phase shifters.

pattern by feed line radiation, it is recommended to install a layer of absorber on the Wilkinson power divider.

Therefore, the maximum power handling capability is determined by the breakdown voltage of this thinner substrate underneath the feed line. According to our simulations and the substrate data-sheet, each input is capable of carrying 36 W of microwave power. The dimensions of different parts of the antenna are obtained with HFSS using particle swarm optimization and are shown in Fig. 33. The radius of each via and the distance between them is 0.5 mm and 2 mm, respectively. In our design we have used a standard LC material GT3-23001 from Merck, which has $\varepsilon_{r||} = 3.28$, $\varepsilon_{r\perp} = 2.46$, $\tan\delta|| = 0.0038$ and $\tan\delta\perp = 0.0.0143$. The length of the LC phase shifter is 60 mm and it can create $\Delta\phi = 30^\circ$ phase

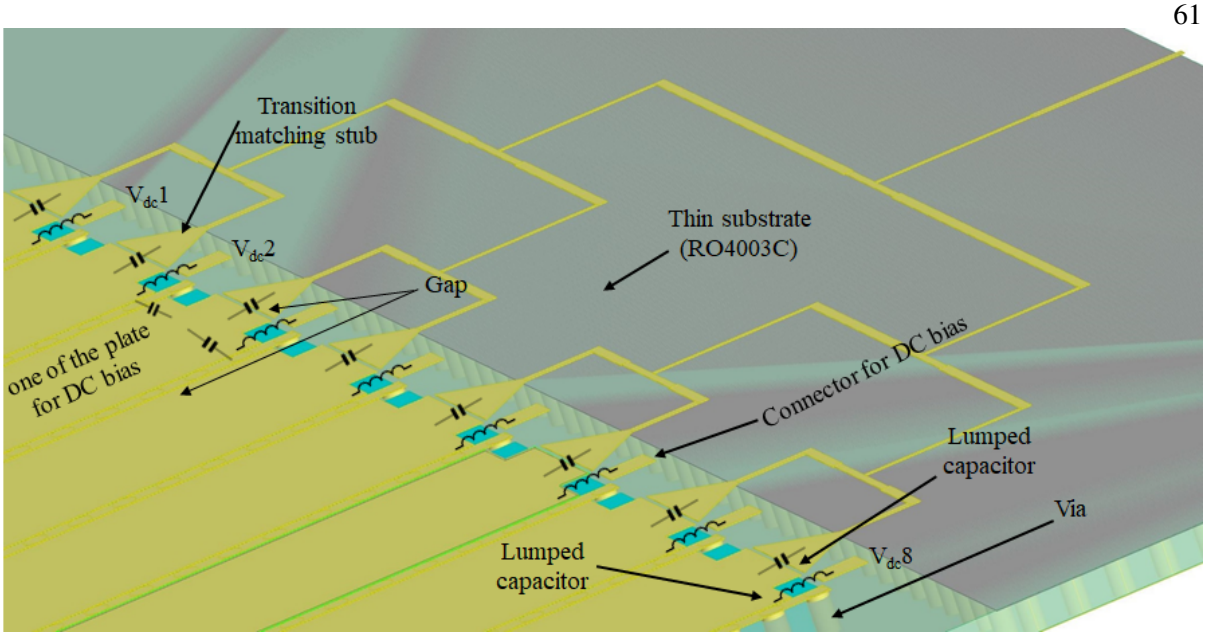

Figure 33: Side view of the antenna. The substrate underneath the feed line is thinner to avoid radiation losses from the feed line.

shift at 12 GHz when the LC epsilon changes from 2.46 to 3.28. 30° phase shifts can rotate the main lobe of the pattern about 11° in each direction. The Wilkinson 1×8 power divider is the third part and is attached to SIW phase shifter with a rectangular transition matching. Each part is DC separated and connected with lumped capacitors for RF connection because each phase shifter should be biased with individual DC voltage. Each DC voltage is applied to the appropriate plate with a lumped inductor for blocking RF signal leakage to the DC sources. As seen in Fig. 54c, the location of some inductors and capacitors are shown.

5.3 Simulation results of the liquid crystal antenna array

In this section, we are going to present the results of our design and simulations. Fig. 35 shows the simulated S-parameter of the antenna. Since slot is a resonant structure, the bandwidth of the antenna is not expected to be large. The frequency range of operation for a VSWR of better than 2 is from 11.85 GHz to 12.25 GHz. The simulated results for the radiation pattern of the antenna at 12 GHz are shown in Fig. 36. As can be seen the maximum of 11° rotation in the main beam can be achieved, which makes it possible to scan a total angle of 22°.

5.4 Introduction to a reconfigurable antenna using metasurface

Reconfigurable antennas are well known and useful in many applications such as satellite communications, radar, and wireless systems. Most reconfigurable antennas are designed using a Rotman

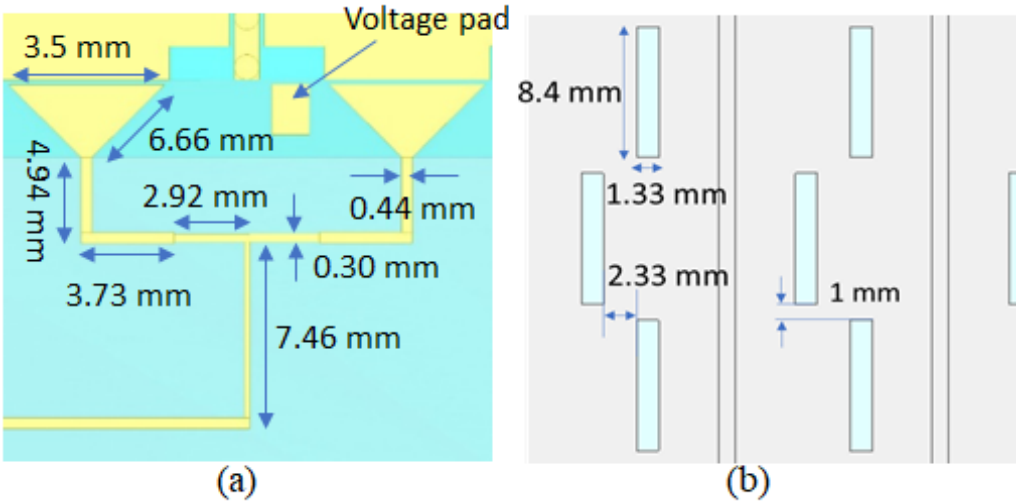

Figure 34: (a) Dimensional parameters of the feed line. The voltage pad is also shown(b) dimension of the slot.

lens (14), a Luneburg lens (9), an active phased array (76) and a metasurface (77). Metasurfaces have attracted a lot of interest recently because they are less bulky compared to phased arrays or lens methods, especially at lower frequencies. Metasurfaces can also be used in nanoscale applications such as nano antennas at radio frequencies and in the optical domain (78).

In particular, many papers have proposed to design antennas containing metasurfaces to provide the excitation. However, the individual radiation elements present in metasurfaces are narrow band; therefore researchers try to address this problem by proposing reconfigurable metasurfaces. Challenges of reconfigurable metasurfaces include occupying larger space and requiring many active lumped elements to control the metasurface unit cells. Some authors proposed using PIN diodes to control the direction of the antenna such as the case of a Yagi-Uda design (79). Therefore, we proposed a design where a

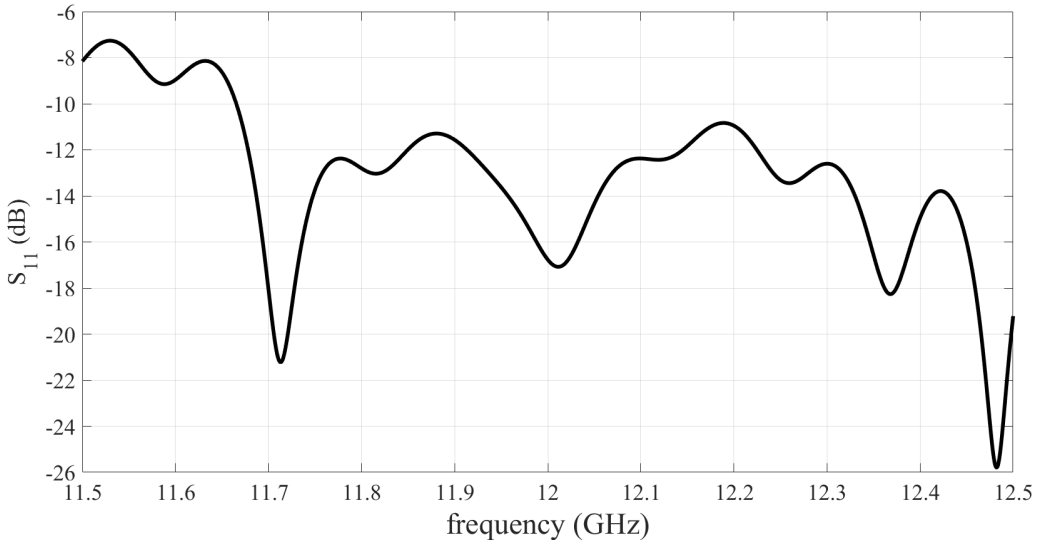

Figure 35: The simulated S-parameter of the proposed antenna.

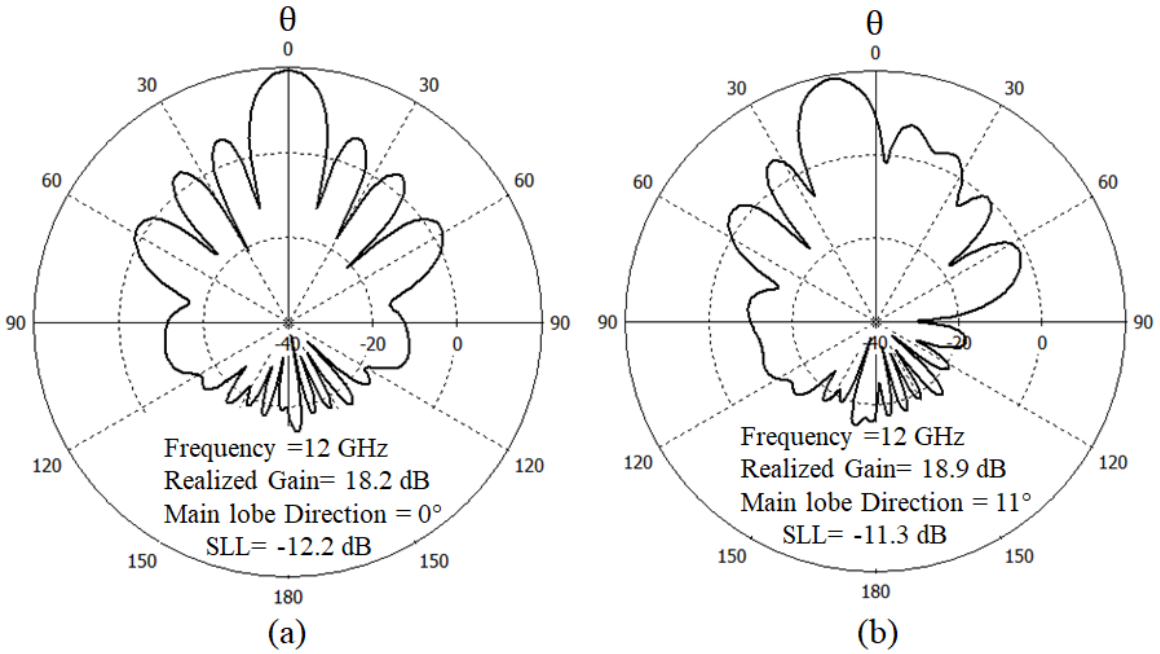

Figure 36: The simulated radiation pattern of the antenna at 12 GHz. (a) No rotation in the pattern (b) The pattern rotates 11°.

metasurface is part of the radiating structure and diodes control the elements that are active to determine the beam direction. Hence, the antenna size can be minimized by using a metasurface and a tapered cross-shaped antenna is used to increase the bandwidth.

5.5 Reconfigurable cross-slot antenna design

The structure of the proposed antenna consists of two sections: a tapered cross slot antenna on a 0.76 mm Rogers FR4-4003 substrate with $\varepsilon_r = 4.2$; and an artificial magnetic conductor (AMC) surface on the same substrate. The whole structure is designed at the center frequency of 5.2 GHz to be used in wireless communication too. The metasurface consists of periodical unit cell patches placed at the

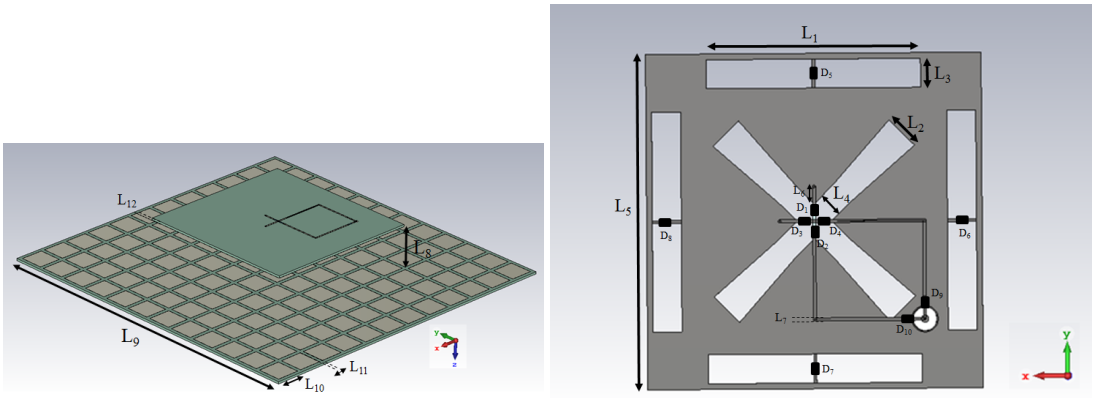

(a) (b)

Figure 37: Geometry of the proposed antenna. (a) Side view,(b) top view of the substrate. The dimensions are given in Table IX.

distance $l_8 = 15$ mm to create unidirectional radiation using a low profile structure. The cross-shaped main slot is one wavelength long and is tapered, therefore obtaining higher bandwidth is easier compared to a $\lambda/2$ long slot which has a higher quality factor (80). Cross slots occupy less real estate and can be fed to obtain two orthogonal polarizations using two orthogonal microstrip stubs. (see Fig. 37). The input slot impedance is adjusted by changing the feed via points so that the return loss can be minimized. There are two paths to feed the antenna to obtain two orthogonal polarizations: for the first path diodes D_3, D_4, and D_9 should be ON and diodes D_1, D_2 and D_{10} should be OFF while for the second path the state of the diodes is reversed. The PIN diodes are BAR50-02, SC-79 from Infineon Technologies with a physical dimension of 1.2 mm $\times$ 0.8 mm $\times$ 0.55 *mm* and have 0.95 V forward voltage bias. All the parasitic elements were included in the simulation. The cross-shaped antenna is surrounded by four slots acting as reflectors. This occurs because the lengths of the slots exceed $\lambda_g/2$ so that their input

TABLE IX: Dimensions of the antenna (mm)

Parameter	L_1	L_2	L_3	L_4	L_5	L_6
Dimension	38	6.2	5	4.2	58	2.9
Parameter	L_7	L_8	L_9	L_{10}	L_{11}	L_{12}
Dimension	0.5	15	120	8.5	1.4	0.76

impedances will be inductive according to the theory of two-element dipole array (80). The reflective slots are used to rotate the beam. Diodes D_5 and D_7 rotate the main beam in the y-z plane and diodes D_6 and D_8 rotate the main beam in the x-z plane. For example, when diode D_5 is ON, and diode D_7 is OFF, the pattern rotates toward the negative y-axis. So, overall we can rotate the beam in four positions by appropriately switching the PIN diodes.

5.6 Reconfigurable cross-slot antenna simulation results

The proposed antenna was simulated with CST software and optimized using its particle swarm algorithm. It has an overall dimension of 120 mm $\times$ 120 mm $\times$ 15 mm. The final dimensions are listed in Table IX. The radiation results when all the slot diodes are OFF, and one of them is ON are compared in Fig. 38b. As shown in Fig. 38a, the main beam rotates about 17°. The simulated S_{11} is also depicted in Fig. 38c.

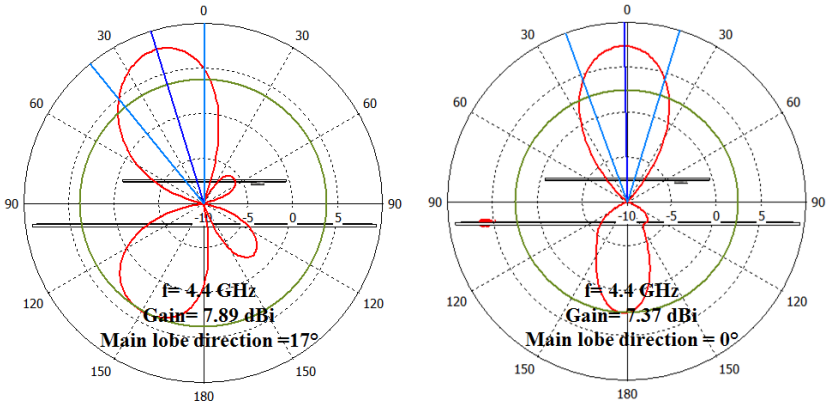

(a)

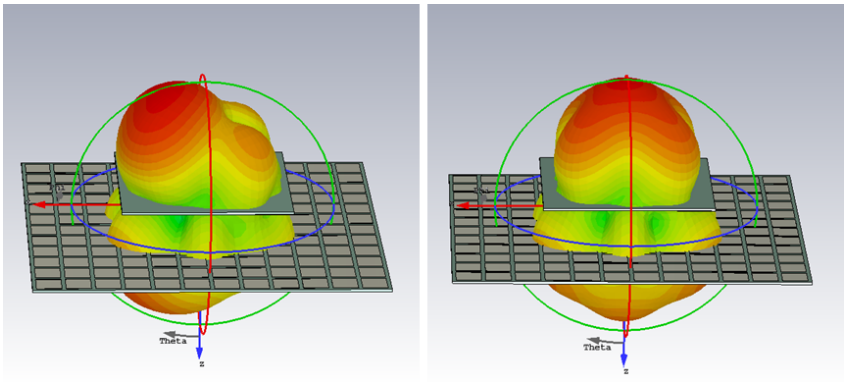

(b)

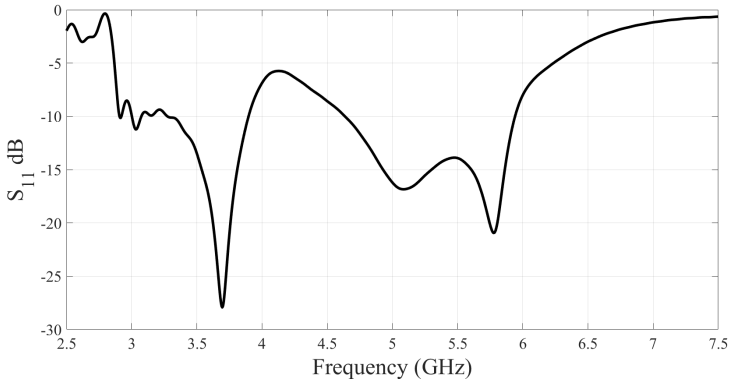

(c)

Figure 38: (a) Simulated radiation patterns in the yz plane at 4.4 GHz, (b) simulated S_{11}.

Part II

Ultra-Wide-Band Antennas

CHAPTER 6

TEM HORN ANTENNA DESIGN

6.1 Literature review of TEM horn antennas

We propose a UWB receiver antenna system that maximizes its operational bandwidth to cover a huge number of bands from 20 MHz to 2.5 GHz. Its design was mainly motivated by a direction finding application (81; 82; 83) where the goal was to replace three different narrowband antenna systems with a more compact UWB single antenna system. Hence, benefits of the new design include (1) a smaller physical size that results from replacing a 2 m monopole antenna with a horn antenna about 5 times smaller in its larger dimension; (2) using a single antenna instead of three; and (3), reducing the cost of the system. Many of these antenna systems may also be used in array configurations. Additional sample applications include radar systems(84), broadband communication systems (85) and electromagnetic compatibility measurement systems.

In the case of direction-finding applications, a transverse electromagnetic (TEM) horn antenna is a suitable candidate for both its directivity and wideband behavior. However, the frequency at which a TEM horn starts to radiate efficiently is not sufficiently low. Therefore, our approach consists of dividing the overall operational bandwidth into two frequency ranges, as shown in the block diagram of Fig. 39. An RF switch is used to select between low and high frequencies. At low frequency, a negative impedance converter (NIC) is introduced to cancel the capacitive impedance of the antenna. At

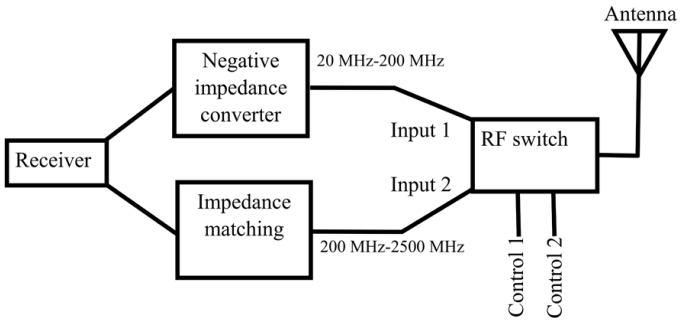

Figure 39: Block diagram of the proposed antenna system. The RF switch is controlled by using control pins (control 1 and control 2) in order to select between low and high frequencies.

high-frequency, an impedance matching network is used. Obviously, this approach can be extended to more than two frequency ranges. The TEM horn antenna, as well as the NIC circuit, are fabricated, and the results of the measurements are reported in the following. Table X compares some parameters of the present work with similar works to the best of the knowledge of the authors (86; 87; 88). As can be seen, the proposed antenna system has the following advantages: (I) it has the largest fractional bandwidth thanks to the active matching circuit; (II) it has both a very wide bandwidth and a good return loss; (III) only one antenna is used to cover the whole operational bandwidth, unlike the others. As a result, the proposed system is simpler, smaller, cheaper and lighter.

6.2 Active antenna design

6.2.1 TEM horn antenna design

TEM horn antennas have been widely used in ground penetrating radar (GPR), EMC measurement systems and broadband communication systems (89). Low distortion of pulse transmission, directional

TABLE X: Comparison with other works.

Reference	Radiating element	Frequency range(MHz) Fractional bandwidth(I)	$\|S_{11}\|(dB)$ (II)	Number of the antennas
this proposal	Active TEM horn	20-2500;1.97	Min=10 Max=33	1
(86)	Conical dipole	20-1300;1.94	Min=1 Max=18	2
(87)	Conformal shaped dipoles	240-3300;1.73	Min=10 Max=35	2
(88)	Microstrip TEM horn	150-3000;1.81	Min=2 Max=10	2

radiation pattern, low cross polarization, and wide bandwidth are some of the properties that make TEM horn antennas interesting for various applications (89; 90).

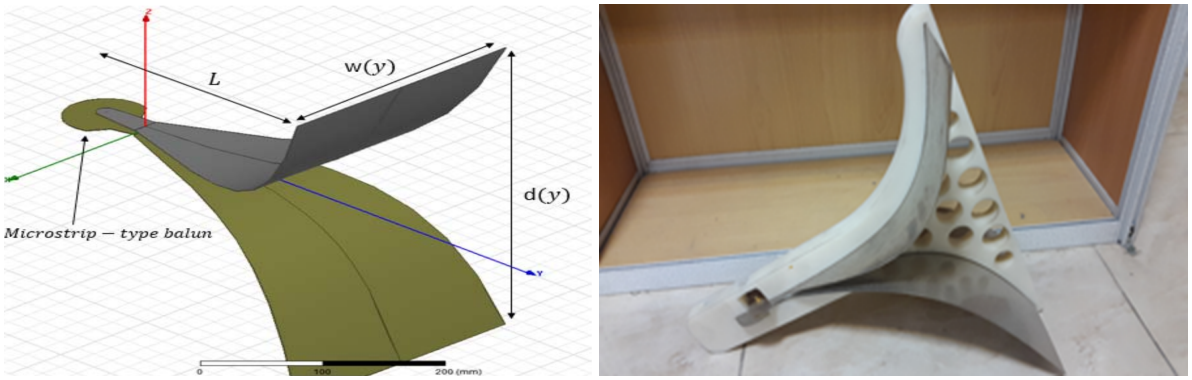

(a) (b)

Figure 40: Dimensional parameters of the TEM horn antenna. At the aperture we have $L = 300\ mm$, $w = 243\ mm$ and $d = 429\ mm$. (b) fabricated TEM horn photo in Amirkabir University antenna laboratory.

Various attempts have been made to improve the radiation characteristics of these antennas. Partial dielectric loading (91) and using a TEM horn antenna with an inductive loop antenna for low frequency radars (92) are among the methods to improve the intensity of the pulse radiation for GPR applications. A wider bandwidth can be achieved by shaping the antenna profile using an exponential (93) or even an elliptical (94) taper. In our design, an exponential taper is employed to match the characteristic

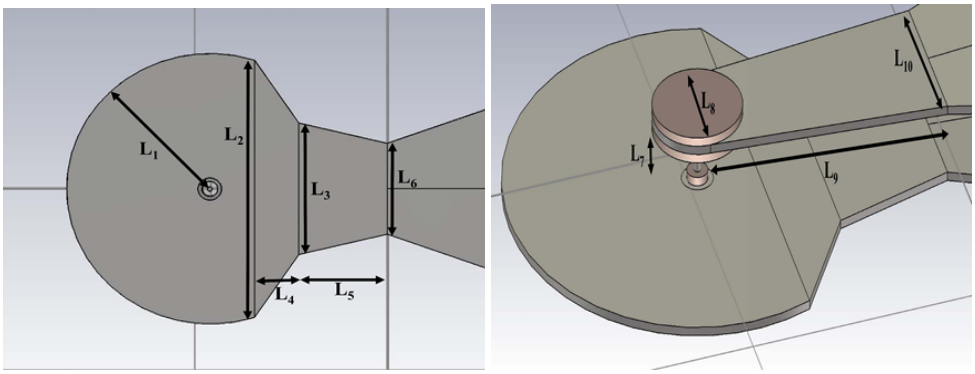

(a) (b)

Figure 41: Dimensions of the microstrip balun (a) bottom view, (b) top view. The discs with diameter L_8 provide mechanical support.

impedance at the feed point to the impedance of free space. The gradual exponential transition keeps the reflections low and makes the bandwidth wider.

The antenna consists of two parts: (1) the horn section, and (2) the balun for matching the impedance of the TEM horn antenna with a balanced structure to an unbalanced coax feedline (95). Design parameters for the horn antenna with an exponential taper are shown in Fig. 40a and Fig. 40b shows the fabricated horn antenna. The distance d(y) between the two plates of an exponentially tapered TEM horn antenna is given by (96)

$$d(y) = 2a\exp(by) \quad (0 \leq y \leq L) \tag{6.1}$$

TABLE XI: Dimensions of the microstrip balun.

Parameter	L_1	L_2	L_3	L_4	L_5
value (mm)	38	71	36	11.5	23
Parameter	L_6	L_7	L_8	L_9	L_{10}
value (mm)	25	7	17	46	25

where a, b are arbitrary coefficients to be determined. The characteristic impedance at any point on the antenna is expressed as (96)

$$Z(y) = Z_0 \exp(\alpha y) \quad \alpha = \frac{1}{L} \ln(Z_L/Z_0) \quad (0 \leq y \leq L) \tag{6.2}$$

where $Z_0 = 50\ \Omega$, $Z_L = 120\pi\ \Omega$ and L is the antenna length. To determine the plate width, the characteristic impedance of a parallel plate waveguide is employed, where the characteristic impedance between two plates is given by (94)

$$Z(y) = 120\pi \frac{d(y)}{w(y)}\ \Omega \tag{6.3}$$

and $w(y)$ is the plate width. The microstrip-type balun (96) to connect the coaxial feed to the antenna is shown in Fig. 41 and the corresponding values of the design parameters are given in Table XI. An alternative for the microstrip feed is to use coax with an elliptical shaped cavity in order to reduce reflections in the coaxial to double-ridged waveguide transition (96). However, according to our requirements, a microstrip balun is more suitable because it has smaller dimensions. As shown in Fig. 41, the width

of the upper plate has an increasing taper whereas the width of the ground plane has a decreasing taper such that a transition from the characteristic impedance of the coaxial line to that of the balanced parallel plates is obtained (90). Unlike the balun proposed in (90), which uses a linear taper, additional optimized tapered sections are used in our design to improve the high frequency performance of the balun. We should also note that the input impedance of the TEM horn antenna must be matched to the output impedance of the balun. Fig. 42 shows the simulated radiation pattern with (49) and the measured radiation pattern at various frequencies for the single TEM horn antenna with microstrip balun. As expected, for direction finding applications, this antenna should be used in an array configuration. The radiation pattern of the antenna is almost omnidirectional at the lower frequencies. However, the beamwidth gets narrower as the frequency increases but there exists a 3 dB beam overlap to cover the azimuth plane. It is worth to mention that at each frequency, sampling algorithm in the software should be calibrated to decrease the errors due to the variations of the power magnitude.

6.2.2 Negative impedance converter (NIC)

For the lower range of frequencies, i.e., below 200 MHz, the antenna remains electrically small and consequently has a narrow bandwidth. For electrically small antennas, passive (Foster) matching cancels the reactive part of the antenna impedance over a very narrow bandwidth (97). However, it is possible to cancel the reactive part of the antenna input impedance over a wide bandwidth with non-Foster elements, such as a negative impedance converter (NIC).

The NIC is an active two-port network that inverts the impedance connected to the other port (98), and one realization was provided by Linville in (99). The schematic of our NIC is provided in Fig. 43, where two transistors are biased in the common emitter configurations and their bases are connected

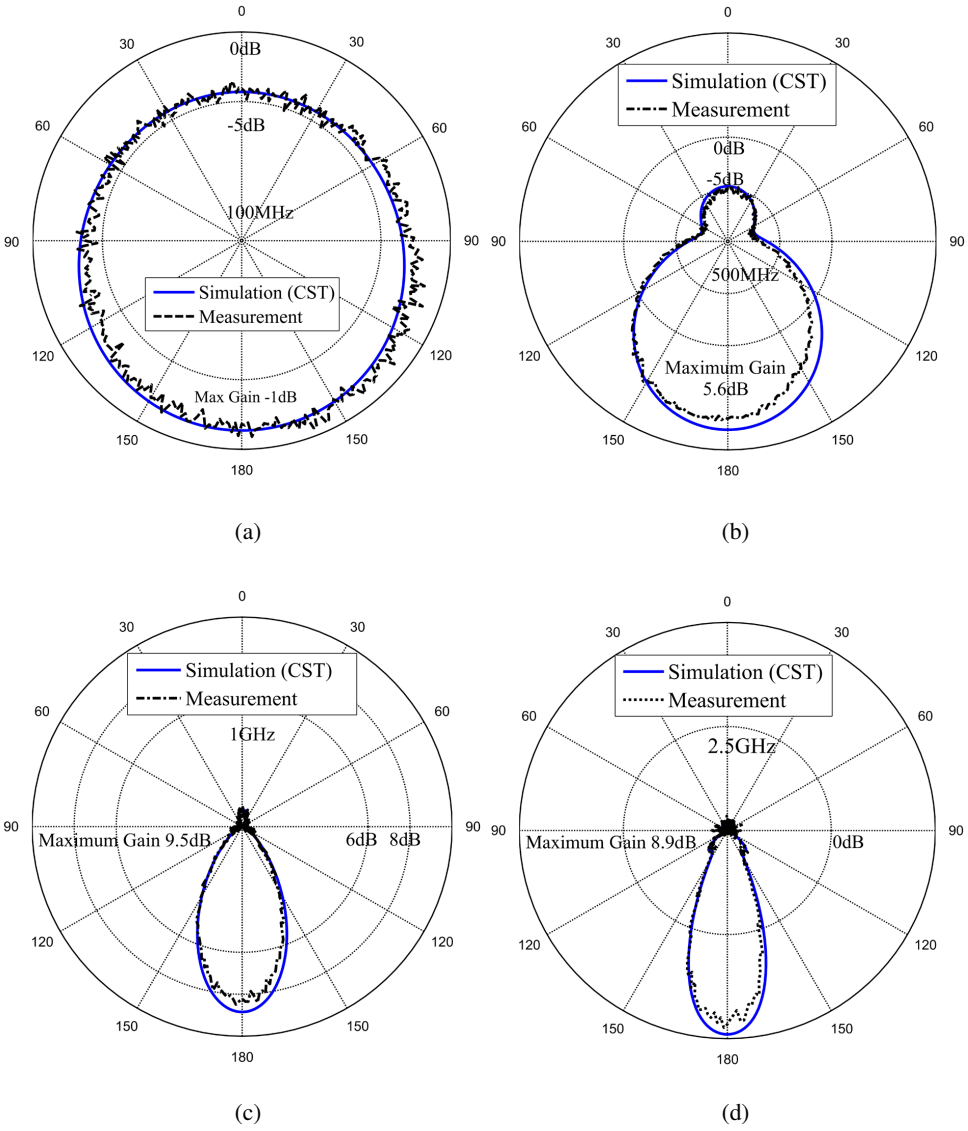

Figure 42: Simulated and measured radiation pattern generated by the TEM horn antenna in the XY plane (see Fig. 2a) at (a) 100 MHz (b) 500 MHz (c) 1 GHz and (d) 2.5 GHz.

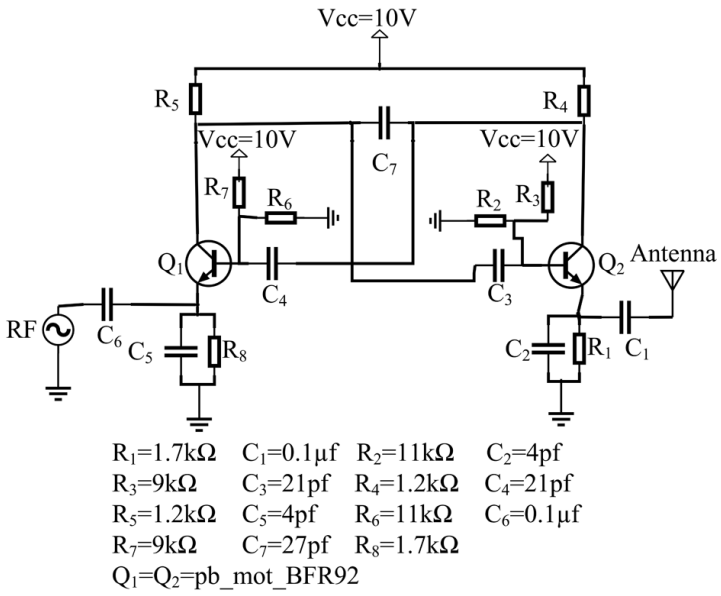

Figure 43: Schematic of the NIC circuit. The values of the elements are also given.

to form a feedback loop (98). Capacitor C_7 is then connected between the two collector leads. The transistors are NPN BJTs (BFR92) with class-A type biasing, which increases the voltage gain and fulfills the condition for having a negative impedance. The circuit is fabricated on FR-4 substrate with permittivity 4.3 and thickness of 1 mm. We should also notice that the active elements exhibit internal losses, noise and bandwidth limitations (100).

Moreover, parasitic reactance must be considered when the circuit is laid out. Therefore, the manufacturer's S parameter file for the transistor is used in our simulations with ADS (101). The output port is connected to a 50 Ω load and the values of the elements, especially the capacitor C_7 of Fig. 43, are optimized to achieve an acceptable matching over the desired frequency band ($|S_{11}| < -10\,dB$). Figs. 45a,

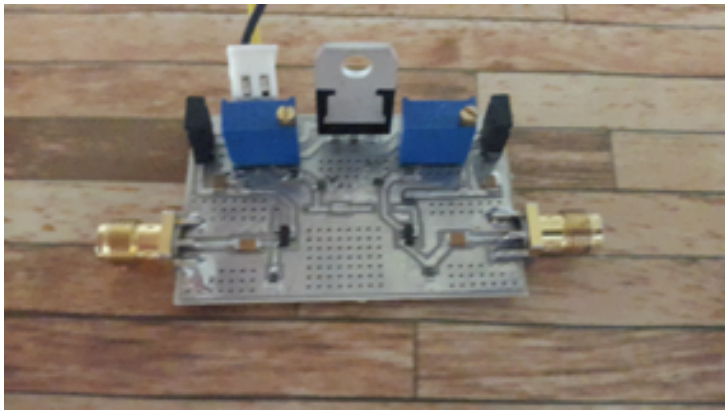

Figure 44: Fabricated NIC circuit.

45b show the real and imaginary parts of the input impedance as well as the reflection coefficient of the isolated antenna and the antenna connected to the NIC. As can be seen from Fig. 45a, the NIC significantly reduces the large capacitive reactance of the antennas at low frequencies. Consequently, the real part of the impedance increases at low frequencies. The influence of the NIC can also be observed in the reflection coefficient in Fig. 45c, where the simulation and measurement results are shown. The NIC significantly reduces the almost full reflection of the antenna at low frequencies as shown in Fig. 45c. The insertion loss of the NIC circuit varies between 2.9 dB and 4.6 dB over the frequency band from 20 MHz to 200 MHz. A RF switch is introduced to bypass the NIC for frequencies above 200 MHz because of the excessive losses introduced by the NIC, as shown by the value of S_{11}. Above 200 MHz the value of S_{11} of the antenna and NIC is below 10 dB; however, the losses are mostly due to the NIC losses and not radiation. The fabricated NIC circuit is shown in Fig. 44. As can be seen from

the simulation and measurement results, the bandwidth of the whole system for VSWR less than 2.0 is about 2.5 GHz (i.e., from 20 MHz to 2.5 GHz).

NIC circuits are potentially unstable since we use positive feedback in this circuit so an efficient stability test is necessary during the design step to prevent any undesired NIC response. Unfortunately, most of the spectral stability tests are not sufficient to predict the system stability because the antenna and matching circuit are used in non-Foster domain (99). In the other words, This NIC is only stable for this antenna and this frequency bandwidth and there is no guaranty to be used with other antennas because each antenna has a different input impedance values. The NIC stability is determined by the system pole locations in the complex plane. So, the positive real parts of the poles create an instability in the NIC. Moreover, the lumped elements, which are used to bias the transistors, have parasitic values that increase the complexity of finding the NIC pole locations. The lumped element values are chosen based on the antenna input impedance value versus the frequency, therefore the stable domain on the smith chart or complex plane, depends on the antenna input impedances. Therefore, solid and straightforward solution to find stable poles is not easy. Consequently, the proposed NIC stability has been checked with ADS software in the whole frequency bandwidth. From 20 MHz to 200 MHz, the NIC circuit K parameter is greater than 1 and the NIC is stable. For higher frequencies, the S_{21} becomes lossy (greater than 20 dB) and the NIC is not useful. Hence, we used a switch to remove the NIC from the RF line regardless of its stability. It is interesting to say that the NIC is unstable at the frequencies above 500 MHz.

6.3 Conclusion

An ultra-wideband antenna system for the frequency range from 20 MHz to 2.5 GHz has been proposed. The operation bandwidth of the passive antenna is from 200 MHz to 2.5 GHz. A NIC circuit is used to reduce the capacitive behavior of the antenna from 20 MHz to 200 MHz, which also improves the return loss. By using a simple RF switch in the antenna feed, the NIC can be switched in and out of the circuit. The insertion loss of the NIC circuit varies between 2.9 dB and 4.6 dB over the frequency band from 20 MHz to 200 MHz. This system has been simulated, optimized, fabricated and measured. A good agreement between the measured and simulated results is observed. Future work will address the mutual coupling between the antennas in an array configuration.

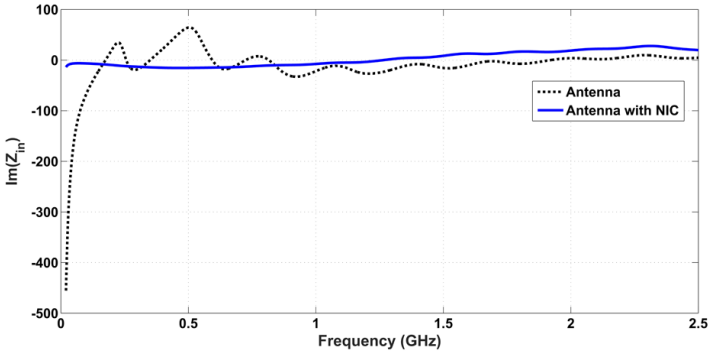

(a)

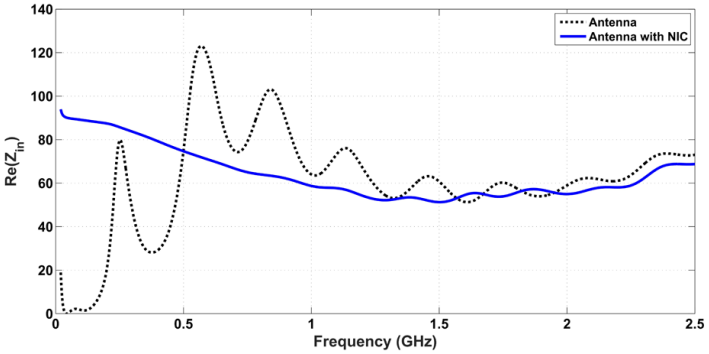

(b)

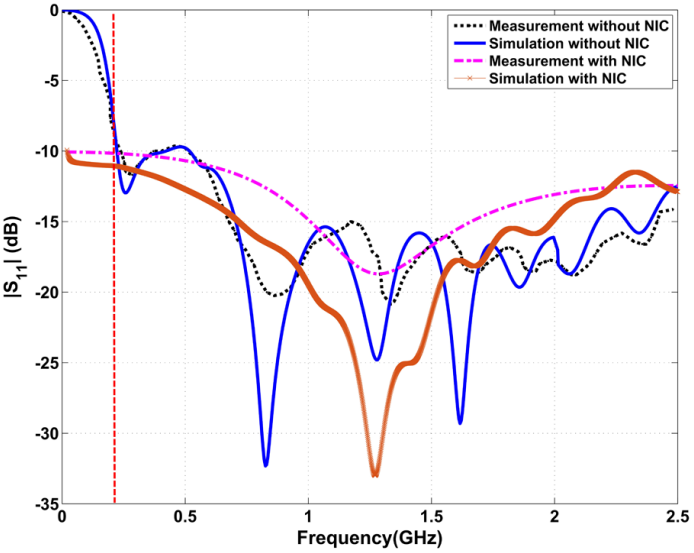

(c)

Figure 45: (a) Imaginary part of the input impedance for the antenna with and without NIC (b) real part of the input impedance for the antenna with and without NIC. (c) S-parameter of the antenna without/with NIC.

CHAPTER 7

UWB DUAL-POLARIZED BICONICAL ANTENNA

7.1 Literature review of the biconical antenna

Biconical antennas are omnidirectional, and they are very attractive because they have a very wide bandwidth, high input impedance, and are easy to fabricate (102; 103). One limitation of biconical antennas is that they are linearly polarized along the direction of their axis of symmetry. Since they are usually placed vertically, they cannot receive horizontally polarized signals.

In this Chapter, we design polarizers that surround a biconical antenna so that the structure resulting from the combination of the polarizers and the biconical antenna can respond to signals that have both horizontal and vertical polarizations.

Specifically, several layers of polarizers are used to rotate the plane of polarization of horizontally and vertically polarized incident signals so that they become polarized at a slant angle of 45°. So, this antenna can received both polarization at the expense of 3 dB loss for vertically polarized incident signals (104; 105). In addition, in order to reduce the reception of signals reflected from the ground, we are going to design an asymmetric biconical antenna such that the maximum of the radiation pattern shifts towards the upper cone and away from the ground (106).

Our design requirements are as follows: omnidirectional radiation pattern with a ripple of less than 0.5 dB in the azimuth plane, 3 dB beamwidth of at least 20° in the elevation plane, to minimize target

ranges estimation errors and bandwidth from 2 GHz to 18 GHz to detect every target at S, C, X and Ku bands and a VSWR below 2.5 to increase the antenna range capabilities.

The design procedure is as follows. First, the biconical antenna is designed and optimized without polarizers in order to obtain the required VSWR and radiation pattern. Then we design and optimize the polarizers, which surround the biconical antenna.

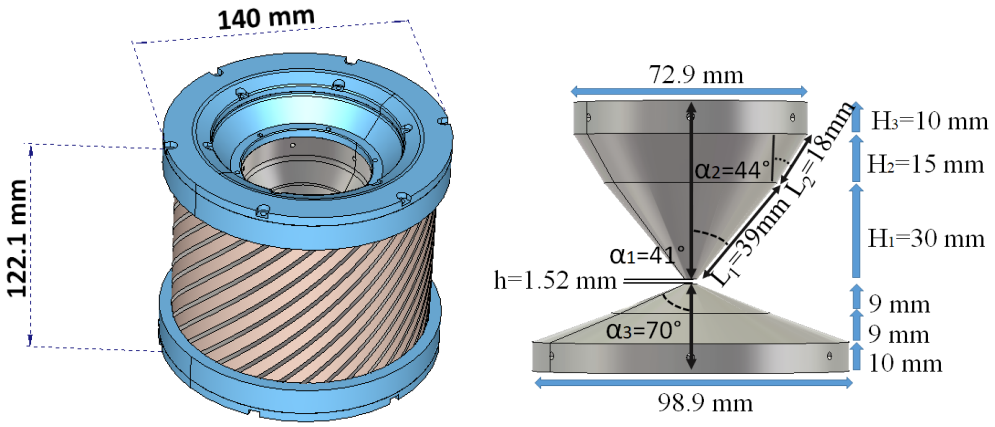

Figure 46: (a) Dimensions of the biconical antenna with polarizers and mechanical fixtures. (b) Dimensions of the asymmetrical biconical antenna. L_1,L_2,H_1, H_2, H_3, α_1, α_2 are optimization parameters.

The conclusion of our simulations is that 5 layers of polarizers are needed to meet our design requirements. Fig. 46 shows the final design consisting of a biconical antenna surrounded by polarizers and the corresponding mechanical fixture. This chapter is organized as follows. In section 7.1.1, we

present the design of the asymmetrical biconical antenna, its parameters as well as simulation results. In section 7.1.2, the design procedure for the multilayer polarizers is discussed together with simulation results and dimensions of the polarization layers. The fabricated sample, as well as measurement results, are shown in section 7.2.

7.1.1 Asymmetric biconical antenna design

An ideal infinite biconical antenna has an input impedance that is frequency independent and is solely determined by the cone half-angle. Actual finite biconical antennas have an input impedance that is determined mostly by the cone half-angle α, and by the frequency of operation, the length of the cone L and the separation distance h between the tips of the cones. At lower frequencies, the impedance bandwidth is determined mostly by the length of the cones. At higher frequencies, the cone half-angles should be chosen between 30° and 60° (106) to have stable radiation pattern and low VSWR.

In this Chapter, we consider the asymmetrical biconical antenna shown in Fig. 46, where for the upper part two different cone angles have been considered to provide a stable pattern shape in the whole frequency bandwidth.

At lower frequencies, the real part of the input impedance of the antenna is low (107). So based on Schelkunoff's formula (108) for the input impedance of a biconical antenna,

$$Z_{in} = 120 \ln \cot \frac{\alpha}{2} \tag{7.1}$$

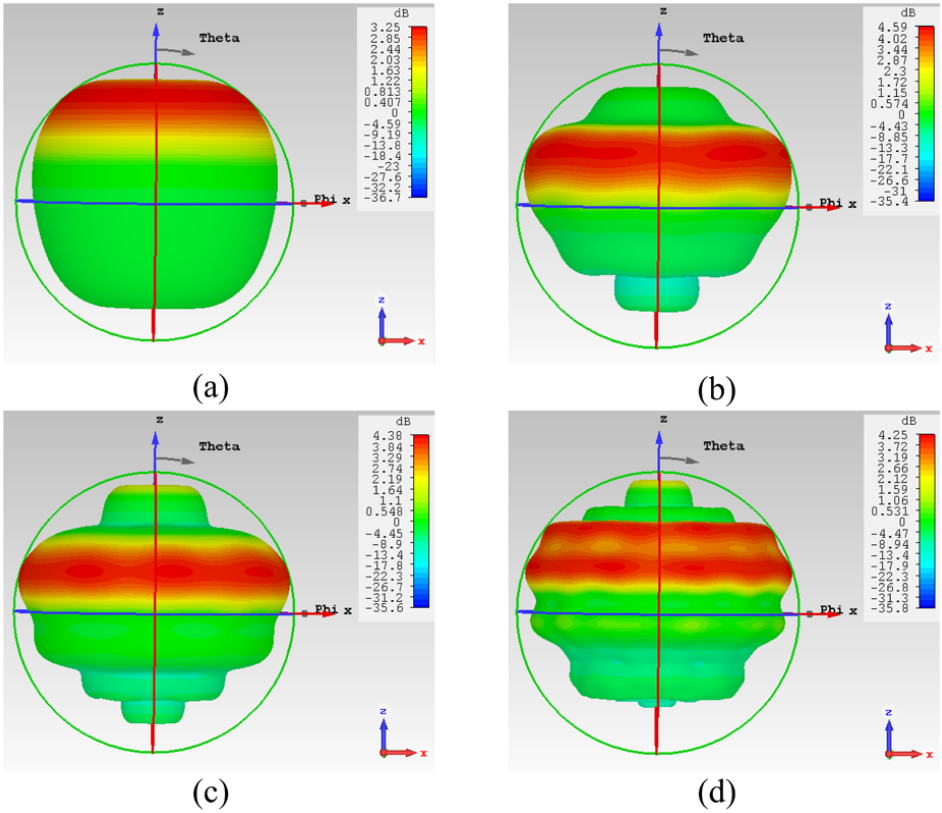

Figure 47: Radiation patterns at several frequencies. (a) 2 GHz (b) 10 GHz (c) 14 GHz (d) 18 GHz.

the cone angle should be chosen smaller to compensate for the low input impedance. At higher frequencies, the real part of the input impedance increases, and the cone angle can be chosen larger and the antenna behavior is similar to the radiation from two parallel plates.

From the point of view of the return loss, the radiating portion of the antenna should have a tapered profile to minimize the return loss, such as the Klopfenstein or the exponential tapers (109). However, such profiles are not easy to fabricate; therefore, we considered the simpler design with two cones of

different aperture angles, α_1 for the lower cone and α_2 as shown in Fig. 46, because satisfactory results were obtained.

At higher frequencies, the dominant radiation occurs between the first (α_1) and the third (α_3) antenna cones. The second cone has a smaller angle ($\alpha_2 < \alpha_1$) and has a higher impedance, according to the equation 7.1.

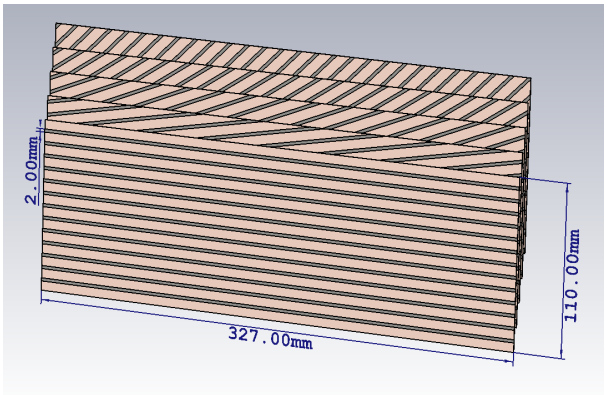

Figure 48: Front view of the 5 layers of polarizers. Each sheet has a dimension of 327 mm by 11 mm and the width of each strip is 2 mm.

From the point of view of the radiation pattern, this should not vary too much with the frequency in the azimuth plane, therefore, the biconical antenna should not be electrically large (and thus behave similar to a traveling wave antenna).

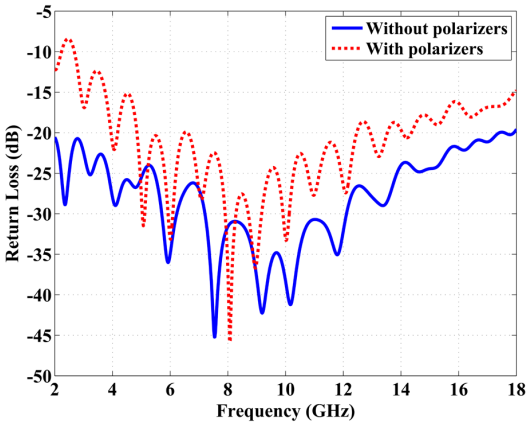

(a)

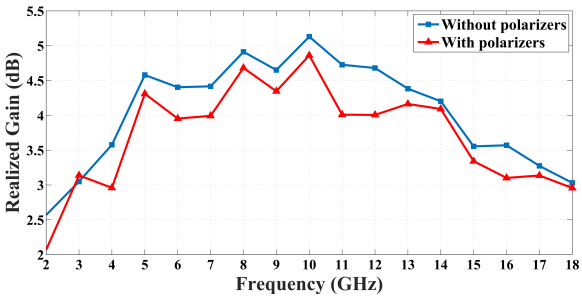

(b)

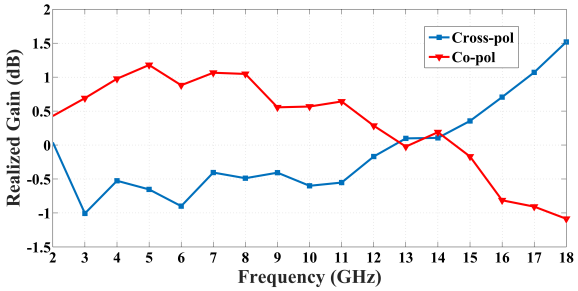

(c)

Figure 49: Simulation results of the biconical antenna with and without polarizers. (a) Return loss (b) Variation of maximum gain versus frequency (c) Co-pol. and cross-pol. gain.

In order to determine the total length $L_1 + L_2$ we need to satisfy two conditions. One condition is about the minimization of the return loss, for which we require that the total length at a characteristic frequency f_c be about one quarter wavelength or $L_1 + L_2 \simeq \lambda(f_c)/4$. The other condition is about having a pattern that does not vary too much with the frequency. In this design, by selecting the characteristic

frequency $f_c = 1.34$ GHz below the minimum operating frequency $f_{\min} = 2\ GHz$ we obtain a pattern that is sufficiently a stable within the operating frequency from 2 GHz to 18 GHz.

The important design parameters are indicated in Fig. 46. Since we require a bandwidth of 9:1 and the pattern variations over the operation bandwidth are large, the angles α_1 and α_2 are used as the tuning parameters to control the radiation pattern. In order to reach the appropriate matching, α_1 and α_2 as well as L_1, L_2, H_1, H_2 and H_3 are optimized using the particle swarm algorithm that is part of CST software (49). During the optimization process, the variations in the antenna pattern and matching are observed, and the variables are adapted to meet the design requirements. The biconical antenna is fed through an SMA cable, where the central pin of the coaxial cable is connected to cone 3 and the shield is connected to cone 1. After several iterations of design, simulation, and measurements, appropriate dimensions for matching and radiation pattern were achieved as shown in Fig. 46. The radiation patterns at different frequencies are shown in Fig. 47. As can be seen, the maximum of the radiation pattern in the elevation plane is shifted away from the center, and the ripple in the radiation pattern throughout the operation bandwidth is less than 3 dB.

7.1.2 Multilayer polarizers design

Designing an antenna with slant polarization makes it possible to receive both vertical and horizontal polarizations. In order to receive both polarizations, the biconical antenna is surrounded by multilayer polarizers (110; 111; 112; 102; 113).

In our design procedure, we started with a single layer polarizer with a slope of 45°, but this could not achieve the design requirements. Hence, we investigated a multilayer polarizer solution with different

polarizing slopes for each layer. At the end of our simulations, we found that 5 layers of polarizers with slopes of 0°, 11.25°, 22.5°, 37.5° and 45°, respectively, are needed to meet our design requirements.

The distance between the layers as well as the polarizing strips are important design parameters and are shown in Fig. 48. The polarizers are designed on a Rogers RO4003 board with a thickness of 0.254 mm. Each sheet has a dimension of 327 mm by 11 mm and the width of each strip is 2 mm, see Fig. 48. The distance between the layers is 3 mm and there is a gradual increase in the angle of the polarizers to provide a smooth transition to a slant polarization. The design is optimized to receive both polarizations in the frequency band from 2 GHz to 18 GHz. After placing the polarizers around the antenna, its return loss degrades by a small amount, which is due to the reflections from the polarizer layers, see Fig. 49a.

Fig. 49 shows the return loss of the biconical antenna with and without polarizers. Moreover, variations of the maximum gain versus frequency with and without polarizers are shown in Fig. 49b, where the polarizers reduce the maximum gain due to their dielectric losses. It is apparent that achieving a slant polarization using polarizers degrades both the return loss and the maximum gain of the antenna. Fig. 50 shows the frequency response of the realized gain for two polarizations in the presence of polarizers.

In order to keep the polarizers fixed in their place, it is necessary to add rings above the antenna. In our first design, Teflon was used to keep the cones of the antenna in a protective layer. However, this layer degrades the radiation pattern of the antenna so that it is necessary to repeat the simulation of the antenna once more to account for the protective layer. In our revised design, however, foam was used instead of Teflon because Teflon is heavy with high losses at high frequencies and high diffraction due to

inhomogeneity. However, foam is much lighter, has lower losses and diffraction, therefore it introduces less ripple in the radiation pattern.

In order to verify that the polarizers work as expected we are going to show their effect on the polarization by a simulation. For doing this the received power in a biconical antenna due to a horizontal polarized plane wave with and without polarizers is determined, which is shown in Fig. 50b and 50c. As can be seen from Fig. 50b the received power by the biconical antenna is increased by an amount of 80 dB compared to the case without polarizers. Moreover, in order to investigate the effect of polarizers on the vertical polarization, the received power in the biconical antenna with and without polarizers are compared. As can be seen from Fig. 50c, adding polarizers introduces about 3 dB of loss in the vertical polarization. Considering the effect of polarizers for both polarizations, it can be concluded that the polarizers improve the antenna reception for horizontal polarizations, while they cause a 3 dB insertion loss for vertical polarization, which shows that a slant polarization has been achieved. It is interesting to say that the received power with polarizer of Fig. 50b and Fig. 50c are the same.

7.2 Fabrication and measurements of the biconical antenna

The biconical antenna with 5 layers of polarizers are fabricated and measured as shown in Fig. 52. The received power at different angles for different frequencies as well as the radiation pattern in azimuth and elevation planes are measured in an anechoic chamber. The results of radiation pattern measurements are shown in Fig. 51. As can be seen, the radiation pattern in azimuth is almost omnidirectional whereas the radiation in elevation shows deviation from an omnidirectional pattern. Moreover, Fig. 53 shows the received power versus the angle at different frequencies. The fluctuations in the received

power are always less than 3 dB, which shows that an acceptable omnidirectional pattern has been obtained.

7.3 Conclusion

In this Chapter an ultra-wideband antenna system for the frequency range from 2 GHz to 18 GHz has been proposed. This system is especially designed to operate as a direction-finding system. Five layers of polarizers are used to introduce slant polarization to enable the biconical antenna to receive both horizontal and vertical polarizations. This system has been simulated, optimized, fabricated and measured. A good agreement between the measured and simulated results is observed.

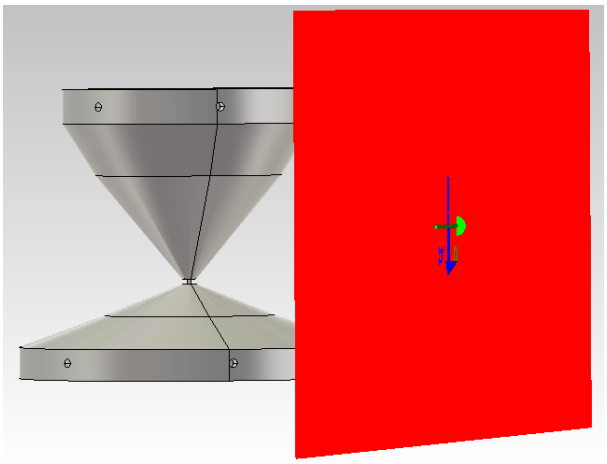

(a)

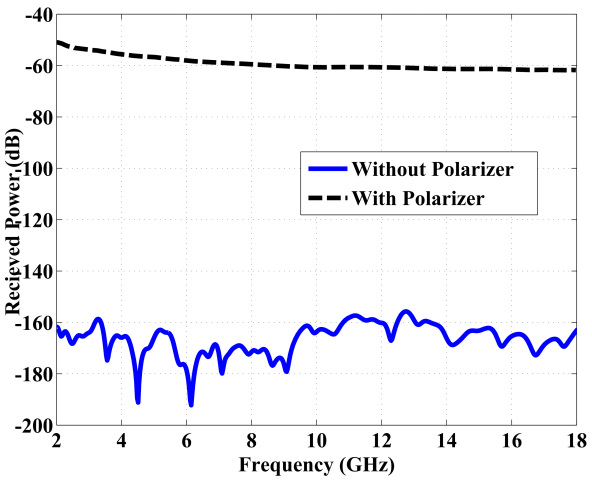

(b)

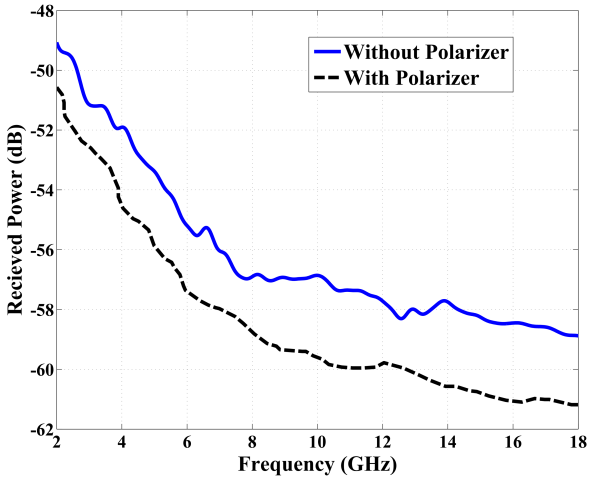

(c)

Figure 50: Simulation of the effect of polarizers by illuminating the structure with a horizontal polarized electromagnetic wave (a) the antenna without and with polarizers. (b) Received power of the horizontal polarized electromagnetic field with and without polarizers. (c) Received power of the vertical polarized electromagnetic field with and without polarizers. The red color plane is the plane of he incident wave containing the electric and magnetic fields.

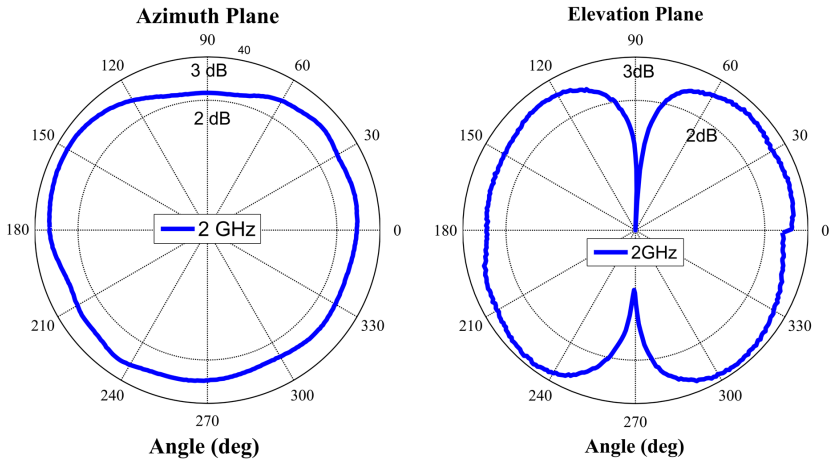

(a)

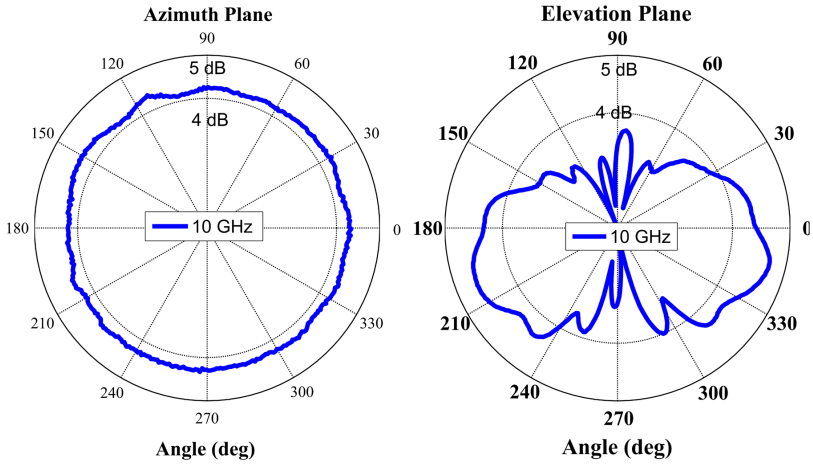

(b)

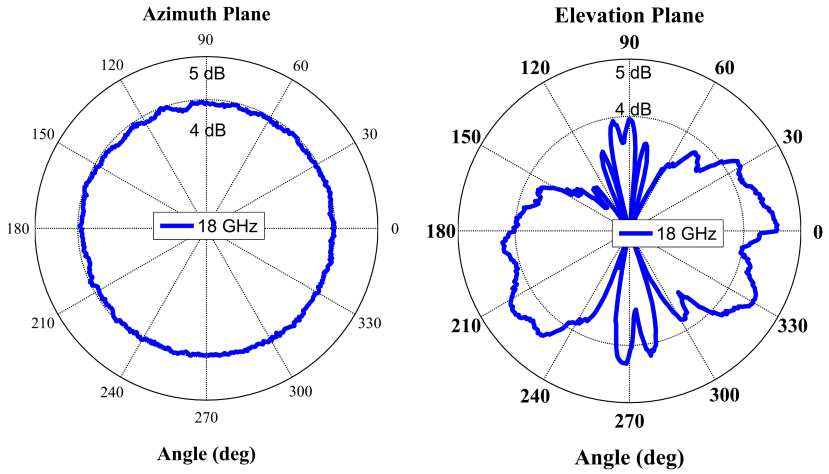

(c)

Figure 51: Measured azimuth and elevation radiation patterns (a) 2 GHz (b) 10 GHz (c) 18 GHz.

Figure 52: (a) Fabricated biconical antenna with polarizers. (b) Measurement of the fabricated sample in anechoic chamber.

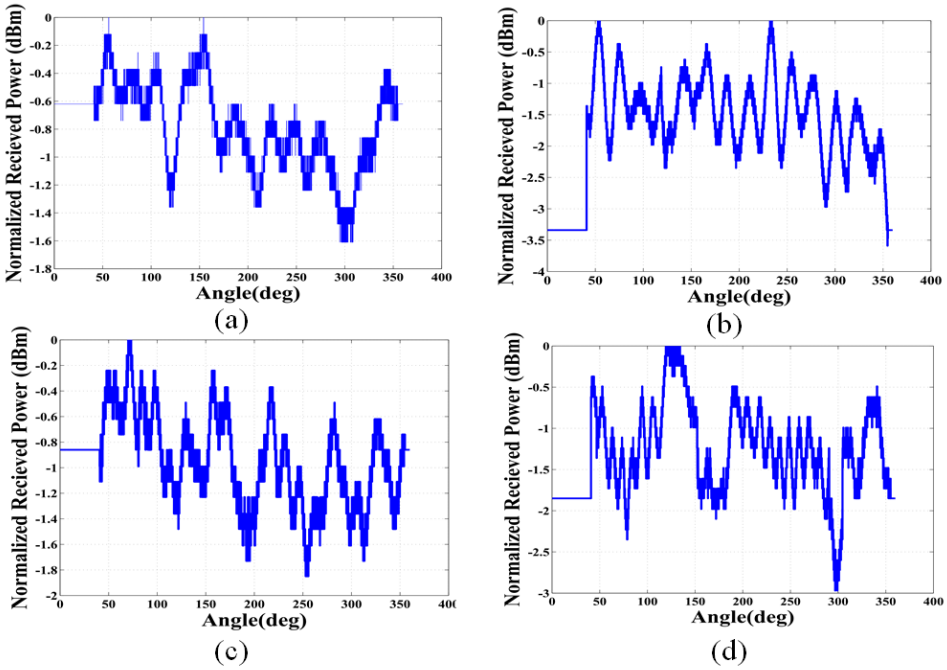

Figure 53: Measured received power in azimuth pattern at different frequencies (a) 2 GHz; (b) 10 GHz; (c) 14 GHz; (d) 18 GHz.

Part IV
Conclusions

CHAPTER 8

CONCLUSIONS

Todays, to detects the location of unknown targets direction finding systems are used. Direction finding systems can be used in radio direction finder for cell phone services, satellite communication systems, medical applications and plane or automobile navigation systems.

Direction finding systems have three main parts: i) the antennas; ii) the receiver; iii) the signal processor and operator display software. This thesis focuses on the direction finding antenna part only. The antenna should have some strict specifications and the primary requirements are mentioned as follows:

i) The antenna should be wideband enough to cover most of the frequency bandwidth of unknown targets; ii) The antenna should have a minimum gain variation in the whole frequency bandwidth to reduce the range targets estimation errors; and, iii) The dimension and number of the antennas should be small as possible to be useful in low frequencies (below VHF band).

The main novelty of the thesis is proposing some reconfigurable antennas instead of ordinary and simple antennas to pass the above requirements and achieve better results compared with previous works. I also designed and fabricated two low frequency and wideband small size antennas.

Reconfirable antennas can detect targets with higher accuracy since the beam can be rotate electronically with higher resolutions. Therefore, we presented an ultra-wide band reconfigurable antenna in the frequency range from 8 GHz to 18 GHz (9), (see Chapter 2) and a UWB phased-array system with a total scanning angle of 56° from the frequency range of 6 GHz to 18 GHz (14) (see Chapetr 3). The lens

antenna creates four distinct radiation beams, each covering a scan angle of 40° in the azimuth plane. and about 30° in the elevation plane. The main advantage of the proposed structure lies in its simple design and high power handling capability. For the excitation a simple coax input and a single dielectric slab are used to manipulate the curvature of the wavefront and obtain a planar wavefront, without any need for multilayer dielectric structures such as Luneburg lens. This antenna has been fabricated and measured. The proposed parallel antenna has a smaller size, wider frequency bandwidth, and easier fabrication process due to using a single layer slab lens than the previous published papers.

The microstrip Rotman lens with eight input ports and ten output ports has been designed, optimized, and fabricated to achieve a minimum phase-error. Considering the properties such as power handling capability, high bandwidth, and small interelement spacing, an E-plane double-ridged horn antenna is designed as the radiating element. Due to the small interelement spacing, it is required to feed the horn antenna from the waveguide cross section. Therefore, an optimized wideband end-launcher coaxial to waveguide adapter has also been designed. This phased-array system has been comprehensively simulated, optimized, fabricated, and measured. Each one of these antennas can be used individually or together with other antennas. The antenna a has wider frequency bandwidth and smaller dimensions than the other proposed Rotman lenses.

To detect higher attitude targets such as aircrafts, we also proposed a multi-feed multi-beam parabolic reflector antenna (see Chapetr 4). We also proposed a method to control the feed arrangement of the feed positions to obtain maximum efficiency and gain. The method is faster than the previous ones. Two types of broadband antennas from 6 GHz to 18 GHz are designed to feed the reflector: i) a double-ridged horn antenna; and, ii) antipodal Vivaldi antenna. The method is approved with HFSS using a genetic al-

gorithm (GA) and is a good substitution for previous optimization methods (15). The proposed reflector antenna fed by two types of antennas (Vivaldi and double-ridged horn antenna) has a wider frequency bandwidth and more stable radiation patterns than the previous antennas.

Direction finding systems can be used for wireless and medical applications such as electromagnetic torso image systems. Therefore, a wideband and miniaturized reconfigurable antenna using a metasurface from 3.5 GHz to 5.5 GHz is proposed (see Chapter 5). This antenna has a simple structure and uses one tapered cross-shaped radiation slot with four parasitic slots and eight PIN diodes. Four diodes are used to control four reflector slots to steer the radiation pattern and other diodes are used to switch the feeding path to modify the polarization of the radiated beam. The metasurface behaves as a reflector and reduces the back lobe. Simulation results are illustrated. The main lobe has a minimum gain of 7 dBi and can be steered along 5 positions 0° and $\pm 17^\circ$ in two perpendicular elevation planes. For a medical application, such as tumor detection, a miniaturized wideband reconfigurable microstrip slot antenna with a grid mesh microstrip surface is proposed. The antenna works from 3.5 GHz to 5.5 GHz. The antenna beam is steered from 0° to $\pm 30^\circ$in the zx and zy planes. Ten PIN diodes are used to select the desired direction and rotate the antenna beam in two principal surfaces. The antenna is fabricated and tested and there is a good agreement between the simulation and measurement results. The antenna can be used in the UHF band. The proposed antenna has a wider frequency bandwidth, smaller dimensions, wider steering angles, and lower number of the PIN diodes than the previous papers.

As mentioned before, to cover low frequency bandwidth (below VHF band) a UWB TEM horn antenna for the frequency range from 20 MHz to 2.5 GHz (12) (see Chapter 6), and a dualband ultra wide band bicone antenna for the frequency range from 2 GHz to 18 GHz (10) (see Chapter 7) as the reference

antenna are proposed. The biconical antenna has five layers of polarizers to introduce slant polarization and enable the biconical antenna to receive both horizontal and vertical polarizations. Direction finding systems compare the target unknown signals with reference antennas to find the approximate location of them. The proposed biconical antenna has the lower ripples on the radiation patterns than the previous works and can receive both vertical and horizontal polarizations while others cannot.

The TEM horn antenna passive bandwidth is from 200 MHz to 2.5 GHz. A NIC circuit is used to reduce the capacitive behavior of the antenna from 20 MHz to 200 MHz, which also improves the return loss. By using a simple RF switch in the antenna feed, the NIC can be switched in and out of the circuit. The insertion loss of the NIC circuit varies between 2.9 dB and 4.6 dB over the frequency band from 20 MHz to 200 MHz. This system has been simulated, optimized, fabricated, and measured. The proposed TEM horn antenna with a NIC circuit has a wider frequency bandwidth, and a smaller size than the previous papers.

To measure the RF power capability of the proposed lens antenna a waveguide directional coupler is proposed (26) (see Appendix 8). The coupler works in the 6 GHz to 18 GHz band, the VSWR of each port is under 1.5, the minimum directivity is 15 dB, and the coupling coefficient is -50 dB. To reduce the return loss, the ridge has been designed with an exponential taper, and some gaps have been added to the connector pins. This structure has been fabricated, and an excellent agreement between measured and simulated results is achieved. The proposed coupler has a wider bandwidth, lower coupling coefficient, and the ripple on its responses than the previous directional coupler specifications.

Appendices

Appendix A

DOUBLE RIDGED WAVEGUIDE DIRECTIONAL UWB COUPLER

A.1 Introduction of a directional coupler

While the thesis focuses on designing some wideband reconfigurable antennas, I have provided some contributions that one of them is collected in the appendices. To measure RF-power or signal sampling in transmitters and direction finding systems couplers can be used. The frequency bandwidth which is considered for most of direction finding systems is from 6 GHz to 18 GHz. Therefore, a directional coupler operating at the C, X, Ka and Ku bands from 6 GHz to 18 GHz is designed and fabricated, where it is required to sample high-power and ultra-wide band (UWB) signals. Its coupling coefficient is below -50 dB and this feature presents the advantage of eliminating the attenuator at the coupling port when sampling in high power applications. The design solution is based on the introduction of a tapered ridge to obtain wider frequency bandwidth. The traditional design of a microwave coupler was based on two waveguides that are coupled through small apertures so that the field could be considered uniform over the apertures. The number of apertures controls the amount of coupling. In the case of a single aperture, the bandwidth is about 5-7 %, which is not sufficient for making a UWB coupler. Augmenting the number of coupling apertures to improve the frequency bandwidth increases the mutual coupling, which is not desirable (114). Various improvements have been made recently (115; 116). To the best of our knowledge, there is not in the literature a directional coupler that meets all the features described

Appendix A (Continued)

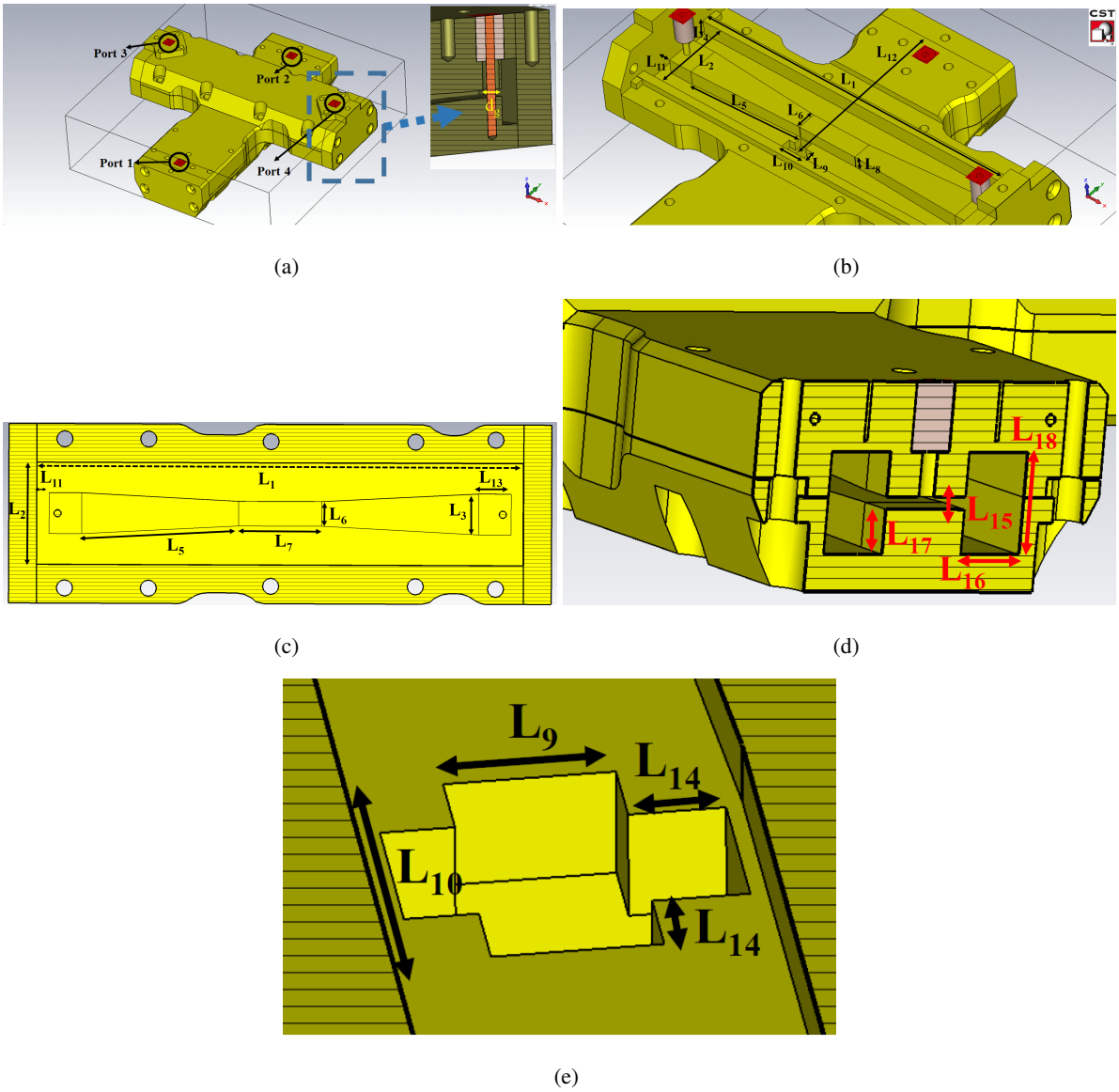

Figure 54: Geometry and parameters of the waveguide directional coupler (a) top view, (b) inside view, (c) one waveguide view, (d) side view (e) coupling hole view. The actual values of the dimensions are given in Table I.

above. The high-power requirement demands that waveguides be considered. In fact, microstrip technology cannot be used because it cannot handle high power levels, even though it satisfies the bandwidth requirements (116; 117).

Appendix A (Continued)

Other types of microwave couplers such as those based on ferrites cannot be considered because of their high losses. On the other hand, coaxial and waveguide directional couplers are the most common high-power solutions when bandwidth requirements are not critical. Hence, we start from a single hole coupler based on waveguide technology to handle high power, and then we improve the design to achieve the UWB requirements.

A.2 Design procedure of designing waveguide directional coupler

The proposed UWB double ridge waveguide coupler is shown in Fig. 54, and it was designed to satisfy requirements including bandwidth, directivity, reduced size, power handling, losses and coupling coefficient(118),(119). The main features of our design are: (1) using a tapered ridge and (2) introducing a gap between the wall and the connector pin. Both these features improve the return loss and extend it over 3 octaves. The starting point of the design is the standard waveguide WRD650, which has the cutoff frequencies of the first two lowest order modes at 3.31 GHz and 18 GHz. An approximation of the dominant mode cutoff frequency is (120),(121)

$$f_c = \frac{3\cdot 10^8}{2(a-s)}\left[1+\frac{4}{\pi}\left(1+0.2\sqrt{\frac{b}{a-s}}\right)\left(\frac{b}{a-s}\right)\ln\csc\frac{\pi d}{2b} \quad +\left(2.45+0.2\frac{s}{a}\right)\left(\frac{sb}{d(a-s)}\right)\right]^{-0.5} \tag{A.1}$$

where the symbols used are defined in Fig 55. The power handling capability of waveguides is related to the maximum power that can be transmitted without causing an electric arc inside the waveguides. One major limiting factor is the distance between metal edges inside waveguides. For double ridge waveguides, this distance is shorter because it corresponds to the separation distance d between upper and lower ridges, shown in Fig 55. Accordingly, it is apparent that these waveguides can handle lower

Appendix A (Continued)

TABLE XII: Physical dimensions of the coupler

Parameter	L_1	L_2	L_3	L_4	L_5	L_6	L_7
Dimension (mm)	87.14	18.29	7.3	3.6	28.19	4.4	14.86
Parameter	L_8	L_9	L_{10}	L_{11}	L_{12}	L_{13}	L_{14}
Dimension (mm)	2.81	3	6	2.21	38	5.8	1.5
Parameter	L_{15}	L_{16}	L_{17}	L_{18}	d_g		
Dimension (mm)	1	5.5	3.6	8.15	2.5		

power than conventional rectangular waveguides. Fortunately, the ranges of levels of power handling capability are acceptable and still significantly higher than those achievable with other couplers such as microstrips. For the WRD650 waveguide, the average power handling is 1.5 KW, and the peak power handling is about 3 KW (122).

The directivity of the cross waveguide depends on the location of the coupling aperture and is defined as (120)

$$D = -20\log\frac{B_a}{A_a}\ \text{dB}, \tag{A.2}$$

where A_a and B_a are the transmission coefficients in the forward and backward directions, respectively, given by (120)

$$A_a = -\frac{Mh_x h_z k_c}{abs_a} - j\frac{Pe_y^2 k^2}{2abs_a\beta}, \tag{A.3}$$

$$B_a = -j\frac{Pe_y^2 k^2}{2abs_a\beta}. \tag{A.4}$$

Appendix A (Continued)

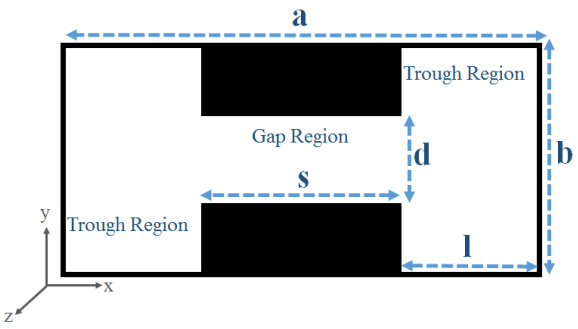

Figure 55: Cross section of the proposed double ridge waveguide coupler.

In the previous expressions, P and M are the electric and magnetic dipoles of the coupling aperture and depend on its shape. These quantities have been determined experimentally for various aperture shapes (114). Our design uses the cross shape because the coupling coefficients for the magnetic and electric fields can be adjusted independently(123). Previous double ridge cross directional couplers use multiple holes to increase the bandwidth, which results in larger coupling coefficient and bulky structures(122). One goal of the proposed design is to avoid the presence of an attenuator, which is required when the coupler is used to measure RF power. In fact, when the output RF power is high, attenuators must be used before RF power meters to protect them against damage. This goal is met by achieving a low value of the coupling coefficient below -50 dB by using only one coupling hole. The drawback of using only one hole is that the bandwidth is reduced; however the reduction in bandwidth is compensated for by introducing the tapering in the internal ridges. A similar approach was used for the different context of the transition from a waveguide to a coaxial cable in (124). In addition, the advantages of using only one hole include (i) a shorter overall length of the coupler and (ii) lower losses. The expressions given in equations (A.3) and (A.4) depend on the TE modes in the trough region, which may be approximated as (125)

Appendix A (Continued)

$$e_x = h_y = \frac{E_x}{E_0} = \frac{\eta k}{\beta}\frac{H_y}{E_0} = \cos\frac{k_c s}{2} \times \sum_{n=1}^{\infty} \frac{2b(\gamma_n^2 + k_c^2)}{(n\pi)^2 \gamma_n \sinh k_{nx} l} \sin\frac{n\pi d}{b} \cosh(\gamma_n x) \sin\frac{n\pi y}{b} \tag{A.5}$$

$$e_y = h_x = \frac{E_y}{E_0} = \frac{-\eta k}{\beta}\frac{H_x}{E_0} = \frac{d}{b}\frac{\cos\frac{k_c s}{2}}{\sin k_c l} \sin k_c x + \sum_{n=1}^{\infty} \frac{2\sin\frac{n\pi d}{b}}{(n\pi)\sinh\gamma_n l} \cos\frac{k_c s}{2} \sinh(\gamma_n x) \sin\frac{n\pi y}{b} \tag{A.6}$$

$$h_z = \frac{-j\eta k}{k_c}\frac{H_z}{E_0} = \cos\frac{k_c s}{2}\left[\frac{d}{b}\frac{\cos k_c x}{\sin k_c l} \times \sum_{n=1}^{\infty} \frac{2k_c \sin\frac{n\pi d}{b}}{n\pi\gamma_n \sinh(\gamma_n l)} \cos\frac{k_c s}{2} \cos\gamma_n x \cos\frac{n\pi y}{b}\right] \tag{A.7}$$

where

$$\beta^2 = k_0^2 - k_c^2,\ \gamma_n^2 = \left(\frac{n\pi}{b}\right)^2 - k_c^2. \tag{A.8}$$

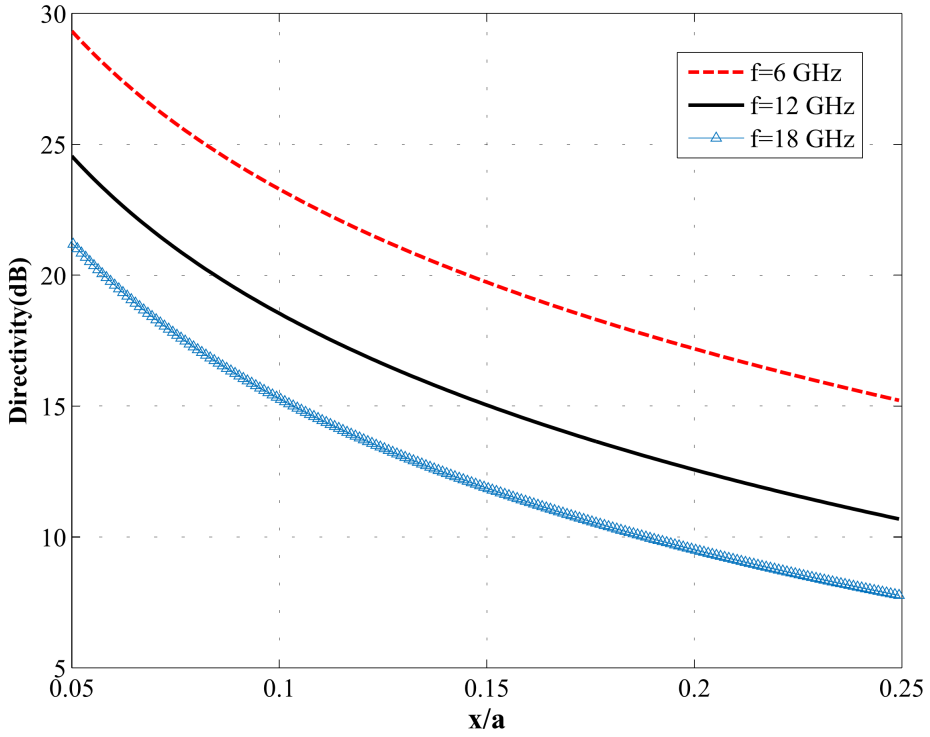

Figure 56: Directivity values versus position of the hole in three different frequencies.

Appendix A (Continued)

The values of the directivity as a function of the position of the coupling aperture are shown in Fig 56. This figure indicates that the directivity decreases when the operating frequency is increased and that the coupling aperture must be located as close as possible to the waveguide wall to obtain the desired value of 15 dB. In principle, this design approach is applicable to other frequency ranges; however, one should bear in mind that below 1 GHz the dimensions of the waveguide increase dramatically and above 30 GHz mechanical fabrication tolerances are very challenging. To reduce the reflection coefficient, the ridges of the waveguides have been tapered using a particle swarm optimization (PSO) algorithm, as it is implemented in the CST software. This results into a profile are similar to an exponential tapering, (see Fig 54). Another parameter that was optimized with the PSO algorithm to reduce the reflection coefficient is d_g, which is shown in Fig 54.

A.3 Fabrication and measurement results

The UWB double ridge cross waveguide coupler was designed using both HFSS and CST, fabricated according to the optimized dimensions reported in Table I, and it is shown in Fig 57. Scattering parameters were measured to verify the validity of the design with a HP8722D network analyzer and the measurement results are given in Fig 56. The measured directivity is shown in Fig 58 and it satisfies the design goal by exceeding the minimum requirement of 15 dB. There is an excellent agreement between the measured and the simulation results obtained with CST and HFSS. The differences between simulation and measurements may be due to mechanical tolerances and the SMA connectors used, which were of low loss type. Measured and simulated results have been shown in Fig 56. As shown in Fig 57, one arm along the direct pass is longer than the other arm. The reason is that in the trough pass higher evanescent modes are created near the aperture hole and, with one arm longer than the other,

Appendix (Continued)

these modes cannot reach the through port. Another reason is that the ridge taper can be designed to be smoother so that S_{11} improves for high power pass.

Appendix (Continued)

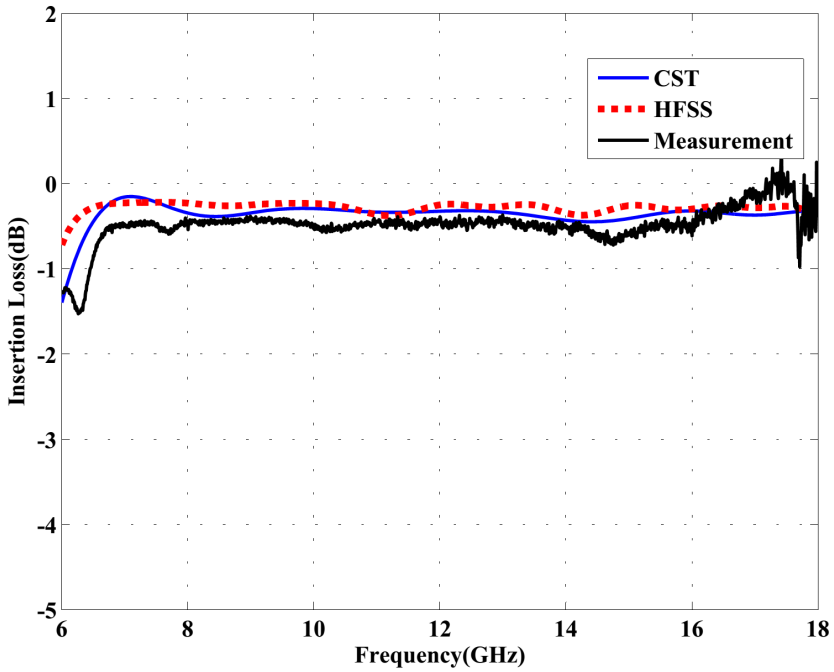

(a)

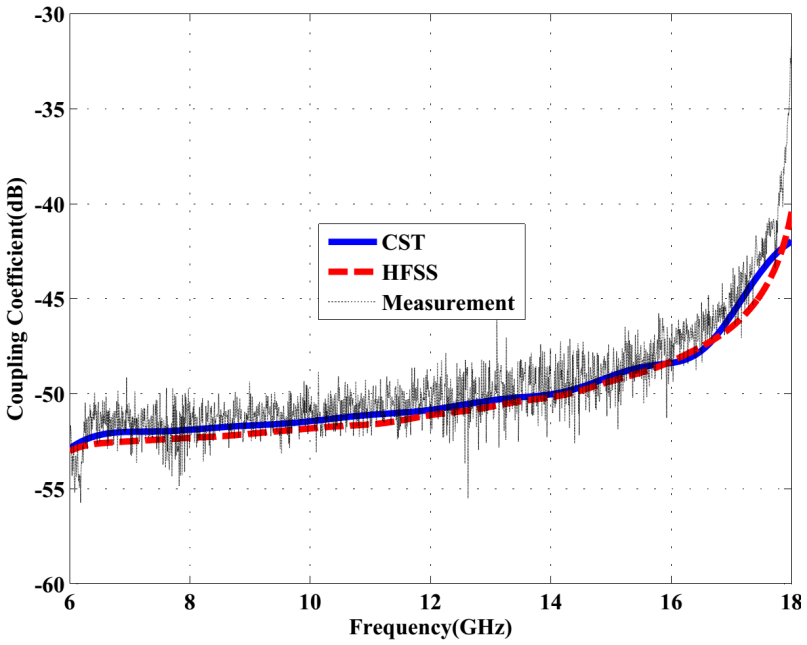

(b)

Appendix (Continued)

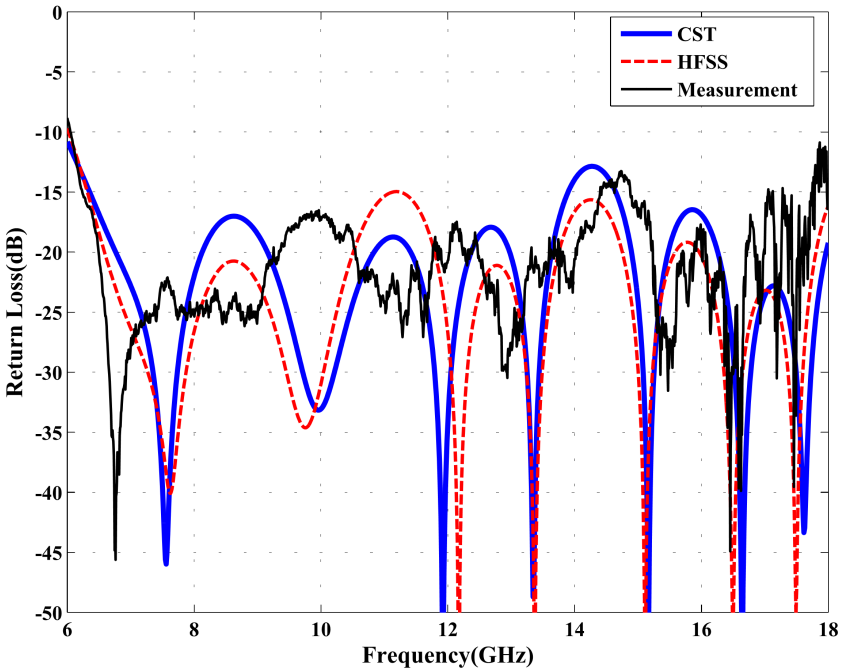

(c)

Figure 56: Measured and simulated results of (a) insertion Loss, (b) coupling coefficient, (c) return loss of the coupler

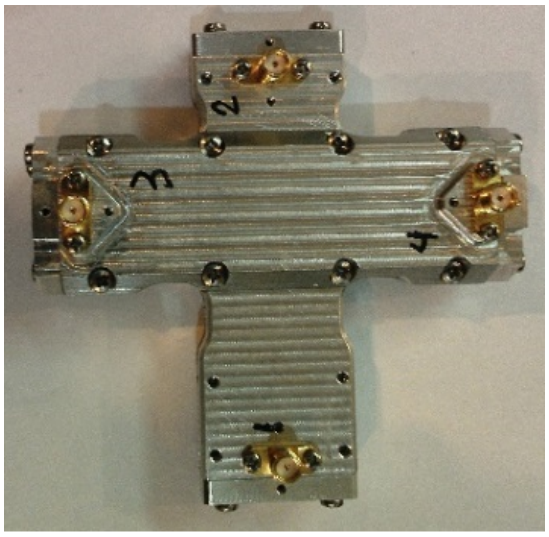

Figure 57: Photo of the coupler.

Appendix (Continued)

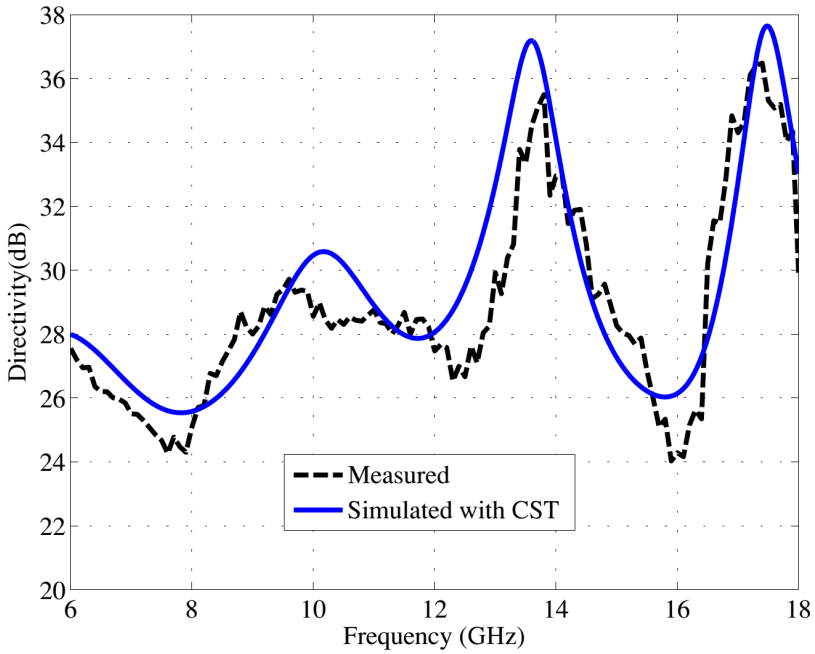

Figure 58: Measured and simulated directivity.

Appendix A

AUTHOR'S BIOGRAPHY

Omid Manoochehri received the B.S. degree in electrical engineering from the Shiraz University of Technology, Shiraz, Iran, in 2007, and the M.S. degree in electrical engineering from Tarbiat Modares University, Tehran, Iran, in 2011. He has been pursuing the Ph.D. degree at the University of Illinois at Chicago, Chicago, IL, USA, since 2015. His current research interests include miniaturized frequency-selective surfaces, phase-array design, scattering of electromagnetic waves, reconfigurable antenna design, LNA and power amplifier design and beam-forming systems.

Appendix B

COPYRIGHT PERMISSIONS

In this appendix, we present the copyright permissions for the articles, whose contents were used in this thesis. The list of the articles includes IEEE Antennas and Wireless Propagation Letters (12). A conference paper (37) following by articles in Journal of IEEE Transactions on Antennas and Propagation (9) and A journal paper in IEEE Transactions on Microwave Theory and Techniques(14). Two conference paper (15; 25). Two journal papers in Microwave and Optical Technology Letters(10; 26).

Title: Wide band multi-beam cylindrical lens

Conference Proceedings: Antennas and Propagation & USNC/URSI National Radio Science Meeting, 2017 IEEE International Symposium on

Author: Amin Darvazehban

Publisher: IEEE

Date: July 2017

Thesis / Dissertation Reuse

The IEEE does not require individuals working on a thesis to obtain a formal reuse license, however, you may print out this statement to be used as a permission grant:

Requirements to be followed when using any portion (e.g., figure, graph, table, or textual material) of an IEEE copyrighted paper in a thesis:

1) In the case of textual material (e.g., using short quotes or referring to the work within these papers) users must give full credit to the original source (author, paper, publication) followed by the IEEE copyright line © 2011 IEEE.
2) In the case of illustrations or tabular material, we require that the copyright line © [Year of original publication] IEEE appear prominently with each reprinted figure and/or table.
3) If a substantial portion of the original paper is to be used, and if you are not the senior author, also obtain the senior author's approval.

Requirements to be followed when using an entire IEEE copyrighted paper in a thesis:

1) The following IEEE copyright/ credit notice should be placed prominently in the references: © [year of original publication] IEEE. Reprinted, with permission, from [author names, paper title, IEEE publication title, and month/year of publication]
2) Only the accepted version of an IEEE copyrighted paper can be used when posting the paper or your thesis on-line.
3) In placing the thesis on the author's university website, please display the following message in a prominent place on the website: In reference to IEEE copyrighted material which is used with permission in this thesis, the IEEE does not endorse any of [university/educational entity's name goes here]'s products or services. Internal or personal use of this material is permitted. If interested in reprinting/republishing IEEE copyrighted material for advertising or promotional purposes or for creating new collective works for resale or redistribution, please go to http://www.ieee.org/publications_standards/publications/rights/rights_link.html to learn how to obtain a License from RightsLink.

If applicable, University Microfilms and/or ProQuest Library, or the Archives of Canada may supply single copies of the dissertation.

Thesis / Dissertation Reuse

The IEEE does not require individuals working on a thesis to obtain a formal reuse license, however, you may print out this statement to be used as a permission grant:

Requirements to be followed when using any portion (e.g., figure, graph, table, or textual material) of an IEEE copyrighted paper in a thesis:

1) In the case of textual material (e.g., using short quotes or referring to the work within these papers) users must give full credit to the original source (author, paper, publication) followed by the IEEE copyright line © 2011 IEEE.
2) In the case of illustrations or tabular material, we require that the copyright line © [Year of original publication] IEEE appear prominently with each reprinted figure and/or table.
3) If a substantial portion of the original paper is to be used, and if you are not the senior author, also obtain the senior author's approval.

Requirements to be followed when using an entire IEEE copyrighted paper in a thesis:

1) The following IEEE copyright/ credit notice should be placed prominently in the references: © [year of original publication] IEEE. Reprinted, with permission, from [author names, paper title, IEEE publication title, and month/year of publication]
2) Only the accepted version of an IEEE copyrighted paper can be used when posting the paper or your thesis on-line.
3) In placing the thesis on the author's university website, please display the following message in a prominent place on the website: In reference to IEEE copyrighted material which is used with permission in this thesis, the IEEE does not endorse any of [university/educational entity's name goes here]'s products or services. Internal or personal use of this material is permitted. If interested in reprinting/republishing IEEE copyrighted material for advertising or promotional purposes or for creating new collective works for resale or redistribution, please go to http://www.ieee.org/publications_standards/publications/rights/rights_link.html to learn how to obtain a License from RightsLink.

If applicable, University Microfilms and/or ProQuest Library, or the Archives of Canada may supply single copies of the dissertation.

Title: Ultra-Wideband Scanning Antenna Array With Rotman Lens

Author: Amin Darvazehban

Publication: Microwave Theory and Techniques, IEEE Transactions on

Publisher: IEEE

Date: Sept. 2017

Thesis / Dissertation Reuse

The IEEE does not require individuals working on a thesis to obtain a formal reuse license, however, you may print out this statement to be used as a permission grant:

Requirements to be followed when using any portion (e.g., figure, graph, table, or textual material) of an IEEE copyrighted paper in a thesis:

1) In the case of textual material (e.g., using short quotes or referring to the work within these papers) users must give full credit to the original source (author, paper, publication) followed by the IEEE copyright line © 2011 IEEE.
2) In the case of illustrations or tabular material, we require that the copyright line © [Year of original publication] IEEE appear prominently with each reprinted figure and/or table.
3) If a substantial portion of the original paper is to be used, and if you are not the senior author, also obtain the senior author's approval.

Requirements to be followed when using an entire IEEE copyrighted paper in a thesis:

1) The following IEEE copyright/ credit notice should be placed prominently in the references: © [year of original publication] IEEE. Reprinted, with permission, from [author names, paper title, IEEE publication title, and month/year of publication]
2) Only the accepted version of an IEEE copyrighted paper can be used when posting the paper or your thesis on-line.
3) In placing the thesis on the author's university website, please display the following message in a prominent place on the website: In reference to IEEE copyrighted material which is used with permission in this thesis, the IEEE does not endorse any of [university/educational entity's name goes here]'s products or services. Internal or personal use of this material is permitted. If interested in reprinting/republishing IEEE copyrighted material for advertising or promotional purposes or for creating new collective works for resale or redistribution, please go to http://www.ieee.org/publications_standards/publications/rights/rights_link.html to learn how to obtain a License from RightsLink.

If applicable, University Microfilms and/or ProQuest Library, or the Archives of Canada may supply single copies of the dissertation.

Title: An Active 20-MHz to 2.5-GHz UWB Receiver Antenna System Using a TEM Horn

Author: Mohammad Ali Salari

Publication: IEEE Antennas and Wireless Propagation Letters

Publisher: IEEE

Date: 2017

Thesis / Dissertation Reuse

The IEEE does not require individuals working on a thesis to obtain a formal reuse license, however, you may print out this statement to be used as a permission grant:

Requirements to be followed when using any portion (e.g., figure, graph, table, or textual material) of an IEEE copyrighted paper in a thesis:

1) In the case of textual material (e.g., using short quotes or referring to the work within these papers) users must give full credit to the original source (author, paper, publication) followed by the IEEE copyright line © 2011 IEEE.
2) In the case of illustrations or tabular material, we require that the copyright line © [Year of original publication] IEEE appear prominently with each reprinted figure and/or table.
3) If a substantial portion of the original paper is to be used, and if you are not the senior author, also obtain the senior author's approval.

Requirements to be followed when using an entire IEEE copyrighted paper in a thesis:

1) The following IEEE copyright/ credit notice should be placed prominently in the references: © [year of original publication] IEEE. Reprinted, with permission, from [author names, paper title, IEEE publication title, and month/year of publication]
2) Only the accepted version of an IEEE copyrighted paper can be used when posting the paper or your thesis on-line.
3) In placing the thesis on the author's university website, please display the following message in a prominent place on the website: In reference to IEEE copyrighted material which is used with permission in this thesis, the IEEE does not endorse any of [university/educational entity's name goes here]'s products or services. Internal or personal use of this material is permitted. If interested in reprinting/republishing IEEE copyrighted material for advertising or promotional purposes or for creating new collective works for resale or redistribution, please go to http://www.ieee.org/publications_standards/publications/rights/rights_link.html to learn how to obtain a License from RightsLink.

If applicable, University Microfilms and/or ProQuest Library, or the Archives of Canada may supply single copies of the dissertation.

Title: A dual-polarized biconical antenna for direction finding applications from 2 to 18 GHz

Author: Omid Manoochehri, Amin Darvazehban, Mohammad Ali Salari, et al

Publication: Microwave and Optical Technology Letters

Publisher: John Wiley and Sons

Date: Apr 24, 2018

Order Completed

Thank you for your order.

This Agreement between University of Illinois at Chicago -- Omid Manoochehri ("You") and John Wiley and Sons ("John Wiley and Sons") consists of your license details and the terms and conditions provided by John Wiley and Sons and Copyright Clearance Center.

Your confirmation email will contain your order number for future reference.

printable details

License Number	4354280791627
License date	May 22, 2018
Licensed Content Publisher	John Wiley and Sons
Licensed Content Publication	Microwave and Optical Technology Letters
Licensed Content Title	A dual-polarized biconical antenna for direction finding applications from 2 to 18 GHz
Licensed Content Author	Omid Manoochehri, Amin Darvazehban, Mohammad Ali Salari, et al
Licensed Content Date	Apr 24, 2018
Licensed Content Volume	60
Licensed Content Issue	6
Licensed Content Pages	7
Type of use	Dissertation/Thesis
Requestor type	Author of this Wiley article
Format	Print and electronic
Portion	Full article
Will you be translating?	No
Title of your thesis / dissertation	Wideband reconfigurable antenna designs
Expected completion date	May 2019
Expected size (number of pages)	120
Requestor Location	University of Illinois at Chicago 851 S Morgan St CHICAGO, IL 60607 United States Attn: University of Illinois at Chicago

Publisher Tax ID	EU826007151
Total	0.00 USD

Would you like to purchase the full text of this article? If so, please continue on to the content ordering system located here: Purchase PDF

If you click on the buttons below or close this window, you will not be able to return to the content ordering system.

ORDER MORE CLOSE WINDOW

Title: A new method for designing high efficiency multi feed multi beam reflector antennas

Conference Proceedings: Electromagnetics in Advanced Applications (ICEAA), 2017 International Conference on

Author: Omid Manoochehri

Publisher: IEEE

Date: Sept. 2017

Thesis / Dissertation Reuse

The IEEE does not require individuals working on a thesis to obtain a formal reuse license, however, you may print out this statement to be used as a permission grant:

Requirements to be followed when using any portion (e.g., figure, graph, table, or textual material) of an IEEE copyrighted paper in a thesis:

1) In the case of textual material (e.g., using short quotes or referring to the work within these papers) users must give full credit to the original source (author, paper, publication) followed by the IEEE copyright line © 2011 IEEE.
2) In the case of illustrations or tabular material, we require that the copyright line © [Year of original publication] IEEE appear prominently with each reprinted figure and/or table.
3) If a substantial portion of the original paper is to be used, and if you are not the senior author, also obtain the senior author's approval.

Requirements to be followed when using an entire IEEE copyrighted paper in a thesis:

1) The following IEEE copyright/ credit notice should be placed prominently in the references: © [year of original publication] IEEE. Reprinted, with permission, from [author names, paper title, IEEE publication title, and month/year of publication]
2) Only the accepted version of an IEEE copyrighted paper can be used when posting the paper or your thesis on-line.
3) In placing the thesis on the author's university website, please display the following message in a prominent place on the website: In reference to IEEE copyrighted material which is used with permission in this thesis, the IEEE does not endorse any of [university/educational entity's name goes here]'s products or services. Internal or personal use of this material is permitted. If interested in reprinting/republishing IEEE copyrighted material for advertising or promotional purposes or for creating new collective works for resale or redistribution, please go to http://www.ieee.org/publications_standards/publications/rights/rights_link.html to learn how to obtain a License from RightsLink.

If applicable, University Microfilms and/or ProQuest Library, or the Archives of Canada may supply single copies of the dissertation.

Title:	UWB double-ridge waveguide coupler with low loss
Author:	Omid Manoochehri, Amin Darvazehban, Danilo Erricolo
Publication:	Microwave and Optical Technology Letters
Publisher:	John Wiley and Sons
Date:	May 27, 2017

Order Completed

Thank you for your order.

This Agreement between University of Illinois at Chicago -- Omid Manoochehri ("You") and John Wiley and Sons ("John Wiley and Sons") consists of your license details and the terms and conditions provided by John Wiley and Sons and Copyright Clearance Center.

Your confirmation email will contain your order number for future reference.

printable details

License Number	4396381367884
License date	Jul 26, 2018
Licensed Content Publisher	John Wiley and Sons
Licensed Content Publication	Microwave and Optical Technology Letters
Licensed Content Title	UWB double-ridge waveguide coupler with low loss
Licensed Content Author	Omid Manoochehri, Amin Darvazehban, Danilo Erricolo
Licensed Content Date	May 27, 2017
Licensed Content Volume	59
Licensed Content Issue	8
Licensed Content Pages	5
Type of use	Dissertation/Thesis
Requestor type	Author of this Wiley article
Format	Print and electronic
Portion	Full article
Will you be translating?	No
Title of your thesis / dissertation	Wideband reconfigurable antenna designs
Expected completion date	May 2019
Expected size (number of pages)	120
Requestor Location	University of Illinois at Chicago 851 S Morgan St CHICAGO, IL 60607 United States Attn: University of Illinois at Chicago
Publisher Tax ID	EU826007151

Total	0.00 USD

Would you like to purchase the full text of this article? If so, please continue on to the content ordering system located here: Purchase PDF

If you click on the buttons below or close this window, you will not be able to return to the content ordering system.

ORDER MORE CLOSE WINDOW

Title: A Parallel Plate Ultrawideband Multibeam Microwave Lens Antenna
Author: Omid Manoochehri
Publication: Antennas and Propagation, IEEE Transactions on
Publisher: IEEE
Date: Sept. 2018

Thesis / Dissertation Reuse

The IEEE does not require individuals working on a thesis to obtain a formal reuse license, however, you may print out this statement to be used as a permission grant:

Requirements to be followed when using any portion (e.g., figure, graph, table, or textual material) of an IEEE copyrighted paper in a thesis:

1) In the case of textual material (e.g., using short quotes or referring to the work within these papers) users must give full credit to the original source (author, paper, publication) followed by the IEEE copyright line © 2011 IEEE.
2) In the case of illustrations or tabular material, we require that the copyright line © [Year of original publication] IEEE appear prominently with each reprinted figure and/or table.
3) If a substantial portion of the original paper is to be used, and if you are not the senior author, also obtain the senior author's approval.

Requirements to be followed when using an entire IEEE copyrighted paper in a thesis:

1) The following IEEE copyright/ credit notice should be placed prominently in the references: © [year of original publication] IEEE. Reprinted, with permission, from [author names, paper title, IEEE publication title, and month/year of publication]
2) Only the accepted version of an IEEE copyrighted paper can be used when posting the paper or your thesis on-line.
3) In placing the thesis on the author's university website, please display the following message in a prominent place on the website: In reference to IEEE copyrighted material which is used with permission in this thesis, the IEEE does not endorse any of [university/educational entity's name goes here]'s products or services. Internal or personal use of this material is permitted. If interested in reprinting/republishing IEEE copyrighted material for advertising or promotional purposes or for creating new collective works for resale or redistribution, please go to http://www.ieee.org/publications_standards/publications/rights/rights_link.html to learn how to obtain a License from RightsLink.

If applicable, University Microfilms and/or ProQuest Library, or the Archives of Canada may supply single copies of the dissertation.

CITED LITERATURE

1. Li, W.-R., Chu, C.-Y., Lin, K.-H., and Chang, S.-F.: Switched-beam antenna based on modified butler matrix with low sidelobe level. Electronics Letters, 40(5):290–292, 2004.

2. Cheng, Y. J., Hong, W., and Wu, K.: Millimeter-wave substrate integrated waveguide multibeam antenna based on the parabolic reflector principle. IEEE Transactions on Antennas and Propagation, 56(9):3055–3058, Sept 2008.

3. Vesnik, M. V.: Compact multibeam reflector antenna for satellite TV signal receiving. 2009.

4. Mailloux, R. J.: Phased Array Antenna Handbook. Boston, Artech House, 1994.

5. Demmerle, F. and Wiesbeck, W.: A biconical multibeam antenna for space-division multiple access. IEEE Transactions on Antennas and Propagation, 46(6):782–787, 1998.

6. Klukas, R. and Fattouche, M.: Line-of-sight angle of arrival estimation in the outdoor multipath environment. IEEE Trans. Veh. Technol., 47(1):342–351, Feb 1998.

7. Lipsky, S. E.: Microwave passive direction finding. SciTech Publishing, 2004.

8. Lie, J. P., See, C. M., and Ng, B. P.: Ultra wideband direction finding using digital channelization receiver architecture. IEEE communications letters, 10(2):85–87, 2006.

9. Manoochehri, O., Darvazehban, A., Salari, M. A., Emadeddin, A., and Erricolo, D.: A parallel plate ultrawideband multibeam microwave lens antenna. IEEE Transactions on Antennas and Propagation, 66(9):4878–4883, Sept 2018.

10. Manoochehri, O., Darvazehban, A., Salari, M. A., Khaledian, S., Erricolo, D., and Smida, B.: A dual-polarized biconical antenna for direction finding applications from 2 to 18 ghz. Microwave and Optical Technology Letters, 60(6):1552–1558, 2018.

11. Emadeddin, A., Salari, M. A., Zoghi, M., Darvazehban, A., and Manoochehri, O.: A compact ultra-wideband multibeam antenna system. IEEE Transactions on Antennas and Propagation, 66(1):125–131, 2018.

12. Salari, M. A., Manoochehri, O., Darvazehban, A., and Erricolo, D.: An Active 20-MHz to 2.5-GHz UWB Receiver Antenna System Using a TEM Horn. IEEE Antennas and Wireless Propagation Letters, 16:2432–2435, 2017.

13. Darvazehban, A., Khaledian, S., Manoochehri, O., and Salari, M. A.: Design of a high-gain omni directional microstrip dipole array with low side lobe level in the elevation plane. Microwave and Optical Technology Letters, 60(3):709–713, 2018.

14. Darvazehban, A., Manoochehri, O., Salari, A., Dehkhoda, P., and Tavakoli, A.: Ultra-wideband scanning antenna array with Rotman lens. IEEE Transactions on Microwave Theory and Techniques, 65(9):3435–3442, 2017.

15. Manoochehri, O., Emadeddin, A., Darvazehban, A., and Erricolo, D.: A new method for designing high efficiency multi feed multi beam reflector antennas. In 2017 International Conference on Electromagnetics in Advanced Applications (ICEAA), pages 551–554, Sept 2017.

16. Darvazehban, A., Emadeddin, A., Manoochehri, O., and Erricolo, D.: Wide band multi-beam cylindrical lens. In 2017 IEEE International Symposium on Antennas and Propagation USNC/URSI National Radio Science Meeting, pages 507–508, July 2017.

17. Manoochehri, O., Farzami, F., Darvazehban, A., and Erricolo, D.: A non-resonant short monopole antenna with lumped circuit for wideband impedance matching. In 2016 USNC-URSI National Radio Science Meeting, Boulder, CO, USA., Jan. 2016.

18. Manoochehri, O., Farzami, F., Darvazehban, A., and Erricolo, D.: Higher order analytical models of planar mesh grids. In 2016 USNC-URSI National Radio Science Meeting, Boulder, CO, USA., Jan. 2016.

19. Darvazehban, A., Emadoddin, A., Manoochehri, O., and Erricolo, D.: Mutual coupling reduction in microstrip patch antenna. In 2016 USNC-URSI National Radio Science Meeting, Boulder, CO, USA., Jan. 2016.

20. Darvazehban, A., Manoochehri, O., Farzami, F., and Erricolo, D.: UWB double ridge waveguide coupler with low loss. In 2016 USNC-URSI National Radio Science Meeting, Boulder, CO, USA., Jan. 2016.

21. Manoochehri, O., Darvazehban, A., Farzami, F., and Erricolo, D.: High gain omnidirectional array antenna with low side lobe levels in the elevation plane. In 2017 USNC-URSI National Radio Science Meeting, Boulder, CO, USA., Jan. 2017.

22. Manoochehri, O., Darvazehban, A., Farzami, F., and Erricolo, D.: High gain miniaturized multi-beam Luneburg lens antenna for satellite communications. In 2017 USNC-URSI National Radio Science Meeting, Boulder, CO, USA., Jan. 2017.

23. Raisi, P., Farzami, P., Khaledian, S., Manoochehri, O., and Erricolo, D.: Low power reflection amplifier using extracted S-parameter of tunnel diode in RFID application. In 2018 USNC-URSI National Radio Science Meeting, Boulder, CO, USA., Jan. 2018.

24. Foroutan, V., Manoochehri, O., Darvazehban, A., Farzami, F., and Erricolo, D.: Ultra-wideband ring-cavity power combiner. In 2018 USNC-URSI National Radio Science Meeting, Boulder, CO, USA., Jan. 2018.

25. Manoochehri, O., Farzami, F., Erricolo, D., and Salari, M. A.: A Substrate Integrated Waveguide Slot Array with Voltage-Controlled Liquid Crystal Phase Shifter. In 2018 IEEE International Symposium on Antennas and Propagation USNC/URSI National Radio Science Meeting, pages 2123–2124, July 2018.

26. Manoochehri, O., Darvazehban, A., and Erricolo, D.: UWB double-ridge waveguide coupler with low loss. Microwave and Optical Technology Letters, 59(8):1787–1791, 2017.

27. D'Abreu, G.: Automotive antenna evaluation. In AMTA 2016 Proceedings, pages 1–6. IEEE, 2016.

28. Bailey, M., Campbell, T., Reddy, C., Kellogg, R., and Nguyen, P.: Compact wideband direction-finding antenna. IEEE Antennas and Propagation Magazine, 54(6):44–68, 2012.

29. Rodrigo, D., Cetiner, B. A., and Jofre, L.: Frequency, radiation pattern and polarization reconfigurable antenna using a parasitic pixel layer. IEEE Transactions on Antennas and Propagation, 62(6):3422–3427, June 2014.

30. Panagamuwa, C. J., Chauraya, A., and Vardaxoglou, J. C.: Frequency and beam reconfigurable antenna using photoconducting switches. IEEE Transactions on Antennas and Propagation, 54(2):449–454, Feb 2006.

31. Rodrigo, D., Jofre, L., and Cetiner, B. A.: Circular beam-steering reconfigurable antenna with liquid metal parasitics. IEEE Transactions on Antennas and Propagation, 60(4):1796–1802, April 2012.

32. Aboufoul, T., Parini, C., Chen, X., and Alomainy, A.: Pattern-reconfigurable planar circular ultra-wideband monopole antenna. IEEE Transactions on Antennas and Propagation, 61(10):4973–4980, Oct 2013.

33. Mookiah, P. and Dandekar, K. R.: Metamaterial-substrate antenna array for mimo communication system. IEEE Transactions on Antennas and Propagation, 57(10):3283–3292, Oct 2009.

34. Simons, R. N., Chun, D., and Katehi, L. P. B.: Polarization reconfigurable patch antenna using microelectromechanical systems (mems) actuators. In IEEE Antennas and Propagation Society International Symposium (IEEE Cat. No.02CH37313), volume 2, pages 6–9 vol.2, 2002.

35. Aboufoul, T., Chen, X., Parini, C. G., and Alomainy, A.: Multiple-parameter reconfiguration in a single planar ultra-wideband antenna for advanced wireless communication systems. IET Microwaves, Antennas Propagation, 8(11):849–857, August 2014.

36. Manoochehri, O., Darvazehban, A., Monticone, F., and Erricolo, D.: Design of Compact Beam-Steering Active Slot Antennas Using a Metasurface. In 2019 USNC-URSI National Radio Science Meeting, Boulder, CO, USA., Jan. 2019.

37. Darvazehban, A., Emadeddin, A., Manoochehri, O., and Erricolo, D.: Wide band multi-beam cylindrical lens. In 2017 IEEE International Symposium on Antennas and Propagation USNC/URSI National Radio Science Meeting, pages 507–508, July 2017.

38. Chen, L., Lei, Z., Yang, R., Fan, J., and Shi, X.: A broadband artificial material for gain enhancement of antipodal tapered slot antenna. IEEE Transactions on Antennas and Propagation, 63(1):395–400, Jan 2015.

39. Hay, S. G., Archer, J. W., Timms, G. P., and Smith, S. L.: A beam-scanning dual-polarized fan-beam antenna suitable for millimeter wavelengths. IEEE Transactions on Antennas and Propagation, 53(8):2516–2524, Aug 2005.

40. Matytsine, L., Lagoiski, P., Matytsine, M., and Matitsine, S.: Large size, lightweight, Luneburg Lenses for multi-beam antenna applications. In 2012 6th European Conference on Antennas and Propagation (EUCAP), pages 2266–2270, 2012.

41. Matytsine, L., Lagoiski, P., Matytsine, M., and Matitsine, S.: Large size, lightweight, Luneburg Lenses for multi-beam antenna applications. In 2012 6th European Conference on Antennas and Propagation (EUCAP), pages 2266–2270, March 2012.

42. Schulwitz, L. and Mortazawi, A.: A new low loss Rotman lens design using a graded dielectric substrate. IEEE Transactions on Microwave Theory and Techniques, 56(12):2734–2741, 2008.

43. Wu, X. and Laurin, J. J.: Fan-Beam Millimeter-Wave Antenna Design Based on the Cylindrical Luneberg Lens. IEEE Transactions on Antennas and Propagation, 55(8):2147–2156, Aug 2007.

44. Hua, C., Wu, X., Yang, N., and Wu, W.: Air-Filled Parallel-Plate Cylindrical Modified Luneberg Lens Antenna for Multiple-Beam Scanning at Millimeter-Wave Frequencies. IEEE Transactions on Microwave Theory and Techniques, 61(1):436–443, Jan 2013.

45. Bailey, M. C., Campbell, T. G., Reddy, C. J., Kellogg, R. L., and Nguyen, P.: Compact wide-band direction-finding antenna. IEEE Antennas and Propagation Magazine, 54(6):44–68, December 2012.

46. Salari, M. A., Manoochehri, O., Darvazehban, A., and Erricolo, D.: An Active 20 MHz to 2.5 GHz UWB Receiver Antenna System Using a TEM Horn. IEEE Antennas and Wireless Propagation Letters, 16:2432–2435, July 2017.

47. Farzami, F., Khaledian, S., Smida, B., and Erricolo, D.: Reconfigurable Dual-Band Bidirectional Reflection Amplifier With Applications in Van Atta Array. IEEE Transactions on Microwave Theory and Techniques, 65(11):4198–4207, Nov 2017.

48. Emadeddin, A., Salari, M. A., Zoghi, M., Darvazehban, A., and Manoochehri, O.: A Compact Ultra-Wideband Multibeam Antenna System. IEEE Transactions on Antennas and Propagation, 66(1):125–131, Jan 2018.

49. Computer Simulation Technology: CST MICROWAVE STUDIO.

50. Balanis, C. A.: Advanced engineering electromagnetics. John Wiley & Sons, 1999.

51. Volakis, J., Chen, C.-C., and Fujimoto, K.: Small antennas: miniaturization techniques & applications. McGraw Hill, 2009.

52. Song, K. and Xue, Q.: Ultra-wideband ring-cavity multiple-way parallel power divider. IEEE Transactions on Industrial Electronics, 60(10):4737–4745, Oct 2013.

53. Robrish, P.: An analytic algorithm for unbalanced stripline impedance. IEEE Transactions on Microwave Theory and Techniques, 38(8):1011–1016, Aug 1990.

54. Schelkunoff, S. A.: Electromagnetic waves. Van Nostrand, 1951.

55. Mailloux, R.: Phased array antenna handbook, volume 2. Artech House Boston, 2005.

56. Rodenbeck, C. T., Kim, S.-G., Tu, W.-H., Coutant, M. R., Hong, S., Li, M., and Chang, K.: Ultra-wideband low-cost phased-array radars. IEEE Transactions on microwave theory and techniques, 53(12):3697–3703, 2005.

57. Rotman, W. and Turner, R.: Wide-angle microwave lens for line source applications. IEEE Transactions on Antennas and Propagation, 11(6):623–632, 1963.

58. balanis, R.: Design trades for Rotman lenses. IEEE Transactions on antennas and propagation, 39(4):464–472, 1991.

59. Manoochehri, O., Farzami, F., Darvazehban, A., Shamim, A., Bagci, H., and Erricolo, D.: Design of a corrugated antipodal Vivaldi antenna with stable pattern. In 2019 USNC-URSI National Radio Science Meeting, Boulder, CO, USA., Jan. 2019.

60. Pour, Z. A. and Shafai, L.: Investigation of virtual array antennas with adaptive element locations and polarization using parabolic reflector antennas. IEEE Transactions on Antennas and Propagation, 61(2):688–699, Feb 2013.

61. Nomoto, S., Mizuguchi, Y., Watanabe, F., and Yamada, M.: Offset multi-focal reflector antenna. In 1986 Antennas and Propagation Society International Symposium, volume 24, pages 267–270, June 1986.

62. Landrac, G., Jehamy, E., and Ney, M.: Optimisation of wide angle scanning antennas by genetic algorithms; application to reflector antennas for automotive radars at 76 GHz.

63. Kira, F., Honma, N., Cho, K., and Mizuno, H.: Modified multi-focal paraboloid design for high aperture efficiency multibeam reflector antenna. In IEEE Antennas and Propagation Society International Symposium (IEEE Cat. No.02CH37313), volume 1, pages 662–665 vol.1, 2002.

64. Kildal, P. S.: Laws of geometrical optics mapping in multi-reflector antennas with application to elliptical apertures. IEE Proceedings H - Microwaves, Antennas and Propagation, 136(6):445–454, Dec 1989.

65. Foudazi, A. and Mallahzadeh, A. R.: Pattern synthesis for multi-feed reflector antennas using invasive weed optimisation. IET Microwaves, Antennas Propagation, 6(14):1583–1589, November 2012.

66. Oliner, A. A., Jackson, D. R., and Volakis, J.: Antenna engineering handbook. McGraw Hill, 2007.

67. Collin, R. E.: Antennas and radiowave propagation. McGraw-Hill College, 1985.

68. Sharma, A., Hoang, A. T., and Reynolds, M. S.: A Coplanar Vivaldi-Style Launcher for Goubau Single-Wire Transmission Lines. IEEE Antennas and Wireless Propagation Letters, 16:2955–2958, 2017.

69. Zhu, S., Liu, H., Chen, Z., and Wen, P.: A Compact Gain-Enhanced Vivaldi Antenna Array With Suppressed Mutual Coupling for 5G mm Wave Application. IEEE Antennas and Wireless Propagation Letters, 17(5):776–779, May 2018.

70. Oktafiani, F., Amrullah, Y. S., Saputera, Y. P., Wahyu, Y., and Wijayanto, Y. N.: Analysis of corrugated edge variations on balanced antipodal Vivaldi antennas. In 2015 International Conference on Radar, Antenna, Microwave, Electronics and Telecommunications (ICRAMET), pages 1–5, Oct 2015.

71. Qiu, L., Xiao, K., Chai, S. L., Qi, H. Y., and Mao, J. J.: A double-layer shaped-beam traveling-wave slot array based on siw. IEEE Transactions on Antennas and Propagation, 64(11):4639–4647, Nov 2016.

72. Wen, Y. Q., Wang, B. Z., and Ding, X.: Wide-beam siw-slot antenna for wide-angle scanning phased array. IEEE Antennas and Wireless Propagation Letters, 15:1638–1641, 2016.

73. Farzami, F. and Norooziarab, M.: Experimental Realization of Tunable Transmission Lines Based on Single-Layer SIWs Loaded by Embedded SRRs. IEEE Transactions on Microwave Theory and Techniques, 61(8):2848–2857, Aug 2013.

74. Algorri, J. F., Urruchi, V., Bennis, N., Sánchez-Pena, J. M., and Otón, J. M.: Cylindrical liquid crystal microlens array with rotary optical power and tunable focal length. IEEE Electron Device Letters, 36(6):582–584, June 2015.

75. Woehrle, C. D., Doyle, D. T., Lane, S. A., and Christodoulou, C. G.: Space radiation environment testing of liquid crystal phase shifter devices. IEEE Antennas and Wireless Propagation Letters, 15:1923–1926, 2016.

76. Duan, Z., Wang, Y., Lv, W., Dai, Y., and Lin, F.: A 6-bit CMOS Active Phase Shifter for Ku-Band Phased Arrays. IEEE Microwave and Wireless Components Letters, 28(7):615–617, July 2018.

77. Cao, Y. F. and Zhang, X. Y.: A wideband beam-steerable slot antenna using artificial magnetic conductors with simple structure. IEEE Transactions on Antennas and Propagation, 66(4):1685–1694, April 2018.

78. Monticone, F., Estakhri, N. M., and Alù, A.: Linear and nonlinear optical nano-antennas. In 2015 USNC-URSI Radio Science Meeting (Joint with AP-S Symposium), pages 345–345, July 2015.

79. Sabapathy, T., Jusoh, M., Ahmad, R. B., Kamarudin, M. R., and Soh, P. J.: A Ground-Plane-Truncated, Broadly Steerable Yagi–Uda Patch Array Antenna. IEEE Antennas and Wireless Propagation Letters, 15:1069–1072, 2016.

80. Wang, C. and Chen, L.: Modeling of stepped-impedance slot antenna. IEEE Transactions on Antennas and Propagation, 62(2):955–959, Feb 2014.

81. Lipsky, S. E.: Microwave passive direction finding. SciTech Publishing, 2004.

82. Guinvarc'h, R., Serhir, M., and Boust, F.: A compact dual-polarized 3: 1 bandwidth omnidirectional array of spiral antennas. IEEE Antennas and Wireless Propagation Letters, 15:1909–1912, 2016.

83. Ebihara, S., Kimura, Y., Shimomura, T., Uchimura, R., and Choshi, H.: Coaxial-fed circular dipole array antenna with ferrite loading for thin directional borehole radar sonde. IEEE Transactions on Geoscience and Remote Sensing, 53(4):1842–1854, 2015.

84. Lie, J. P., See, C. M., and Ng, B. P.: Ultra wideband direction finding using digital channelization receiver architecture. IEEE communications letters, 10(2):85–87, 2006.

85. Klukas, R. and Fattouche, M.: Line-of-sight angle of arrival estimation in the outdoor multipath environment. IEEE transactions on vehicular technology, 47(1):342–351, 1998.

86. Cho, C., Park, I., and Choo, H.: Design of a small antenna for wideband mobile direction finding systems. IET microwaves, antennas & propagation, 4(7):930–937, 2010.

87. Caratelli, D., Liberal, I., and Yarovoy, A.: Design and full-wave analysis of conformal ultra-wideband radio direction finders. IET microwaves, antennas & propagation, 5(10):1164–1174, 2011.

88. Ozturk, M. E., Korkmaz, E., and Kebeli, M.: Rounded-edge bow-tie antenna for wideband mobile direction finding system. IET Microwaves, Antennas & Propagation, 9(15):1809–1815, 2015.

89. Chung, K., Pyun, S., and Choi, J.: Design of an ultrawide-band tem horn antenna with a microstrip-type balun. IEEE Transactions on Antennas and Propagation, 53(10):3410–3413, 2005.

90. Tan, A. E.-C., Jhamb, K., and Rambabu, K.: Design of transverse electromagnetic horn for concrete penetrating ultrawideband radar. IEEE Transactions on Antennas and Propagation, 60(4):1736–1743, 2012.

91. Elsherbini, A. and Sarabandi, K.: Envelop antenna: a class of very low profile uwb directive antennas for radar and communication diversity applications. IEEE Transactions on Antennas and Propagation, 61(3):1055–1062, 2013.

92. Chang, T., Burnside, W. D., et al.: An ultrawide-bandwidth tapered resistive tem horn antenna. IEEE Transactions on antennas and propagation, 48(12):1848–1857, 2000.

93. Blume, S. and Grafmuller, B.: Biconical antennas and conical horns with elliptic cross section. IEEE transactions on antennas and propagation, 36(8):1066–1070, 1988.

94. McLean, J. S., Sutton, R., Medina, A., Foltz, H., and Li, J. F.: The experimental characterization of uwb antennas via frequency-domain measurements. IEEE Antennas and Propagation Magazine, 49(6):192–202, 2007.

95. Shao, J., Fang, G., Fan, J., Ji, Y., and Yin, H.: Tem horn antenna loaded with absorbing material for gpr applications. IEEE antennas and wireless propagation letters, 13:523–527, 2014.

96. Church, J., Chieh, J.-C. S., Xu, L., Rockway, J. D., and Arceo, D.: Uhf electrically small box cage loop antenna with an embedded non-foster load. IEEE Antennas and Wireless Propagation Letters, 13:1329–1332, 2014.

97. Elfrgani, A. M. and Rojas, R. G.: Biomimetic antenna array using non-foster network to enhance directional sensitivity over broad frequency band. IEEE Transactions on Antennas and Propagation, 64(10):4297–4305, 2016.

98. White, C. R., Colburn, J. S., and Nagele, R. G.: A non-foster vhf monopole antenna. IEEE Antennas and Wireless Propagation Letters, 11:584–587, 2012.

99. Gannett, D. K.: Transistor negative impedance converters, May 8 1956. US Patent 2,745,068.

100. Sussman-Fort, S. E. and Rudish, R. M.: Non-foster impedance matching of electrically-small antennas. IEEE Transactions on Antennas and Propagation, 57(8):2230–2241, 2009.

101. Advanced Design System: Keysight technologies.

102. Blech, M. D., Ott, A. T., and Eibert, T. F.: A two octave bandwidth dielectric loaded biconical antenna with high sidelobe suppression. In 2009 3rd European Conference on Antennas and Propagation, pages 1006–1010, March 2009.

103. McDonald, J. L. and Filipovic, D. S.: Biconical antenna over ground plane. IEEE Trans. Antennas Propag., 60(4):2093–2096, April 2012.

104. Gimeno, B., Cruz, J. L., Navarro, E. A., and Such, V.: A polarizer rotator system for three-dimensional oblique incidence. IEEE Transactions on Antennas and Propagation, 42(7):912–919, Jul 1994.

105. Dietlein, C., Luukanen, A., Popovi, Z., and Grossman, E.: A W-Band Polarization Converter and Isolator. IEEE Transactions on Antennas and Propagation, 55(6):1804–1809, June 2007.

106. Amert, A. K. and Whites, K. W.: Miniaturization of the biconical antenna for ultrawideband applications. IEEE Transactions on Antennas and Propagation, 57(12):3728–3735, Dec 2009.

107. Schantz, H. G.: Introduction to ultra-wideband antennas. In Ultra Wideband Systems and Technologies, 2003 IEEE Conference on, pages 1–9. IEEE, 2003.

108. Balanis, C. A.: Antenna theory: analysis and design. Microstrip Antennas, third edition, John wiley & sons, 2005.

109. Pozar, D. M.: Microwave Engineering 3e. Transmission Lines and Waveguides, pages 143–149, 2005.

110. Arnaud, E., Chantalat, R., Koubeissi, M., Monediere, T., Rodes, E., and Thevenot, M.: Global Design of an EBG Antenna and Meander-Line Polarizer for Circular Polarization. IEEE Antennas and Wireless Propagation Letters, 9:215–218, June 2010.

111. Chu, R.-S. and Lee, K.-M.: Analytical method of a multilayered meander-line polarizer plate with normal and oblique plane-wave incidence. IEEE Transactions on Antennas and Propagation, 35(6):652–661, June 1987.

112. Bhattacharyaa, A. K.: Analysis of multilayer infinite periodic array structures with different periodicities and axes orientations. IEEE Transactions on Antennas and Propagation, 48(3):357–369, Mar 2000.

113. Wu, T.-K.: Meander-line polarizer for arbitrary rotation of linear polarization. IEEE Microwave and Guided Wave Letters, 4(6):199–201, June 1994.

114. Levy, R.: Improved single and multiaperture waveguide coupling theory, including explanation of mutual interactions. IEEE Transactions on Microwave Theory and Techniques, 28(4):331–338, Apr. 1980.

115. Mira, F., Blas, A. A. S., Boria, V. E., and Gimeno, B.: Wideband modelling of cascaded h-plane waveguide junctions using the generalised impedance matrix representation. IET Microwaves, Antennas Propagation, 3(4):580–590, June 2009.

116. Hrobak, M., Sterns, M., Seler, E., Schramm, M., and Schmidt, L. P.: Design and construction of an ultrawideband backward wave directional coupler. IET Microwaves, Antennas Propagation, 6(9):1048–1055, June 2012.

117. Lopez-Berrocal, B., de Oliva-Rubio, J., Marquez-Segura, E., Moscoso-Martir, A., Molina-Fernandez, I., and Uhlig, P.: High Performance 1.8-18 GHz 10-dB Low Temperature Co-Fired Ceramic Directional Coupler. Progress In Electromagnetics Research, 104:99–112, 2010.

118. Chu, Q. X., Kang, Z. Y., Wu, Q. S., and Mo, D. Y.: An in-phase output ka -band traveling-wave power divider/combiner using double ridge-waveguide couplers. IEEE Transactions on Microwave Theory and Techniques, 61(9):3247–3253, Sept. 2013.

119. Liu, H., Fang, S., and Wang, Z.: Modified coupled line trans-directional coupler with arbitrary power divisions and its application to a 180 hybrid. IET Microwaves, Antennas Propagation, 9(7):682–688, 2015.

120. Helszajn, J.: Ridge waveguides and passive microwave components. Number 49. IET, 2000.

121. Chen, T. S.: Calculation of the parameters of ridge waveguides. IRE Transactions on Microwave Theory and Techniques, 5(1):12–17, Jan. 1957.

122. Lee, H. Y., Jun, D. S., Kim, D. Y., Lee, S. S., and Choi, I. G.: Wideband HNRD guide directional coupler based on multi-hole coupling structure for V-band. Electronics Letters, 40(20):1277–1278, Sept. 2004.

123. Fickenscher, T.: Theoretical and experimental results of aperture coupling between image guides. IET Microwaves, Antennas Propagation, 1(5):1042–1045, October 2007.

124. Morgan, M. A. and Boyd, T. A.: A 10-100 GHz Double-Ridged Horn Antenna and Coax Launcher. IEEE Transactions on Antennas and Propagation, 63(8):3417–3422, Aug. 2015.

125. Cohn, S. B.: Determination of aperture parameters by electrolytic-tank measurements. Proceedings of the IRE, 39(11):1416–1421, Nov. 1951.

VITA

NAME: Omid Manoochehri

EDUCATION: Ph.D., Electrical and Computer Engineering, University of Illinois at Chicago, Chicago, Illinois, 2019

M.S., Electrical Engineering, Tarbiat Modares University, Tehran, Iran, 2011

B.S., Electrical Engineering, Shiraz University of Technology, Shiraz, Iran, 2008

PUBLICATIONS:

O. Manoochehri, et al, "A Parallel Plate Ultra-Wideband Multibeam Microwave Lens Antenna," in *IEEE Transactions on Antennas and Propagation*. vol. 66, no. 9, pp. 4878-4883, Sept. 2018.

O. Manoochehri, et al, "A dual-polarized biconical antenna for direction finding applications from 2 to 18 GHz," *Microwave and Optical Technology Letters*, 2018.

O. Manoochehri, et al, " A short broadband monopole antenna," *AEU-International Journal of Electronics and Communications*, 2018.

A. Emadeddin, M. A. Salari, M. Zoghi, A. Darvazehban and **O. Manoochehri**, " A Compact Ultra-Wideband Multibeam Antenna System," *IEEE Transactions on Antennas and Propagation*, 2018.

O. Manoochehri, et al, " An improved formula for the inductance of mesh grids," *Microwave and Optical Technology Letters*, 2017.

A. Darvazehban, **O. Manoochehri**, et al, " Ultra-Wideband Scanning Antenna Array With Rotman Lens," *IEEE Transactions on Microwave Theory and Techniques*, 2017.

O. Manoochehri, et al, " UWB double-ridge waveguide coupler with low loss," *Microwave and Optical Technology Letters*, 2017.

M. A. Salari, **O. Manoochehri**, et al, "An Active 20 MHz to 2.5 GHz UWB Receiver Antenna System Using a TEM Horn," *IEEE Antennas and Wireless Propagation Letters*, 2017.

O. Manoochehri, et al, "Π-Model Dual-Band Impedance Transformer for Unequal Complex Impedance Loads," *IEEE Microwave and Wireless Components Letters*, 2015.

S. Abbasiniazare, **O. Manoochehri**, et al " A reconfigurable printed dipole antenna using RF PIN diodes," *Microwave and Optical Technology Letters*, 2014.

O. Manoochehri, et al, "Design of a 2×2 tapered dielectric-loaded helical antenna array for Inmarsat satellite system," *Microwave and Optical Technology Letters*, 2013.

M. A. Salari, **O. Manoochehri**, et al, "Miniaturized Microstrip Ring Hybrid with Defected Microstrip Structure" *Microwave and Optical Technology Letters*, 2013.

S. Abbasiniazare, K. Forooraghi, A. Torabi, and **O. Manoochehri**, " Mutual Coupling Compensation for a 1×2 Short Helical Antenna Array Using Split-Ring Resonators (SRRs)," *Journal of Electromagnetic Waves and Applications*, 2013.

O. Manoochehri, et al " A Second-Order BPF Using a Miniaturized-Element Frequency Selective Surface with Reduced Angular Sensitivity," *Progress In Electromagnetics Research C*, 2012.

M. A. Salari, S. Abbasiniazare, **O. Manoochehri** " The Effect of Electromagnetic Waves on Multilayer Orthogonal Microstrip Lines With and Without Defected Microstrip Structure," *IEEE Antennas and Wireless Propagation Letters*, 2012.

A. Torabi, K. Forooraghi, **O. Manoochehri** and S. Abbasiniazare, " Compact microstrip bandpass filters using dual mode stub loaded resonators and capacitive inductive source load coupling," *Microwave and Optical Technology Letters*, 2011.

O. Manoochehri,et al," Wide band multi-beam cylindrical lens," *2017 IEEE International Symposium on Antennas and Propagation USNC/URSI National Radio Science Meeting*, San Diego, CA, 2017.

O. Manoochehri, et al, "A new method for designing high efficiency multi feed multi beam reflector antennas," *2017 International Conference on Electromagnetics in Advanced Applications (ICEAA)*, Verona, 2017.

O. Manoochehri, et al," High gain miniaturized multi-beam Luneburg lens antenna for satellite communications," *USNC-URSI National Radio Science Meeting*, Boulder, CO, Jan. 4-7, 2017.

O. Manoochehri, et al," High gain miniaturized multi-beam Luneburg lens antenna for satellite communications," *USNC-URSI National Radio Science Meeting*, Boulder, CO, Jan. 4-7, 2017.

O. Manoochehri, et al, " A non-resonant short monopole antenna with lumped circuit for wideband impedance matching," *USNC-URSI National Radio Science Meeting*, Boulder, CO, Jan. 6-9, 2016.

O. Manoochehri, F. Farzami, D. Erricolo "Higher order analytical models of planar mesh grids," *USNC-URSI National Radio Science Meeting*, Boulder, CO, Jan. 6-9, 2016.

A. Darvazehban, A. Emadoddin, **O. Manoochehri**, D. Erricolo," Mutual coupling reduction in microstrip patch antenna," *USNC-URSI National Radio Science Meeting*, Boulder, CO, Jan. 6-9, 2016.

A. Darvazehban, **O. Manoochehri**, et al, " UWB double ridge waveguide coupler with low loss," *USNC-URSI National Radio Science Meeting*, Boulder, CO, Jan. 6-9, 2016.